Polynomial Inflation and Its Aftermath

Dissertation
zur
Erlangung des Doktorgrades (Dr. rer. nat.)
der
Mathematisch-Naturwissenschaftlichen Fakultät
der
Rheinischen Friedrich-Wilhelms-Universität Bonn

von
Yong Xu
aus
Henan, China

Bonn, 2022

Abstract

Cosmic inflation elegantly resolves problems in the standard cosmology. The most simple inflationary theory invokes a single scalar field ϕ, slowly rolling down from a flat potential of a *monomial* form. However latest Cosmic microwave background (CMB) experiments have ruled out the monomial scenarios. In this thesis, we show that a simple and well motivated small field *polynomial* of degree four, with a near inflection-point at $\phi_0 \lesssim M_P$, can fit comfortably well on current CMB data. This model predicts a testable running of the spectral index $\sim -10^{-3}$. A full model parameter space has been obtained by considering Big Bang nucleosynthesis (BBN) constraint on reheating temperature as well as radiative stability conditions; this yields a lower bound $\phi_0 > 3 \times 10^{-5} M_P$. The inflationary scale within the parameter space can be as low as ~ 1 MeV, or as high as $\sim 10^{10}$ GeV. Similarly, the reheating temperature can lie between its lower bound of ~ 4 MeV and about $4 \times 10^8 (10^{11})$ GeV for fermionic (bosonic) inflaton decays.

Since any cosmological model has to give rise to successful post-inflationary phenomena, e.g. producing correct dark matter (DM) and baryon densities, we then show that the aftermath of polynomial inflation can easily account for DM production and Baryogenesis (via Leptogenesis) by simply extending the model with a DM field, e.g. singlet fermion or boson and right handed neutrinos (RHNs). It turns out that DM field with mass in the range: $O\,(\text{KeV}) \lesssim m_\chi \lesssim O(10^{11})$ GeV can account for the correct relic density while being consistent with inflationary predictions and constraints from Lyman$-\alpha$ and kinematic threshold. For leptogenesis, one can have either thermal channel if the lightest RHN mass lies in 10^{10} GeV $\lesssim M_1 \lesssim 10^{11}$ GeV or non-thermal channel if 10^8 GeV $\lesssim M_1 \lesssim 10^{10}$ GeV, while being consist with neutrino oscillation data and inflationary predictions. Finally we consider the extension to a large field scenario with $\phi_0 \geq 1 M_P$. We work out the parameter space consistent with latest CMB measurements at 2σ level, and obtain an upper bound $\phi_0 \lesssim 21.5 M_P$. We show that the tensor-to-scalar ratio r ranges from $O(10^{-8})$ to $O(10^{-2})$, being testable in the near future.

This thesis *i*) offered the most complete analysis for the polynomial inflation to date, and *ii*) showed that the aftermath of polynomial inflation can account for successful post-inflationary phenomena without jeopardizing the inflationary predictions, hence *iii*) demonstrated that polynomial inflation is an acceptable cosmological framework.

Acknowledgements

List of Publications

- [1] M. Drees and **Yong Xu**, Overshooting, Critical Higgs Inflation and Second Order Gravitational Wave Signatures, 1905.13581,
  Published in **Eur.Phys.J.C 81 (2021) 2, 182**. https://doi.org/10.1140/epjc/s10052-021-08976-2

- [2] M. Drees and **Yong Xu**, Small Field Polynomial Inflation: Reheating, Radiative Stability and Lower Bound, 2104.03977,
  Published in **JCAP 09 (2021) 012**. https://doi.org/10.1088/1475-7516/2021/09/012

- [3] N. Bernal and **Yong Xu**, Polynomial Inflation and Dark Matter, 2106.03950,
  Published in **Eur.Phys.J.C 81 (2021) 10, 877**. https://doi.org/10.1140/epjc/s10052-021-09694-5

- [4] N. Bernal, F. Hajkarim and **Yong Xu**, Axion Dark Matter in the Time of Primordial Black Holes, 2107.13575,
  Published in **Phys.Rev.D 104 (2021) 075007.** https://doi.org/10.1103/PhysRevD.104.075007.

- [5] N. Bernal, Y. F. Perez-Gonzalez, **Yong Xu** and Ó. Zapata, ALP Dark Matter in a Primordial Black Hole Dominated Universe, 2110.04312,
  Published in **Phys.Rev.D 104 (2021) 123536**. https://doi.org/10.1103/PhysRevD.104.123536

- [6] B. Barman, N. Bernal, **Yong Xu** and Ó. Zapata, Ultraviolet Freeze-in with a Time-dependent Inflaton Decay, 2202.12906,
  Published in **JCAP 07 (2022) 019**. https://doi.org/10.1088/1475-7516/2022/07/019

- [7] N. Bernal, Y. F. Perez-Gonzalez, **Yong Xu**, Superradiant Production of Heavy Dark Matter from Primordial Black Holes, 2205.11522,
  Published in **Phys.Rev.D 106 (2022) 1, 015020.** https://doi.org/10.1103/PhysRevD.106.015020

- [8] M. Drees and **Yong Xu**, A Minimal Model for Inflation, Neutrino Masses and Leptogenesis [In preparation]

- [9] M. Drees and **Yong Xu**, Large Field Polynomial Inflation: Parameter Space, Predictions and (Double) Eternal Nature, 2209.07545

- [10] N. Bernal and **Yong Xu**, WIMPs during Reheating, 2209.07546

This thesis is based on Refs. [2, 3, 8, 9], which cover phenomenology of small field polynomial inflation, including the parameter space and predictions [2]; its aftermath related with (p)reheating [2]; dark matter production [3], leptogenesis [8]; and a generation to large field model [9].

Contents

Introduction

The evolution of the Universe was governed by a set of differential equations from the intersection of general relativity (GR) and quantum field theory (QFT). Almost immediately after the Big Bang, an exponential expansion phase–inflation started. After that, energy transferred from the field driven inflation, namely the inflaton field, to other lighter degrees of freedom, leading to an extremely hot and thermal Universe with temperature as high as $T \sim O(10^{16})$ GeV. (A reminder: 1 GeV $\simeq 10^{13}$ Kelvin.) In such a high temperature environment, the Grand Unified Theory (GUT) is believed to hold, and all elementary particles behave freely (namely not bounded) in a cosmic fireball with interacting forces which are not distinct from each other. With the cosmic expansion, the temperature of the Universe decreased. Gradually, the three unified forces, namely strong, weak and electromagnetic interactions separated, free particles amalgamated into bound states, dark matter and neutrinos ceased to interact with the surrounding environment, nuclei formed, electrons and nuclei combined into atoms, photons started to propagate away. Finally, cosmic structures grew under gravitation, stars formed, galaxies assembled, and the Universe became the form as we observe today. See Fig. 1.1 for a quick glimpse at
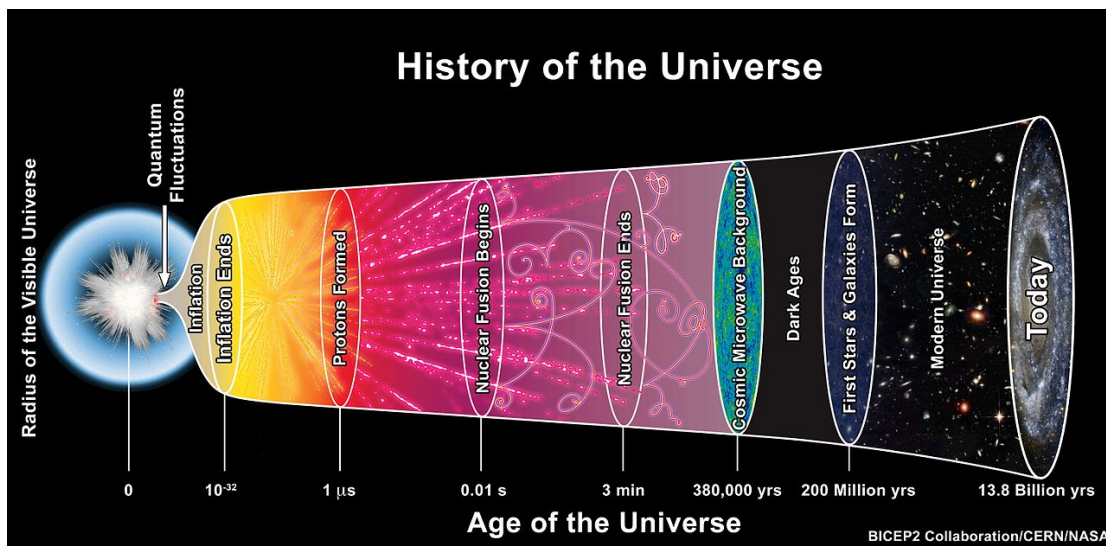
Figure 1.1: History of Universe from $t = 0$ till today $t = 13.8$ Billions years [11].
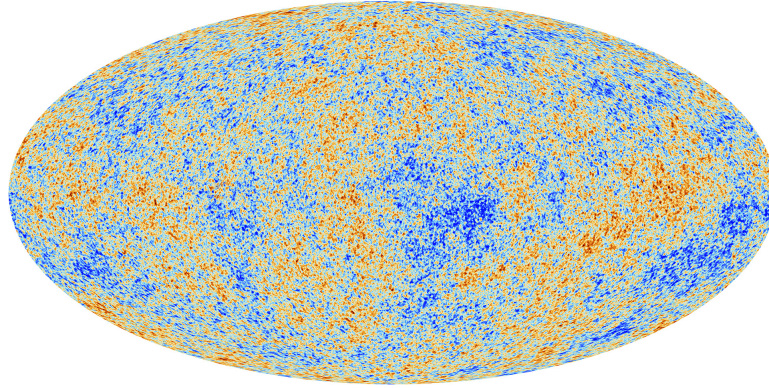
Figure 1.2: CMB map from Planck [14].

the history of the Universe from the Big Bang till today.

A special point of the cosmic history is about 380000 years after the Big Bang, corresponding to the recombination of electrons and nuclei. At that point the temperature of the Universe had become low enough to allow (stable) atoms to form. After that, photons stopped scattering with the free electrons in the thermal plasma, and started to propagate through the Universe. Some of these photons travelled about 13.8 billion years, and finally reached to us as a faint microwave radiation–cosmic microwave background (CMB), as shown in Fig. 1.2, where the blue and red dots correspond to photons with smaller and larger energy, respectively. Due to the comic expansion, matter contents as well as geometry of the Universe, the spectrum of the photons show certain features. By comparing with the measured CMB spectrum, we are then able to obtain the main parameters governing the evolution of the Universe. The cosmological model based on these parameters is quoted as ΛCDM model in which the Universe consists primarily of dark energy denoted by Λ, and cold dark matter (CDM).

In Fig. 1.3, the dotted data points correspond to the temperature temperature power spectrum $\mathcal{D}_\ell^{\mathrm{TT}} \equiv \ell(\ell+1)C_\ell/(2\pi)$[1] measured by Planck 2018 [13], which can be well fitted by a few parameters in ΛCDM model, in particular non-baryonic DM and baryonic matter density are respectively fitted to be [13]:

$$\Omega_c h^2 = 0.120 \pm 0.001 \, ; \tag{1.1}$$

$$\Omega_b h^2 = 0.0224 \pm 0.0001 \, , \tag{1.2}$$

where $\Omega \equiv \rho/(3H_0^2 M_P^2)$ denotes the energy density parameter and $h \simeq 67.4$ is the dimensionless Hubble parameter, defined as $H_0 = 67.4 \pm 0.5 (\mathrm{km/s})\mathrm{Mpc}^{-1} \equiv 100\, h\, (\mathrm{km/s})\mathrm{Mpc}^{-1}$.

Though the ΛCDM model is quite successful to explain the measured data, there are still some questions that it is incapable to answer, e.g.

- Why does the CMB spectrum look so homogeneous?

- What is the origin of the tiny inhomogeneities?

---

[1] The observed CMB temperature anisotropies can be expanded in spherical harmonics with summation of different angular multipole ℓ; C_ℓ here denotes the angular power spectrum [12].
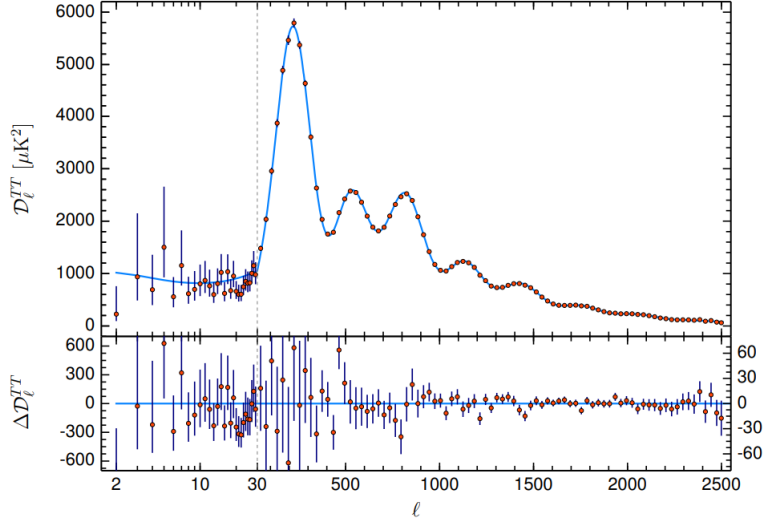
Figure 1.3: Red points are temperature temperature power spectrum measured by Planck 2018 [13]; blue curve corresponds to the fit.

- Why is the Universe so flat geometrically?

On the other hand, at microscopic scales the most successful theory, namely the Standard Model (SM) of particle physics, offers no answer regarding:

- What is nature DM? And how was DM generated in the early Universe?

- What are the dynamics for generation of net baryon densities?

- What is the origin of neutrino mass?

These questions imply that the standard model in both cosmology and particle physics are not complete and a further framework is needed in order to resolve the aforementioned puzzles.

This thesis is intended to answer these questions with a most minimal framework based on empirical facts and the principle of simplicity[2]. In particular we extend the SM of particle physics with a scalar field (acting as inflaton) and a DM field, which could be Dirac fermion, scalar or vector boson, and three right-handed neutrinos (RHNs) for the purpose of generating neutrino masses as well as Baryogenesis (via leptogenesis). The action for this model can be written as

$$S = \int d^4x \sqrt{-g} \left[\mathcal{L}_{SM} + \mathcal{L}_{EH} + \mathcal{L}_{inflaton} + \mathcal{L}_{DM} + \mathcal{L}_{RHNs} \right] , \qquad (1.3)$$

with g being the determinant of spacetime metric $g_{\mu\nu}$ and R the Ricci scalar; $\mathcal{L}_{SM}$ corresponding to the Lagrangian for the SM of particle physics; $\mathcal{L}_{EH} = \frac{M_P^2}{2} R$ describing the usual Einstein-Hilbert term for GR; $\mathcal{L}_{inflaton}$, $\mathcal{L}_{DM}$ and $\mathcal{L}_{RHN}$ denoting Lagrangian for inflaton, DM, and RHNs respectively, which will be explained detailedly in the following. We will show that such a simple setup can account

---

[2] The simplest theory that describes all data should be preferred; this is usually quoted as Occam's razor.

for inflation, DM production, neutrino mass as well as Baryogenesis. Before investigating the detailed phenomenology of this model, we first present some necessary background knowledge, and explain the aforementioned questions in detail.

The outline of this thesis is as follows. In Chapter 2, we offer short review of necessary background knowledge, including GR and standard cosmology; motivations for and dynamics of cosmic inflation; the SM of particle physics; experimental hints for the existence of non-baryonic DM; see-saw mechanism for neutrino mass and a dynamical mechanism for Baryogenesis, namely leptogenesis. In Chapter 3, we present the small field polynomial inflation model as well as its predictions. In Chapter 4, reheating after small field polynomial inflation is investigated, where we work out the radiative stability condition and further estimate the allowed reheating temperature. In Chapter 5, DM production after small field polynomial inflation is studied. In Chapter 6, we are devoted to investigating leptogenesis as well as see-saw mechanism for light neutrino masses. In Chapter 7, we explore the phenomenology of polynomial inflation at large field regime, namely $\phi_0 \gtrsim M_P$. Finally Chapter 8 summarises the findings in this thesis and outlines several future research directions based on this work.

Background Knowledge

In this chapter we revisit several essential background knowledge and further motivations for our model setup (1.3).

2.1 General Relativity

The evolution of spacetime of the Universe is governed by General Relativity (GR). The equations of motion can be obtained by using $\delta S = 0$, with $S = \int dx^4 \sqrt{-g} \left(\frac{M_P^2}{2} R + \mathcal{L}_M \right)$ where g corresponds to the determinant of spacetime metric $g_{\mu\nu}$ and $\mathcal{L}_M$ denotes the Lagrangian for matter components. This leads to the famous Einstein field equation [15]:

$$G_{\mu\nu} = 8\pi G\, T_{\mu\nu} - \Lambda g_{\mu\nu}\,, \tag{2.1}$$

where Λ donates the cosmological constant, and the matter energy momentum tensor is given by

$$T_{\mu\nu} = \frac{-2}{\sqrt{-g}} \frac{\delta \left(\sqrt{-g} \mathcal{L}_M \right)}{\delta g_{\mu\nu}}\,. \tag{2.2}$$

The Einstein tensor is defined as

$$G_{\mu\nu} = R_{\mu\nu} - \frac{1}{2} R g_{\mu\nu}\,, \tag{2.3}$$

where $R = g^{\mu\nu} R_{\mu\nu}$ denotes the Ricci scalar. Eq. (2.1) relates the geometry of spacetime with mass contents. From Eq. (2.2), one also has the energy and pressure densities of the mass contents, which are given by $\rho \equiv T_0^0$ and $p \equiv - \sum_{i=1}^{3} T_i^i / 3$, respectively.

2.1.1 Cosmological Constant Problem

Before moving on, we would like to mention more about the interesting cosmological constant Λ, whose value remains a mystery and might hint more fundamental structure of spacetime. Using values reported in Planck 2018 for Dark Energy density $\Omega_\Lambda = 0.6847 \pm 0.0073$ and Hubble constant $H_0 = 67.4 \pm 0.5 (\text{km/s}) \text{Mpc}^{-1}$, one has $\Lambda = 3 H_0^2 \Omega_\Lambda \simeq 4.24 \times \left(10^{-33}\,\text{eV} \right)^2$ [13], and further

$\rho_\Lambda^0 = M_P^2 \Lambda \simeq 10^{-11}$ eV^4. Note that ρ_Λ denotes the energy density of vacuum states. Since the SM holds up to TeV scale, one would expect that the vacuum energy shall be at least $\rho_\Lambda^{\text{expected}} \gtrsim 10^{48}$ eV^4. But why the measured ρ_Λ^0 is so small compared to the expected value? This is known as *cosmological constant problem* [16]. It is actually very similar to the fate of Higgs mass in the SM of particle physics.

2.1.2 GR as an Effective Theory

Note that GR is a (low energy) effective theory with a coupling denoted as the Newton constant

$$G = \frac{1}{8\pi M_P^2} \, , \qquad (2.4)$$

with $M_P \simeq 2.4 \times 10^{18}$ GeV denoting the reduced Planck mass. Newton constant is actually very similar to Fermi constant appearing in the 4-Fermi effective theory $\mathcal{L}_{\text{Fermi}} = G_F \bar{\psi}_p \psi_n \bar{\psi}_e \psi_\nu$ for β-decay; the cross section scales like $\sigma \propto s G_F^2$ with s denoting the squared centre of mass energy. The Fermi constant is given by

$$G_F \equiv \frac{\sqrt{2}}{8} \frac{g_2^2}{m_W^2} \equiv \frac{\alpha_W}{m_W^2} \, , \qquad (2.5)$$

where g_2 corresponds to the gauge coupling and $m_W \simeq 80.4$ GeV the W boson mass. Note that the 4-Fermi effective theory only works in the regime where the energy scale $\sqrt{s} \ll m_W$. And one has to invoke the electroweak theory with W and Z bosons once $E \ll m_W$ is not satisfied.

Similarly one can rewrite Newton constant as [17]

$$G = \frac{1}{8\pi M_P^2} \equiv \frac{\alpha_g}{M_g^2} \, , \qquad (2.6)$$

with M_g denoting some scale, which is close to M_P if assuming $\alpha_g \sim O(1)$. Once the energy scale is above M_g, some new degree(s) of freedom emerge, similar to the W and Z bosons in the electroweak theory. In such cases classical GR is not valid anymore and a quantum version is needed. We would like to stress that throughout this thesis, we will be working on an energy scale much lower than the quantum gravity scale so that classical GR can be safely applied.

2.2 FLRW Cosmology

Applying the cosmological principle that the Universe at large scale being homogeneous and isotropic, one has the so-called Friedmann -Lemaître-Robertson-Walker (FLRW) metric [18]:

$$ds^2 = dt^2 - a^2(t) \left[\frac{dr^2}{1 - K r^2} + r^2(d\theta^2 + \sin^2 \theta \, d\phi^2) \right] \, , \qquad (2.7)$$

where (t, r, θ, ϕ) are comoving coordinates and $a(t)$ donates the scale factor. The physical distance is obtained by multiplying the scale factor $R = a(t)r$, and $K = +1, 0, -1$ correspond to space with

positive, zero and negative curvature respectively. Using the FLRW metric and zero component with $\mu = \nu = 0$ of Eq. (2.1), one has the first Friedmann equation

$$\mathcal{H}^2 \equiv \left(\frac{\dot{a}}{a}\right)^2 = \frac{\rho}{3\,M_P^2} - \frac{K}{a^2} + \frac{\Lambda}{3}\,, \tag{2.8}$$

describing how the size of the Universe evolves given some energy density; here $\dot{a} = da/dt$. Utilizing the $i\,j$ component of Eq. (2.1), one obtains the second Friedmann equation:

$$\frac{\ddot{a}}{a} = -\frac{4\pi G}{3}(\rho + 3p) + \frac{\Lambda}{3}\,, \tag{2.9}$$

which shows whether the expansion of the Universe is accelerated or not. For example, the Universe today is dominated by a positive and constant vacuum energy Λ, giving rise to an accelerating Universe. This has been verified in 1998 by measuring the brightness against red-shift for type Ia supernova; see e.g. Ref. [19]. In the early Universe, one can neglect the cosmological constant term (since there the energy density is not dominated by vacuum energy), and then the Fridmann equations read:

$$\mathcal{H}^2 = \left(\frac{\dot{a}}{a}\right)^2 = \frac{1}{3}\rho - \frac{K}{a^2}; \tag{2.10}$$

$$\dot{\mathcal{H}} + \mathcal{H}^2 = \frac{\ddot{a}}{a} = -\frac{1}{6}(\rho + 3p), \tag{2.11}$$

where we have set $M_P = 1/\sqrt{8\pi G}$ to be unity. Assuming the term $\frac{K}{a^2}$ to be subdominant, the above two equations can be combined, yielding the continuity equation:

$$\frac{d\rho}{dt} + 3\mathcal{H}(\rho + p) = 0 \implies \frac{d\ln\rho}{d\ln a} = -3(1 + \omega)\,, \tag{2.12}$$

where the equation-of-state parameter ω is defined as $\omega \equiv \frac{p}{\rho}$. Integrating Eq. (2.12), one has

$$\rho \propto a^{-3(1+\omega)}, \tag{2.13}$$

which together with Eq. (2.10) imply that the scale factor behaves as:

$$a(t) \propto \begin{cases} t^{\frac{2}{3}(1+w)} & \text{if } \omega \neq -1; \\ e^{\mathcal{H}t} & \text{if } \omega = -1\,. \end{cases} \tag{2.14}$$

In particular, in a radiation phase with $\omega = 1/3$, $a(t) \propto t^{1/2}$ and $a(t) \propto t^{2/3}$ at matter domination epoch with $\omega = 0$.

2.3 Inflation

In this section, we first revisit the problems in standard cosmology. Then we show how an inflation phase can elegantly resolve these problems. After that we briefly review the dynamics of inflation as well as the corresponding phenomenology. Finally we investigate the current status of the simple

monomial inflation model.

2.3.1 Problems of Standard Cosmology and Motivations for Inflation

- *Horizon problem.*

  An outstanding feature of Einstein's special relativity is that the speed of light is limited (though it is very large); this leads that at a fixed time scale, there is a boundary of the viable Universe (usually quoted as Horizon), giving rise to a domain beyond which causality is lost. CMB decoupling happened at time scale $t \sim 380000$ years, at which the maximum length that one photon could travel (referred as particle horizon) is far smaller than the viable size of the Universe at that time. This means that there were many causally disconnected patches of Universe at the moment of last scattering, and the length scale between each other is so large that they could not have been causally contacted!

  But the observed CMB photons turn out to be very uniform as shown in Fig. 1.2 and (almost) feature the same temperature. How could this be possible if these photons have not contacted each other before CMB decoupling? This is the *horizon problem.*

- *Flatness problem.*

  The first Friedmann equation (2.10) can be rewritten as

  $$1 - \Omega(a) = \Omega_K \,, \tag{2.15}$$

  with $\Omega(a) \equiv \frac{\rho(a)}{\rho_{\text{crit}}(a)}$ and $\rho_{\text{crit}}(a) = 3\mathcal{H}(a)^2$. The observed Universe today turns out to be spatially very flat. In particular current bound on the curvature energy by Planck is [13]

  $$\Omega_{K,0} = -\frac{K}{a_0^2 \mathcal{H}_0^2} < 0.0007 \pm 0.0019 \,. \tag{2.16}$$

  Note that $\mathcal{H}^2$ scales as a^{-4} (a^{-3}) in standard radiation (matter) domination epoch, which correspondingly implies that $|\Omega_K| \propto a^2 (a)$ after Big Bang. This means that one has to significantly fine tune the initial $\Omega_{K,i}$ in order to match the current bound. This is the *Flatness problem.*

- *Origin of initial inhomogeneity.*

  Though homogeneous, CMB photons do feature some tiny anisotropies as shown in Fig. 1.2. *But where the initial seeds for (tiny) CMB anisotropies come from?*

- *Monopole Problem.*

  The early Universe after the Big Bang was an extremely high energy scale and hot environment, where Grand Unified Theory (GUT) was believed to have played a significant role. GUT theories predict copious production of magnetic monopoles, which are heavy and stable particles that could have become the primary constituent of the Universe. Where are these magnetic Monopoles and why have they not been observed in nature? This is the *Monopole problem.*

In the standard cosmology, the Universe was assumed to start to evolve from a radiation epoch after the Big Bang, and there is no solution for the aforementioned problems.

2.3.2 Theory and Phenomenology of Inflation

Inflation corresponds to a phase where the space accelerates exponentially, driven by a (nearly) constant vacuum energy, which is usually quoted as potential energy $V(\phi)$ of a scalar inflaton field ϕ. With inflation, the aforementioned problems in standard cosmology can be elegantly resolved.

- *Horizon problem* reexamined.

  The Universe could have experienced an inflationary phase, where the spatial size of the Universe expands exponentially (from much smaller tiny size). This means that those causally disconnected parts of the Universe at CMB decoupling could have been contacted with each other during inflation, where the size of the Universe could be as small as (well) within the particle horizon.

- *Flatness problem* reloaded.

  Due to inflation, the scale factor grows exponentially, which quickly stretches the size of space. Recall the curvature energy density $\Omega_K = -\frac{K}{a^2 \mathcal{H}^2}$, one sees that an exponential growth of scale factor a (with a near constant $\mathcal{H}$) can dynamically evolve an initial $\Omega_K \sim \mathcal{O}(1)$ to be as small as observed today cf. Eq. (2.16). In other words, no initial fine tuning is needed if there is an inflationary epoch after the Big Bang.

- *Origin of initial inhomogeneity from inflaton.*

  Assuming inflation is driven by some fundamental field, the inflaton field ϕ. The quantum nature of ϕ and uncertainty principle leave a fluctuated field: $\phi = \bar{\phi} + \delta\phi$ with $\bar{\phi}$ denoting the background; the fluctuation $\delta\phi$ can source the inhomogeneities for CMB and act as initial seeds for large scale structure formation.

- *Monopole problem* revisited.

  Due to the exponential expansion, the density of the monopoles can be significantly diluted so that they are too rare to be observed today.

Having shown the power of cosmic inflation to resolve problems in the standard cosmology, we now turn to investigate the conditions for and dynamics of inflation. Inflation corresponds to an accelerated period of expansion with $\ddot{a} > 0$, which implies (cf. Eq. (2.11)) that the condition for inflation is:

$$(\rho + 3p) < 0 \Leftrightarrow p < -\frac{1}{3}\rho \Leftrightarrow \omega < -\frac{1}{3}. \tag{2.17}$$

On the other hand, one can write

$$\frac{\ddot{a}}{a} = -\frac{1}{6}(\rho + 3p) = \mathcal{H}^2(1 - \epsilon_H), \tag{2.18}$$

with

$$\epsilon_H \equiv \frac{3}{2}(\omega + 1) = -\frac{\dot{\mathcal{H}}}{\mathcal{H}^2} = \frac{1}{2}\left(\frac{\dot{\phi}}{\mathcal{H}}\right)^2, \tag{2.19}$$

denoting the Hubble slow-roll parameter [20]. Thereafter $\epsilon_H < 1$ also denotes the condition for inflation being equivalent to $\omega < -\frac{1}{3}$.

The dynamics of inflation is governed by a slow rolling inflaton field ϕ, minimally coupled to gravity. The action of this model is given by

$$S = \int d^4x \sqrt{-g} \left[\frac{1}{2}R + \frac{1}{2}g^{\mu\nu}\partial_\mu\phi\partial_\nu\phi - V(\phi) \right],$$
(2.20)

where $g_{\mu\nu} = \text{diag}\left(1, -a^2, -a^2, -a^2\right)$ denoting the spatial flat metric. Using the Euler-Lagrange equation, one has the equation of motion for (background) ϕ

$$\ddot{\phi} + 3\mathcal{H}\dot{\phi} + \frac{dV}{d\phi} = 0.$$
(2.21)

Using Eq. (2.2), one can write down the energy momentum tensor $T_{\mu\nu}$, with which one can obtain the energy density $\rho_\phi \equiv T_0^0$ and pressure $p_\phi \equiv -\sum_i T_i^i/3$:

$$\rho_\phi = \frac{1}{2}\dot{\phi}^2 + V(\phi); \quad p_\phi = \frac{1}{2}\dot{\phi}^2 - V(\phi).$$
(2.22)

The equation of state is then given by

$$\omega_\phi = \frac{p_\phi}{\rho_\phi} = \frac{\frac{1}{2}\dot{\phi}^2 - V(\phi)}{\frac{1}{2}\dot{\phi}^2 + V(\phi)}.$$
(2.23)

Thereafter if the potential energy dominates over the kinetic energy, one has $\omega_\phi \sim -1 < -\frac{1}{3}$, satisfying the aforementioned condition for inflation. This is usually quoted as slow-roll inflation, where ϕ slowly rolls down from a flat potential. Except the slow-roll parameter ϵ_H we have introduced in Eq. (2.19), a second slow-roll parameter is also needed:

$$\eta_H = -\frac{\ddot{\phi}}{\mathcal{H}\dot{\phi}}.$$
(2.24)

A small η_H is needed in order to ensure the accelerated term is small (hence small kinetic energy.) Thereafter the (sufficient) conditions for a slow-roll inflationary phase are $\epsilon_H, \eta_H \ll 1$. These conditions can be guaranteed if the the inflaton potential $V(\phi)$ is flat enough with the potential slow-roll parameters $\epsilon_V = 1/2(V'/V)^2$ and $\eta_V = V''/V$ being small. Note that slow-roll inflation ends when $\text{Max}\{\epsilon_V, \eta_V\} = 1$.

Quantum fluctuation of the inflaton field $\delta\phi$ leads to fluctuations of both matter distribution as well as geometry (metric) of the Universe, thus leaving some imprints in the CMB photons. From the CMB power spectrum, one is then able to extract information about the inflaton dynamics as well as the shape of the potential. Having shown the conditions as well as dynamics of inflation, we are now trying to investigate the possible candidate(s) for the inflaton field. Let's first look at the most simple inflationary scenario and then check if there is any candidate in the SM of particle physics.

2.3.3 Monomial Inflation and Current Status

The most simple inflationary model is the monomial chaotic scenario [21], where the potential admits a form $V \sim \phi^p$. The directives are $V' = p\phi^{p-1}, V'' = p(p-1)\phi^{p-2}$. Thereafter the potential slow-roll

parameters are $\epsilon_V = p^2/(2\phi^2)$ and $\eta_V = p(p-1)/\phi^2$. Note that $\epsilon_V \geq |\eta_V|$ for $2/3 \leq p \leq 2$. One can compute the number of e-folds that the Universe has expanded from the point when the pivot scale $k_\star = 0.05\ \mathrm{Mpc}^{-1}$ crossed out of the horizon (when $\phi = \phi_{\mathrm{CMB}}$) to the end of inflation [20]:

$$N = \int_{\phi_{\mathrm{CMB}}}^{\phi_{\mathrm{end}}} \frac{1}{\sqrt{2\epsilon_V}} d\phi = \frac{1}{p} \int_{\phi_{\mathrm{CMB}}}^{\phi_{\mathrm{end}}} \phi\, d\phi = \frac{1}{2p} \left(\phi_{\mathrm{CMB}}^2 - \phi_{\mathrm{end}}^2 \right) \simeq \frac{\phi_{\mathrm{CMB}}^2}{2p} . \tag{2.25}$$

where $\phi_{\mathrm{CMB}} \gg \phi_{\mathrm{end}}$ has been assumed[1]. As mentioned earlier fluctuation of inflaton leads to perturbations of metric, hence generation of gravitational waves, whose amplitude is usually quantified as the so-called tensor-to-scalar ratio r. During slow-roll inflation, $r = 16\epsilon_v$ [20]. Thereafter for monomial scenario

$$r = \frac{8\,p^2}{\phi_{\mathrm{CMB}}^2} \approx \frac{4p}{N} . \tag{2.26}$$

Considering a typical $N \simeq 60$ and the latest bound $r < 0.035$ from latest CMB experiments [22], we are then able to conclude that only models $p < 1/2$ are not excluded. Potential with such a small (fraction) power is usually not easy to realize in particle physics. As shown in the next section, no such candidate in the SM of particle physics.

2.4 Standard Model of Particle Physics

The SM of particle physics is the building block of physics at microscopic scale, which is based on quantum field theory (QFT)–a combination of quantum mechanics and special relativity [24]. In QFT, every particle is described by a field that pervades space-time; the dynamics and kinematics of the field are controlled by the Lagrangian. And the construction of SM is then to write down the most general renormalizable Lagrangian obeying some symmetries. In SM, these symmetries are the local $SU(3) \times SU(2) \times U(1)$ gauge symmetry, and a global Poincaré symmetry. Particle content of the SM is shown in Fig. 2.1, consisting of three generations of quarks/leptons, force carriers and Higgs boson (which sources masses via the Higgs mechanism). Regarding a possible candidate for inflaton field, the only known scalar field in the SM is the Higgs boson, admitting a potential of form

$$V(H) \supset \lambda_H (H^\dagger H)^2 , \tag{2.27}$$

which is similar to a ϕ^4 chaotic model and has been ruled out since it is too steep to satisfy the current experimental bound on tensor-to-scalar ratio. In literature, it has been shown that the SM Higgs potential could be flattened with the help of non-minimal coupling to Ricci scalar $\xi R H^\dagger H$, thus making Higgs a possible candidate for inflaton. However it turns out that in order to be consistent with CMB experiments, a rather large coupling ξ is needed, leading to issues of unitarity violation. See Ref. [25] for a recent review regarding Higgs inflation.

In this thesis we will investigate some alternatives, in particular we will consider some fundamental scalar field beyond the SM acting as the inflaton. See Chapter 3 for more details, where we will show that a simple and well motivated polynomial inflationary scenario can match the current CMB

---

[1] We will confirm this assumption in Sec. 7.1.2 with more details.

Standard Model of Elementary Particles

	three generations of matter (fermions)			interactions / force carriers (bosons)	
	I	II	III		
mass charge spin	≈2.2 MeV/c² ⅔ ½ **u** **up**	≈1.28 GeV/c² ⅔ ½ **c** **charm**	≈173.1 GeV/c² ⅔ ½ **t** **top**	0 0 1 **g** **gluon**	≈124.97 GeV/c² 0 0 **H** **higgs**
	≈4.7 MeV/c² −⅓ ½ **d** **down**	≈96 MeV/c² −⅓ ½ **s** **strange**	≈4.18 GeV/c² −⅓ ½ **b** **bottom**	0 0 1 **γ** **photon**	
	≈0.511 MeV/c² −1 ½ **e** **electron**	≈105.66 MeV/c² −1 ½ **μ** **muon**	≈1.7768 GeV/c² −1 ½ **τ** **tau**	≈91.19 GeV/c² 0 1 **Z** **Z boson**	
	<1.0 eV/c² 0 ½ **νe** **electron neutrino**	<0.17 MeV/c² 0 ½ **νμ** **muon neutrino**	<18.2 MeV/c² 0 ½ **ντ** **tau neutrino**	≈80.39 GeV/c² ±1 1 **W** **W boson**	

QUARKS (rows 1–2, left), **LEPTONS** (rows 3–4, left), **GAUGE BOSONS / VECTOR BOSONS**, **SCALAR BOSONS**

Figure 2.1: Particle content of the standard model [23].

experiments well.

2.5 Dark Matter

In this section, we present several compelling experimental results to hint the existence of non-baryonic DM.

2.5.1 Experimental Hints for the existence of DM

- Galactic rotation curves.

  Assuming a spherical symmetry of a galaxy with radius R_0, its mass $M(R) \propto R^3$ if $R \leq R_0$ and $M(R) \propto R_0^3$ if $R \geq R_0$. Using Newton's (third) law of motion

  $$\frac{1}{2}m\frac{v^2}{R} = \frac{G\,M(R)\,m}{R^2}\,,\tag{2.28}$$

  one finds that for bodies with mass m and a radius R far from the centre of galaxy admitting a
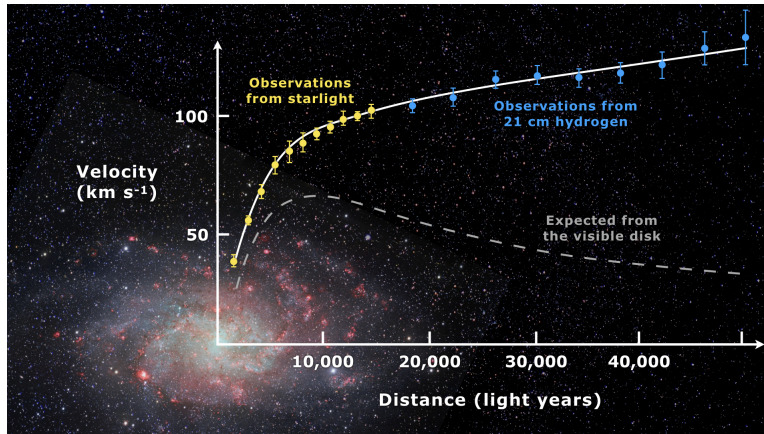
Figure 2.2: Rotation curve of galaxy Messier 33 [26, 27].

circular velocity

$$v(R) \propto \sqrt{\frac{G\,M(R)}{R}}\,. \tag{2.29}$$

It is then expected that in the regime $R > R_0$, $v(R)$ shall decrease as $1/\sqrt{R}$, however observation implies that $v(R)$ increases as shown in Fig. 2.2. The dashed line corresponds to the expected rotation curve taking the visible matter in the stellar disc into account. However the data clearly shows that some dark components are needed. In particular, extra mass from some dark component with a distribution $M(R) \propto R^{\alpha}$ (with $\alpha > 1$) is needed in order to explain the observation.

- Bullet cluster.

  Cluster of galaxies is a structure that consists of hundreds to thousands of galaxies that are gravitationally bound together, in which DM account for about 90% of the total mass, the intergalactic gas (consist of ionized hydrogen and helium) makes 9%, and the rest is stars bounded within the galaxies [28]. When two clusters collide with each other, the hot gases interact with each other electromagnetically, causing them to slow down. However, DM particles which interact very weakly with each other, would pass through each other. In Fig. 2.3, the green lines correspond to the gravitational lensing of the matter (mainly DM) distribution of the two clusters. The red and bright yellow regions correspond to the colliding hot gas (seen via X-ray). If clusters are primarily made from baryonic matter, most of them shall not be so far away from the hot gases after colliding. Fig. 2.3 clearly implies the existence of DM.

- Fitted from CMB.

  In Fig. 2.4, we depict the temperature temperature power spectrum with varying DM density. This figure was generated by using the program CAMB [30, 31]. The solid curve with $\Omega_c h^2 = 0.12$ corresponds to the best fitted value for Planck 2018 data. There we fix $\Omega_b h^2 = 0.00224$ and allow $\Omega_b h^2$ to vary. One can see that increasing DM densities leads to a reduction of peaks as shown in Fig. 2.4. Clearly DM is needed in order to explain the CMB data.
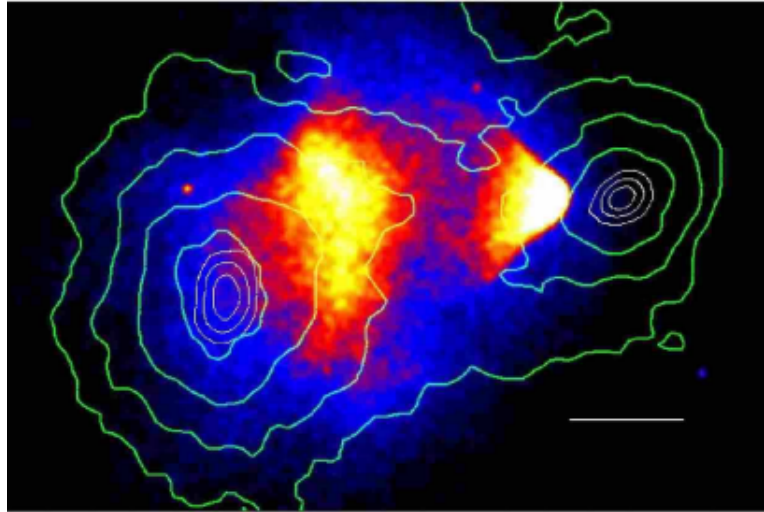
Figure 2.3: Image of the merging cluster 1E0657-558 [29].

Having shown the evidence for the existence of DM, we now list several possible DM candidates considered in literature.

2.5.2 Models of Dark Matter

Candidates for DM [32]:

- *i*) have to be cold i.e. non-relativistic in order to allow structure to form;

- *ii*) must be stable on cosmological time scales;

- *iii*) must interact very weakly with electromagnetic radiation.

Possible candidates widely considered in literature include particles e.g. weakly interacting massive particles (WIMPs) [33], feebly interacting massive particles (FIMP) [34], axions [35], sterile (gauge singlet) neutrinos [36], and non-particle objects like Primordial Black Holes (PBHs) [37][2]. For PBHs, the most simple scenario corresponds to gravitational collapse of large density perturbations, generatre during inflation. However usually a fine tuning (on shape of the inflaton potential) is needed to generate sufficient large perturbations. See Ref. [37] for a review regarding recent development on PBHs as DM, and Ref. [38] for a comprehensive review on DM from historical perspective.

In this thesis, we will assume a simple particle DM scenario, where DM is a gauge singlet field [39–44]. We will show that a correct DM relic density can be sourced during reheating after polynomial inflation. More details can be found in Chapter 5.

---

[2] It is called "Primordial" in the sense that the time scale for formation of those Black Holes has to be earlier than Big Bang Nucleosynthesis [32].
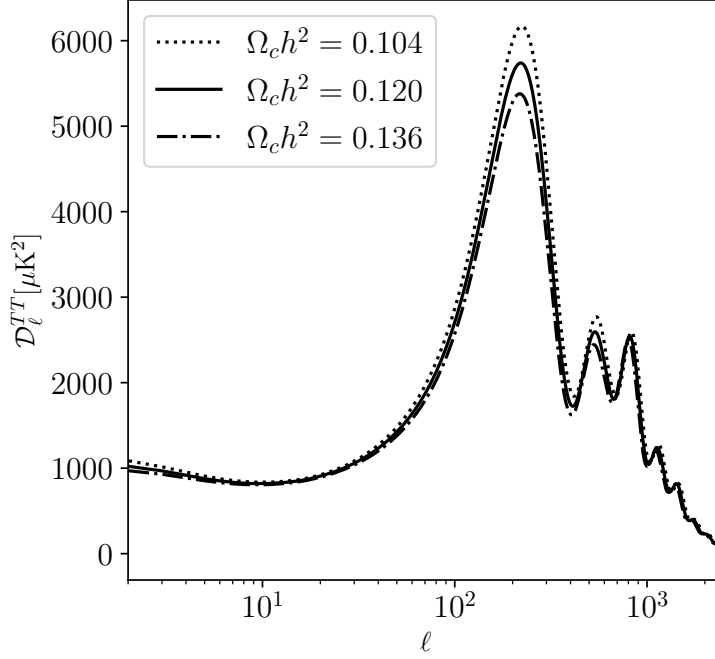
Figure 2.4: Temperature temperature power spectrum with varying DM density.

2.6 Neutrino Oscillations and Masses

The phenomena that neutrinos can oscillate from one flavor to another have been convincingly verified, indicating that there is a mismatch between the mass eigenstate $\nu_i = (\nu_1, \nu_2, \nu_3)$ and flavor eigenstate $\nu_\alpha = (\nu_e, \nu_\mu, \nu_\tau)$ and that neutrinos have tiny masses [45]. Such mismatch is quantified as the so-called Pontecorvo-Maki-Nakagawa-Sakata (PMNS) matrix U, which appears in the weak charged-current [46]:

$$\mathcal{L}_{cc} = -\frac{g}{\sqrt{2}} U^{\alpha i} \left(\bar{e}_{L\,\alpha} \displaystyle{\not}W \nu_{L\,i} + \text{h.c.} \right) , \qquad (2.30)$$

where $\displaystyle{\not}W \equiv \gamma^\mu W_\mu^-$ and $\nu_{L\,\alpha} = U^{\alpha i} \nu_{L\,i}$ or in a more explicit matrix form:

$$\begin{pmatrix} \nu_e \\ \nu_\mu \\ \nu_\tau \end{pmatrix}_L = U \begin{pmatrix} \nu_1 \\ \nu_2 \\ \nu_3 \end{pmatrix}_L = \begin{pmatrix} U_{e1} & U_{e2} & U_{e3} \\ U_{\mu1} & U_{\mu2} & U_{\mu3} \\ U_{\tau1} & U_{\tau2} & U_{\tau3} \end{pmatrix} \begin{pmatrix} \nu_1 \\ \nu_2 \\ \nu_3 \end{pmatrix}_L . \qquad (2.31)$$

The PMNS matrix in general can be parametrized as

$$U = \begin{pmatrix} c_{12}c_{13} & s_{12}c_{13} & s_{13}e^{-i\delta} \\ -s_{12}c_{23} - c_{12}s_{13}s_{23}e^{i\delta} & c_{12}c_{23} - s_{12}s_{13}s_{23}e^{i\delta} & c_{13}s_{23} \\ s_{12}s_{23} - c_{12}s_{13}c_{23}e^{i\delta} & -c_{12}s_{23} - s_{12}s_{13}c_{23}e^{i\delta} & c_{13}c_{23} \end{pmatrix} \begin{pmatrix} 1 & & \\ & e^{i\rho} & \\ & & e^{i\sigma} \end{pmatrix}, \qquad (2.32)$$

with mixing angles $c_{ij} \equiv \cos\theta_{ij}$, $s_{ij} \equiv \sin\theta_{ij}$, one Dirac phase δ and two Majorana phases[3] ρ, σ. For the three flavor oscillations, it is governed by 6 independent parameters, namely three mixing angle θ_{12} θ_{13} θ_{23}, a Dirac CP phase δ and two distinctive neutrino mass-squared differences $m_{21}^2 \equiv m_2^2 - m_1^2$ and $m_{31}^2 \equiv m_3^2 - m_1^2$ (or $\equiv m_{32}^2 \equiv m_3^2 - m_2^2$). In this thesis we will focus on the most simple case with $m_1 = 0$ assume $m_1 < m_2 < m_3$. We consider the best fit from Ref. [47]:

$$m_2 = \sqrt{\Delta m_\odot^2} = (8.6 \pm 0.1) \times 10^{-3}\,\text{eV}\,, m_3 = \sqrt{\Delta m_{\text{atm}}^2} = (5.02 \pm 0.03) \times 10^{-2}\,\text{eV}\,. \tag{2.33}$$

and $31.6° < \theta_{12} < 36.3°$, $40.9° < \theta_{23} < 52.2°$ $8.22° < \theta_{13} < 8.98°$ and $135° < \delta < 366°$ at 3σ.

2.6.1 Models for Neutrino Masses

Similar to how the masses for the charged leptons are generated, one could introduce (gauge singlet) right handed neutrino N:

$$\mathcal{L}_{\text{mass}} = -Y_\nu \bar{L}\tilde{H}N + \text{h.c.}\,, \tag{2.34}$$

where $\tilde{H} \equiv i\sigma_2 H^\star$. After electroweak symmetry breaking, it gives rise to a Dirac mass term:

$$M_D = Y_\nu\,\text{v}\,. \tag{2.35}$$

Here v = 174 GeV denotes the Higgs vev. Considering the neutrino mass $m < 0.1$ eV (cf. Eq. (2.33)), one finds that the Yukawa coupling $Y_\nu < O(10^{-12})$, which is several magnitudes smaller than other lepton Yukawa couplings. (See e.g. in the SM, the electron Yukawa coupling is $Y_e \simeq 3 \times 10^{-6}$.) Now one may ask why Y_ν is so small compared to other Yukawa couplings?

Another scenario is the so-called Majorana mass term, which can be generated via Weinberg dim-5 oprerator [48]

$$\mathcal{L}_{\text{dim-5}} = -\frac{1}{2}\frac{y_{ij}}{\mathcal{E}}\left(\bar{L}^i\tilde{H}\right)\left(\tilde{H}\,L^j\right)^\dagger\,, \tag{2.36}$$

where $\mathcal{E}$ denotes an energy scale above which the operator breaks down, and one shall invoke a theory with some new degree of freedom. After electroweak symmetry, the operator Eq. (2.36) gives rise to a Majorana mass term:

$$M_M = \frac{y\,\text{v}^2}{\mathcal{E}}\,. \tag{2.37}$$

Considering coupling $y \sim O(0.1)$, one has then $\mathcal{E} \gtrsim 10^{13}$ GeV is needed in order to generate a small neutrino mass $m < 0.1$ eV.

2.6.2 See-Saw Mechanism

Indeed, by extending the SM with a heavy singlet right-handed neutrino N, the operator shown in Eq. (2.36) can naturally appear (once integrating out N). Introducing a basis (ν, N), and the full mass

---

[3] The Majorana phase plays no role in neutrino oscillations and in relevant for neutrinoless double-beta decay.

matrix can be written as:

$$\mathcal{M} = \begin{pmatrix} 0 & M_D^T \\ M_D & M_N \end{pmatrix}, \tag{2.38}$$

where M_N denotes the mass for N. After diagonalization, it yields a light neutrino mass as [49]

$$m_\nu = -M_D^T M_N^{-1} M_D. \tag{2.39}$$

Note that the larger M_N is, the smaller m_ν would be; such a mechanism is called Type-I See-Saw Mechanism, which is the most simple theory to account for the tiny Neutrino mass. We will come back to this in Chapter 6.

2.7 Baryogenesis

Particle and antiparticle have the same mass, and it is expected that equal numbers of baryons and antibaryons shall have been generated in the early Universe. However observation implies that current Universe contains mostly matter and no ambient antimatter [13]:

$$\eta_B = \frac{n_B}{n_\gamma} = \frac{n_b - n_{\bar{b}}}{n_\gamma} \simeq 6 \times 10^{-10}, \tag{2.40}$$

where n_B is the baryonic number density [45]

$$n_B = \frac{\rho_B}{m_B} = \frac{\Omega_B \rho_c}{m_B} = 1.05 \times 10^{-5} \Omega_B h^2 \text{ cm}^{-3} \tag{2.41}$$

and n_γ denotes the photon number density, and is given by[4]

$$n_\gamma = \frac{2\,\zeta(3)}{\pi^2} T_0^3 = 410.7 \left(\frac{T_0}{2.7255\,K}\right)^3 \text{ cm}^{-3}. \tag{2.42}$$

This asymmetry can not be explained in standard cosmology and shall have been generated via some dynamical mechanisms.

In this section we first present the essential conditions for Baryogenesis. Then we will revisit a simple and attractive scenario, namely leptogenesis which could resolve Baryogenesis and (light) neutrino masses simultaneously.

2.7.1 Sakharov Conditions

There are three necessary conditions for baryogenesis, including [50]

1. Baryons number violation;

2. C (charge conjugation symmetry) and CP (the product of charge conjugation and parity) violation;

---

[4] For a spatial size of one Sugar Cube, there are roughly 400 CMB photons; these photons have travelled roughly 13.8 billion years!

3. Departure from thermal equilibrium.

Apparently it has to be involved with the baryon number violation process $i \rightarrow f$ (with initial baryon number not equal to the final states, namely $B(i) \neq B(f)$). Violation of charge conjugation symmetry is required, otherwise the conjugated process $\bar{i} \rightarrow \bar{f}$ would totally cancel out the generated baryons. CP violation has to be present since if CP is invariant, which is equivalent to time-invariance, and leads to a process $i(\mathbf{r}_i, \mathbf{p}_i, \mathbf{s}_i) \rightarrow f(\mathbf{r}_j, \mathbf{p}_j, \mathbf{s}_j)$ being the same as $f(\mathbf{r}_j, -\mathbf{p}_j, -\mathbf{s}_j) \rightarrow i(\mathbf{r}_i, -\mathbf{p}_i, -\mathbf{s}_i)$. Thereafter though it is possible to generate some net baryons in a certain region of the phase space, but integrating over all momenta $\mathbf{p}$ and summing over all spins $\mathbf{s}$ would still generate a vanishing baryon asymmetry [51]. Finally an out of equilibrium process is needed, since otherwise the inverse process $f \rightarrow i$ would totally washout the generated baryons.

2.7.2 Baryon and Lepton Conversion

Baryon and Lepton numbers are global (accidental) symmetry (in the SM), which is preserved at classical level, but anomalous at quantum level. In electroweak theory, the anomalous current is [46]:

$$\partial_\mu J_B^\mu = \partial_\mu J_L^\mu = N_f \frac{g^2}{32\pi^2} \epsilon^{\mu\nu\alpha\beta} W_{\mu\nu}^a W_{\alpha\beta}^a , \tag{2.43}$$

where $W_{\mu\nu}^a$ is the SU(2) field strength tensor and N_f the number of generations (being 3 in the SM). Note that $B - L$ is still conserved, however B, L and $B + L$ are not. By integrating the anomalous current Eq. (2.43), one can deduce the corresponding change of B and L quantum numbers [52]:

$$\Delta B = \Delta L = \int d^4 x \, \partial_\mu J_B^\mu = \int d^4 x \, N_f \frac{g^2}{32\pi^2} \epsilon^{\mu\nu\alpha\beta} W_{\mu\nu}^a W_{\alpha\beta}^a \equiv N_f \Delta N_{\text{CS}} , \tag{2.44}$$

where $\Delta N_{\text{CS}} = \pm 1 \pm 2 \ldots$ denotes the change of Chern-Simons number. Thereafter in the SM, transition from one EW vacuum to the other via the so-called sphaleron process, leading to a violation of baryon/lepton number in a unit of $\Delta B = \Delta L = \pm 3 \pm 6 \ldots$ Hence it is possible to mediate lepton numbers into baryon numbers via sphalerons. In particular for a thermal equilibrium environment with some nonzero $(B - L)$, both baryon and lepton numbers would not vanish

$$B = C(B - L) ; \qquad L = (C - 1)(B - L) , \tag{2.45}$$

with

$$C = \frac{8N_f + 4N_H}{22N_f + 13} . \tag{2.46}$$

In the SM, $N_f = 3$ and $N_H = 1$ denoting the number of fermion generations and Higgs doublets, so $C = \frac{28}{79}$. At low temperature, the transition from one vacuum to another is suppressed due to the sphaleron energy barriers between vacuum states. However when the temperature is sizable enough $T \gtrsim 100$ GeV, the transition is very efficient [52]. In the next section we will introduce a mechanism, namely leptogenesis, to generate some nonzero $(B - L)$ numbers at high temperatures in the early Universe.
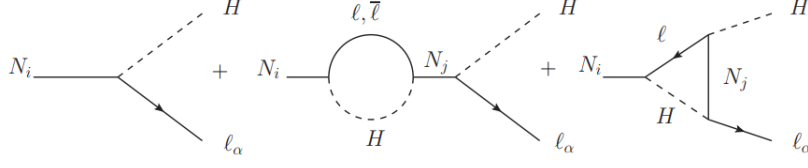
Figure 2.5: Feynman diagram for decay of RHN N_i [54].

2.7.3 Leptogenesis

A simple and attractive scenario for Baryogenesis is Leptogenesis [53], which can also resolve light neutrino mass via Type-I see-saw. The model can be described by the following Lagrangian,

$$\mathcal{L}_N \supset - \left(\frac{1}{2} M_N \overline{N_i^c} N_i + h.c. \right) - \left(Y_{\alpha i} \, \bar{\ell}_\alpha \tilde{H} N_i + h.c. \right) , \tag{2.47}$$

where M_N denotes mass for right-handed neutrinos (RHNs), violating lepton numbers by two. Thereafter the first Sakharov condition is satisfied. Due to the complex nature of the Yukawa coupling, it turns out that the interference between the tree and loop diagrams (see Fig. 2.5) leads to a CP asymmetry parameter. For a fixed lepton species α, this CP asymmetry parameter is quantified as the difference of the decay rate γ between $N_i \to \ell_\alpha H$ and its conjugated, given by [54]

$$\epsilon_{i\alpha} = \frac{\gamma \left(N_i \to \ell_\alpha H \right) - \gamma \left(N_i \to \overline{\ell_\alpha} H^* \right)}{\sum_\alpha \gamma \left(N_i \to \ell_\alpha H \right) + \gamma \left(N_i \to \overline{\ell_\alpha} H^* \right)} . \tag{2.48}$$

Summing over the lepton famlies, one has

$$\epsilon_i \equiv \sum_\alpha \epsilon_{i\alpha} = \frac{1}{8\pi} \frac{1}{\left(Y^\dagger Y \right)_{ii}} \sum_{j \neq i} \mathrm{Im} \left[\left(Y^\dagger Y \right)_{ji}^2 \right] g \left(\frac{M_j^2}{M_i^2} \right) , \tag{2.49}$$

with the Loop function given by

$$g(z) = \sqrt{z} \left[\frac{1}{1-z} + 1 - (1+z) \ln \left(\frac{1+z}{z} \right) \right]$$

$$\simeq -\frac{3}{2} \left(\frac{1}{z} \right)^{1/2} - \frac{5}{6} \left(\frac{1}{z} \right)^{3/2} + O \left(\frac{1}{z} \right)^{5/2} \quad \text{for} \quad z \gg 1 . \tag{2.50}$$

In this thesis we will focus on the most simple case with $i = 1, 2, 3$, and assume $M_3 \gg M_2 \gg M_1$ such that only N_1 can be generated, thereafter only ϵ_1 is of interest here. Note that ϵ_1 is not zero due to complex nature of Yukawa coupling matrix Y, in particular the term $\left(Y^\dagger Y \right)_{21}^2$ in Eq. (2.49). This satisfies the second Sakharov condition. Because of the expansion of the Universe, the decay of N_1 would be out of equilibrium once the expansion rate is larger than the interaction rate between N_1 and the thermal plasma, hence satisfying the third Sakharov condition. Thereafter we see that by

extending the SM with RHNs, all the three Sakharov conditions can be satisfied. As one might guess, the generated net lepton numbers would be quantified by three key factors, namely the CP asymmetry parameter ϵ_1; the density of N_1 in the equilibrium and how much deviation of the decay is out of the equilibrium (this is usually quantified as the efficiency factor κ_f). We will present more details in Chapter 6 and Appendix B.

2.8 Summary

In this chapter, we briefly revisited the theoretical background knowledge for this thesis. We listed the problems in the standard cosmology and argued that cosmic inflation can elegantly resolve them. We investigated the conditions for inflation as well as its phenomenology. We showed that the simple monomial inflationary scenarios with $V \sim \phi^p$ have been ruled out except for $p < 1/2$, which is not easy to realize in particle physics. In the SM of particle physics, there is no such inflaton candidate, appealing to an extension of it. We gave several compelling experimental evidence to argue the existence of non-baryonic DM. In order to resolve the DM problem, one needs to introduce a new degree(s) of freedom beyond the SM. We revisited the see-saw mechanism for light neutrino masses as well as conditions for Baryogenesis. We showed that by extending the SM with RHNs, one could resolve neutrino masses and Baryogenesis (via leptogenesis) simultaneously.

Based on these empirical facts, we proposed a minimal and simple extension of the SM of particle physics, as shown in (1.3). In the following chapters, we are devoted to demonstrating that this model can account for inflation, reheating, DM production, neutrino masses as well as Baryogenesis.

Small Field Polynomial Inflation

As aforementioned, inflationary theory can neatly resolve the horizon, flatness and monopole problems of standard cosmology [21, 55–57]. And the simplest inflation scenario invokes a single elementary scalar "inflaton" field ϕ to drive slow–roll (SR) inflation, with a monomial $\lambda\phi^p$ potential. At sufficiently large field values, this also allows eternal inflation, where the inflaton field undergoes random walk [58, 59]. However the recent BICEP/Keck 2018 results [22] have disfavored those models with $p \gtrsim 1/2$: these potentials are too steep and therefore predict too large a tensor–to–scalar ratio r. (See the discussion in Sec. 2.3.3). Consistence with these observations can be obtained for smaller values of p, which however are not easy to realize in complete particle physics models. We refer to ref. [60] for a review for inflationary modes.

In this Chapter, we will consider the most general renormalizable single–field model, where the potential is a polynomial of degree four [61–65]. We assume that the density perturbations observed in the CMB and other cosmological probes were generated when the inflaton field had values not larger than the Planck scale, so that the energy scale during inflation is far below the Planck scale; thereafter imposing renormalizability is reasonable. Then a polynomial potential of degree four would be the most general inflaton potential once considering the inflaton field to be a sector in some UV complete theory. Note that the linear term can be removed via a shift of the inflaton field and the cosmological constant term is at most of the order of today's cosmological constant, which is essentially zero compared to the energy scales during inflation, the potential only contains three terms. We will see that all three terms, namely ϕ^2, ϕ^3, ϕ^4, are needed in order to reproduce the CMB measurements by the Planck collaboration where the potential shall be flat enough in order to satisfy the bound on tensor-to-scalar ratio. In our case here the potential is sufficiently flat only if it features a (near) inflection point where both the first and the second derivative of the potential are very small. We note that such an inflection point might arise from radiative corrections [66–75], but here we allow it at the tree level.

In literature models feature an inflection point of the potential have been discussed in a supersymmetric context, often using non–renormalizable potentials or only analyzing the motion of the field around the inflection point; see e.g. Refs. [76–82]. Note that our polynomial inflation model does allow for eternal inflationary epoch, at much larger (trans–Planckian) field values but still sub–Planckian energy densities. With an early phase of "eternal" inflation, one can alleviate the initial condition problems for inflation. Eternal inflation can also help to populate a "landscape", i.e. a (complicated) potential with a very large number of minima [83]. For reviews on eternal inflation, see e.g. Refs. [84, 85]. We

will turn back to discussion on eternal inflation soon.

Our goal here is to study the non–supersymmetric small field polynomial inflation model. In particular we are devoted to exploring the entire allowed parameter space in a complete model, including couplings that allows the inflaton to decay and transfer energy. This is required so that the Universe can be reheated after inflation and then enters a radiation epoch. We will analytically compute number of e–folds and inflationary predictions, including power spectrum, tensor–to–scalar ratio, spectral index and its running. Once the power spectrum and the spectral index have been fixed, essentially only the location ϕ_0 of the near–inflection point remains as a free parameter.

As will be shown in chapter 4, ϕ_0 has to be bounded from below by the requirement that the reheating temperature is sufficiently high [86, 87], with inflaton couplings that are sufficiently small not to jeopardize the flatness of the potential through radiative corrections. This leads to ϕ_0 has to be larger than $3 \cdot 10^{-5}$ (in Planckian units). The tensor–to–scalar ratio within the parameter space is much too small to be detectable in the near future. But the running of the spectral index turns out to be independent of ϕ_0, which might be detectable in future precision measurements. Within the allowed parameter space, we find the inflationary scale can be as low as $H_{\mathrm{inf}} \sim 1$ MeV; such a low inflationary energy scale might help to embed the QCD axion as dark matter with a wider cosmologically allowed window, i.e. larger decay constant f_a than is usually considered [88, 89], and could also greatly alleviate the cosmological moduli problem [90]. On the other hand, for larger values of ϕ_0 the reheating temperature can exceed 10^{10} GeV, thus allowing standard thermal leptogenesis [53, 91]; however, this requires an inflationary Hubble parameter of order 10^9 GeV (which might bring the moduli problem back). We will explore leptogenesis in Chapter 6 in detail; in particular we will discuss a non-thermal channel for leptogenesis with much lower reheating temperature, with which the moduli problem could potentially be relaxed.

The primary aim of this Chapter is to investigate the SR predictions for small field polynomial inflation. The full parameter space based on reheating constraints and radiative conditions will be explored in Chapter 4. The rest of this Chapter is organized as follows. In Sec. 3.1 we offer a complete analytical description for our model. Then in Sec. 3.2 the model parameters as well as predictions of observables are presented. Finally, we summarize our results in Sec. 3.3. This chapter is based on Ref. [2].

3.1 The Setup

In this Section we first introduce our potential, with focus on small field values, $\phi_0 \leq 1$ in Planckian units. We will show that CMB observables can be fitted only in the presence of a very flat region, which requires that the potential almost possesses a saddle point at ϕ_0.

3.1.1 The Potential

A general potential for a single real scalar inflaton ϕ respecting renormalizability contains terms $\propto \phi^n$ with $n \in \{0, 1, 2, 3, 4\}$. Here, the linear term can be absorbed by shifting the field, such that the potential minimizes at origin, namely $\phi = 0$. One can also neglect the cosmological constant term, which is small compared to the inflaton energy density during inflation. This leads to a potential of a form

$$V(\phi) = b\,\phi^2 + c\,\phi^3 + d\,\phi^4 \,. \tag{3.1}$$

Note that we require $d > 0$ is needed in order to guarantee the potential to be bounded from beloW; the origin at $\phi = 0$ is the absolute minimum of the potential if $b > 0$. Since the potential is symmetric under the transformation $c \rightarrow -c$, $\phi \rightarrow -\phi$, one take $c \leq 0$ without loss of generality. If not specified, throughout this chapter we work in Planckian units, where we set the reduced Planck mass $M_P \simeq 2.4 \cdot 10^{18}$ GeV to be unity.

Derivatives of the potential Eq. (3.1) are:

$$V'(\phi) = 2b\phi + 3c\phi^2 + 4d\phi^3 \; ;$$
$$V''(\phi) = 2b + 6c\phi + 12d\phi^2 \; . \tag{3.2}$$

One has a true saddle point with $V'(\phi_0) = V''(\phi_0) = 0$ at

$$\phi_0 = -\frac{3c}{8d} \, , \tag{3.3}$$

if the model parameters satisfy the relation

$$b = \frac{9c^2}{32d} \, . \tag{3.4}$$

In general the parameters will not obey Eq. (3.4), which could however help to reparametrize the potential Eq. (3.1). Here we allow the cubic term to deviate from this relation Eq. (3.4) by a factor $1 - \beta$, leading to

$$\begin{aligned} V(\phi) &= d \left[\phi^4 + \frac{c}{d} (1 - \beta) \phi^3 + \frac{9}{32} \left(\frac{c}{d} \right)^2 \phi^2 \right] \\ &= d \left[\phi^4 + A (1 - \beta) \phi^3 + \frac{9}{32} A^2 \phi^2 \right] \, , \end{aligned} \tag{3.5}$$

where we have introduced the quantity

$$A = -\frac{8}{3} \phi_0 \, , \tag{3.6}$$

controlling the location of the (near) inflection point.

As mentioned in the Introduction, for small field values ($\phi \leq 1$) inflation can occur only if the potential indeed "almost" has a saddle point, i.e. β has to be small. This can be seen as follows. As well already discussed in Sec. 2.3.2, SR inflation requires the parameters $\epsilon_V = 1/2(V'/V)^2$ and $\eta_V = V''/V$ to be small [92]. For the potential Eq. (3.1), we find

$$\epsilon_V = \frac{8}{\phi^2} f(\phi) \; ;$$
$$\eta_V = \frac{12}{\phi^2} g(\phi) \, . \tag{3.7}$$

Here the functions f and g approach 1 for $\phi \gg |A|$; in the opposite limit, $\phi \ll |A|$, we have $f(\phi) \rightarrow 1/4$, $g(\phi) \rightarrow 1/6$. "Generically" these functions will therefore be of order unity, or slightly below. The detailed forms for the functions f and g will be presented in Chapter 7. Clearly SR

inflation would then require $\phi \gg 1$, i.e. large field values. Here we are interested in small–field inflation, $\phi \lesssim 1$. Since $f \propto (V')^2$, $g \propto V''$, ϵ_V and η_V can evidently only be simultaneously small if for some range of field values both the first and the second derivative of V are small; which requires the existence of a near saddle point, i.e. we need $|\beta| \ll 1$.

The parameter β controls the flatness of the potential for $\phi \sim \phi_0$, i.e. the larger β is, the more the potential around ϕ_0 deviates from a flat plateau. Note that if $\beta < 0$, the slope at ϕ_0 is negative, and there is a second minimum at some $\phi > \phi_0$. Allowing the inflaton passes this minimum would require some fine tuning of initial conditions, since the universe could easily get "stuck" there if ϕ was initially large. We therefore will assume $\beta \geq 0$ throught this work.

Now we briefly discuss how the model parameters control the shape of the potential. As already noted, the model parameter A determines the location of the saddle point (or flat region of the potential). Parameter d determines the amplitude of the potential, which can be constrained by the power spectrum near the plateau.

Note that although the inflaton potential (3.5) only contains three parameters: d, A and β, the predictions for cosmological observables also depend on the value of the inflaton field ϕ at the time when observable density perturbations were generated. As we will show in the following, this four–dimensional parameter space can be explored fully analytically in the region of interest.

3.1.2 Analytical Analysis

Here we consider $\phi_0 \leq 1$, and the generation to $\phi_0 > 1$ will be discussed in Chapter 7. In the small field case, it turns out that ϕ_{CMB} (the field value when the "pivot" scale $k_\star = 0.05\,\mathrm{Mpc}^{-1}$ crossed out of the horizon) is very close to ϕ_0 (see Fig. 3.1). This guides us to introduce the field parameter δ:

$$\phi = \phi_0(1 - \delta), \tag{3.8}$$

so decreasing ϕ corresponds to increasing δ. Since both δ and β are rather small (as we will see, $\beta \ll \delta \ll 1$), we will keep terms up to linear β and up to quadratic in δ in our analysis, and also drop terms $O(\beta\delta)$.
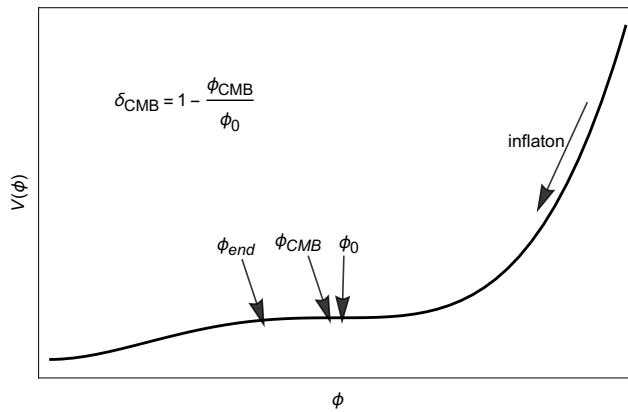
Figure 3.1: Schematic plot for inflaton potential with an (near) inflection-point at ϕ_0.

The following definitions for SR parameters, number of e-folds and inflationary predictions are

based on standard literature, see e.g. Ref.[92]. For our model the SR parameters are given by:

$$\epsilon_V = \frac{1}{2}\left(\frac{V'}{V}\right)^2 \simeq \frac{72\left(-2\beta(\delta-1)+\delta^2\right)^2}{\phi_0^2} \simeq \frac{72\left(2\beta+\delta^2\right)^2}{\phi_0^2}\,;$$

$$\eta_V = \frac{V''}{V} \simeq \frac{12\left(-4\beta(\delta-1)+\delta(3\delta-2)\right)}{\phi_0^2} \simeq \frac{24\left(2\beta-\delta\right)}{\phi_0^2}\,; \qquad (3.9)$$

$$\xi_V^2 = \frac{V'V'''}{V^2} \simeq \frac{288(4\beta^2+\beta(2-10\delta)+\delta^2)}{\phi_0^4} \simeq \frac{288(2\beta+\delta^2)}{\phi_0^4}\,.$$

As already stated, SR requires ϵ_V, $|\eta_V| < 1$. The first two Eqs. (3.9) show that $\epsilon_V \ll |\eta_V|$ in our case, i.e. the beginning and the end of inflation is controlled by $|\eta_V| = 1$, corresponding to

$$\delta_{\text{end}} \simeq \phi_0^2/24\,. \qquad (3.10)$$

The third slow–roll parameter ξ_V^2 turns out to always be small if $|\eta_V| < 1$, and it affects the running of the spectral index, as will be shown shortly.

The number N_{CMB} of e−folds of inflation after the pivot scale $k_\star = 0.05\ \text{MPC}^{-1}$ crossed out of the horizon is given by:

$$\begin{aligned}
N_{\text{CMB}} &= \int_{\phi_{\text{end}}}^{\phi_{\text{CMB}}} \frac{1}{\sqrt{2\epsilon_V}}\,d\phi \\
&= -\frac{\phi_0^2}{12}\int_{\delta_{\text{end}}}^{\delta_{\text{CMB}}} \frac{d\delta}{\left(2\beta+\delta^2\right)} \\
&= -\frac{\phi_0^2}{12\sqrt{2\beta}}\left[\arctan\left(\frac{\delta_{\text{CMB}}}{\sqrt{2\beta}}\right) - \arctan\left(\frac{\delta_{\text{end}}}{\sqrt{2\beta}}\right)\right] \\
&\simeq \frac{\phi_0^2}{12\sqrt{2\beta}}\left[\frac{\pi}{2} - \arctan\left(\frac{\delta_{\text{CMB}}}{\sqrt{2\beta}}\right)\right]\,,
\end{aligned} \qquad (3.11)$$

where δ_{CMB} can be obtained from Eq. (3.8):

$$\delta_{\text{CMB}} = 1 - \frac{\phi_{\text{CMB}}}{\phi_0}\,. $$

To resolve the flatness and horizon problems, sufficient expansion is need with at least 50 e−folds. Here we will take $N_{\text{CMB}} = 65$ as typical value. Eq. (3.11) then implies $\sqrt{2\beta} \ll \phi_0^2/12$, i.e. δ_{end} of Eq. (3.10) is much larger than $\sqrt{2\beta}$ so that $\arctan(\delta_{\text{end}}/\sqrt{2\beta}) \simeq \pi/2$.

From Eq. (3.11), one also sees that δ_{CMB} cannot be much larger than $\sqrt{2\beta}$, but it does not exclude the possibility $\delta_{\text{CMB}} \ll \sqrt{2\beta}$. In order to decide this, we look at at the spectral index of the density perturbations :

$$n_s = 1 - 6\epsilon_V + 2\eta_V \simeq 1 - \frac{48(\delta-2\beta)}{\phi_0^2}\,. \qquad (3.12)$$

Experiments imply a near scale invariant spectrum with $n_s < 1$, leading to $\delta_{\mathrm{CMB}} > 0$. The second term in the last line of Eq. (3.11) therefore reduces the number of $e-$folds of inflation. Ignoring this term and requiring $N_{\mathrm{CMB}} > 50$ gives $\beta < 3.4 \cdot 10^{-6} \phi_0^4$, which in turn shows that the term $\propto \beta$ in Eq. (3.12) can be neglected:

$$\delta_{\mathrm{CMB}} \simeq \left(1 - n_s\right) \frac{\phi_0^2}{48} . \tag{3.13}$$

Eq. (3.11) then requires $\sqrt{2\beta}$ to be of order δ_{CMB}, so that $\beta \sim O(\delta_{\mathrm{CMB}}^2) \ll \delta_{\mathrm{CMB}}$, as claimed at the beginning of this Section.

During slow-roll inflation, the power spectrum of curvature perturbation can be approximated as:

$$\mathcal{P}_\zeta = \frac{V}{24\pi^2 \epsilon_V} \simeq \frac{d \phi_0^6}{5184\pi^2 (\delta^2 + 2\beta)^2} , \tag{3.14}$$

which is the only observable of interest that depends on the strength of the quartic coupling d.

There are two additional observables, whose values are currently not so well known but significant progress is expected in the coming years. One is the running of the spectral index, which is given by:

$$\alpha = 16\epsilon_V \eta_V - 24\epsilon_V^2 - 2\xi_V^2 \simeq -\frac{576(2\beta + \delta^2)}{\phi_0^4} . \tag{3.15}$$

Owing to the smallness of ϵ_V, η_V, the value of α is dominated by the contribution $\propto \xi_V^2$, and is negative in our model. The second observable is the power in gravitational fields generated during inflation. It is usually quantified by the tensor–to–scalar ratio r, given by:

$$r = 16\epsilon_V \simeq \frac{1152 \left(2\beta + \delta^2\right)^2}{\phi_0^2} . \tag{3.16}$$

3.2 Model Parameters and Inflationary Predictions

Any potentially realistic model of inflation has to reproduce known facts, in particular the Planck 2018 measurements[1] [93] at the pivot scale $k_\star = 0.05 \ \mathrm{Mpc}^{-1}$:

$$\mathcal{P}_\zeta = (2.1 \pm 0.1) \times 10^{-9} \, ; \ n_s = 0.9649 \pm 0.0042 \, ; \ \alpha = -0.0045 \pm 0.0067 \, ; \ r < 0.061 \, , \tag{3.17}$$

from which one sees that two quantities, $\mathcal{P}_\zeta$ and n_s, are already known quite accurately. In addition, we have to satisfy Eq. (3.11) with $N_{\mathrm{CMB}} \simeq 65$. This essentially allows to fix three of the four free parameters of our model.

We allow ϕ_0 as a free parameter. The model parameter δ_{CMB} is fixed by the spectral index using Eq. (3.13). Choosing a value of N_{CMB} then fixes β via Eq. (3.11). Finally, the quartic coupling d can be fixed by the power spectrum Eq. (3.14).

---

[1] Note that the recent BICEP/Keck 2018 results have improved the bound to be $r < 0.035$ [22]; we will apply the updated bounds in Chapter 7 when discussing large field inflation, where the bound on r turns out to constrain the upper value of ϕ_0.

Considering the central values of n_s and $\mathcal{P}_\zeta$ and our standard choice $N_{\text{CMB}} = 65$, we have

$$\delta_{\text{CMB}} = 7.31 \times 10^{-4} \phi_0^2 \, ; \tag{3.18}$$

$$\beta = 9.73 \times 10^{-7} \phi_0^4 \, ; \tag{3.19}$$

$$d = 6.61 \times 10^{-16} \phi_0^2 \, . \tag{3.20}$$

The scaling with powers of ϕ_0 can be traced back to Eq. (3.13); the numerical factor in (3.18) corresponds to the result with $n_s = 0.9649$ and $\phi_0 = 1$. Since $\delta_{\text{CMB}} \propto \phi_0^2$, we see from (7.9) that β should be $\propto \phi_0^4$ in order to yield a fixed N_{CMB}. The numerical pre–factor in (3.19) comes from the numerical factor in (3.18) and $N_{\text{CMB}} = 65$. Finally, $d \propto \phi_0^2$ (from Eq. (3.14)) is required to have a fixed power $\mathcal{P}_\zeta = 2.1 \times 10^{-9}$.

With Eqs. (3.18), (3.19) and (3.16), one obtains the prediction for the tensor-to-scalar ratio:

$$r = 7.09 \times 10^{-9} \phi_0^6 \, . \tag{3.21}$$

For $\phi_0 \leq 1$ this is well below the sensitivity of any currently conceivable observation. Varying N_{CMB} and n_s over their allowed ranges does not change this conclusion. We will see in Chapter 7 that r is testable if one has $\phi_0 \sim O(10)$. On the other hand, Eq. (3.15) predicts for the running of spectral index

$$\alpha = -1.43 \times 10^{-3} \, , \tag{3.22}$$

which might be within the sensitivity of a combination of future CMB measurements with greatly improved investigations of structures at smaller scale, in particular the so–called Lyman$-\alpha$ forest [94]. We note that α is independent of ϕ_0, i.e. this is a clear prediction of our model.

Before moving on, we would like to comment on the possibility to allow PBHs formation in the current model. Recently there has been quite a bit of interest in production mechanisms of primordial black holes (PBHs). In principle they can be produced by the gravitational collapse of domains that have a high over–density after inflation. However, this requires [37] a power of $O(10^{-2})$. From Eq. (3.14) we see that in our model the highest power occurs at $\delta = 0$; however, Eqs. (3.19) and (3.20) show that this maximal power only amounts to $O(10^{-8})$, independent of ϕ_0. Moreover, Eq. (7.10) implies that the power decreases monotonically as δ increases, i.e. with decreasing scale, as also indicated by $n_s < 1$ and $\alpha < 0$. Hence the current model does not lead to PBH formation from primordial density fluctuations.

Note that any prediction has to carry errors, and Eqs. (3.18) to (3.22) hold for the central value of n_s and $N_{\text{CMB}} = 65$. Deviations from these values are explored in Fig. 3.2. We see that β is of order $10^{-6} \phi_0^4$ for the entire allowed parameter space. The results shown in this figure can again be understood analytically. To that end we first expand (around the central values)

$$1 - n_s = 0.0351 (1 + \epsilon_n) \tag{3.23}$$

and

$$\sqrt{\frac{\beta}{\phi_0^4}} = 9.86 \cdot 10^{-4} (1 + \epsilon_b) \, . \tag{3.24}$$
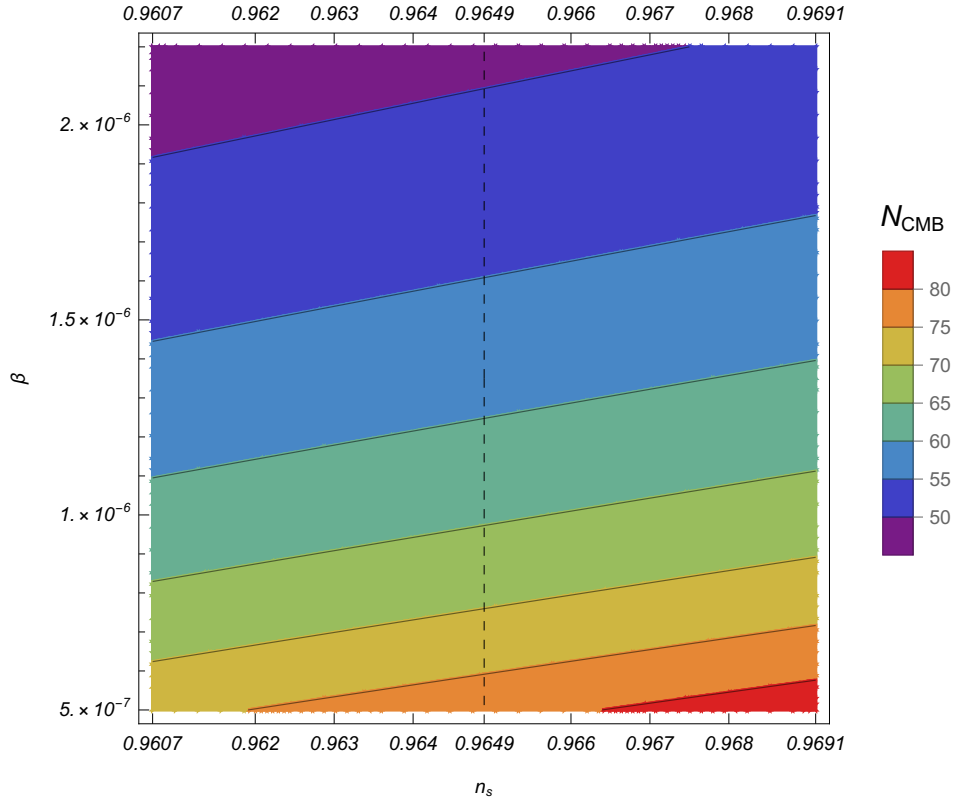
Figure 3.2: N_{CMB} as function of n_s and β for $\phi_0 = 1$; for other values of ϕ_0, β has to be rescaled by ϕ_0^4. The vertical black line denotes the current central value of n_s, which crosses the contour line with $N_{\mathrm{CMB}} = 65$ for $\beta = 9.73 \times 10^{-7}$.

Taylor expanding the arctan function in Eq. (7.9) around the central value then yields:

$$\epsilon_b = \frac{65 - N_{\mathrm{CMB}}}{40.4} - 0.61\epsilon_n \,. \tag{3.25}$$

Eq. (3.25) enables us to obtain an analytical expression for β as function of N_{CMB} and n_s:

$$\sqrt{\frac{\beta}{\phi_0^4}} = 9.86 \times 10^{-4} \left\{ 1 + \left[\frac{65 - N_{\mathrm{CMB}}}{40.4} - 0.61 \left(\frac{1 - n_s}{0.0351} - 1 \right) \right] \right\} \,, \tag{3.26}$$

which agrees very well with the numerical results shown in Fig. 3.2.

As already mentioned r remains tiny, only of order $10^{-8}\phi_0^6$, over the entire allowed parameter space.

The dependence of the running of the spectral index α on n_s and N_{CMB} is given by

$$\alpha = -\frac{576(2\beta + \delta^2)}{\phi_0^4}$$

$$= -1.43 \cdot 10^{-3} - 5.56 \cdot 10^{-5}\Big[65 - N_{\text{CMB}}\Big] + 0.02149\Big[0.9649 - n_s\Big] - 0.25\Big[0.9649 - n_s\Big]^2,$$

(3.27)

which still does not depend on ϕ_0; the result is shown in Fig. 3.3.
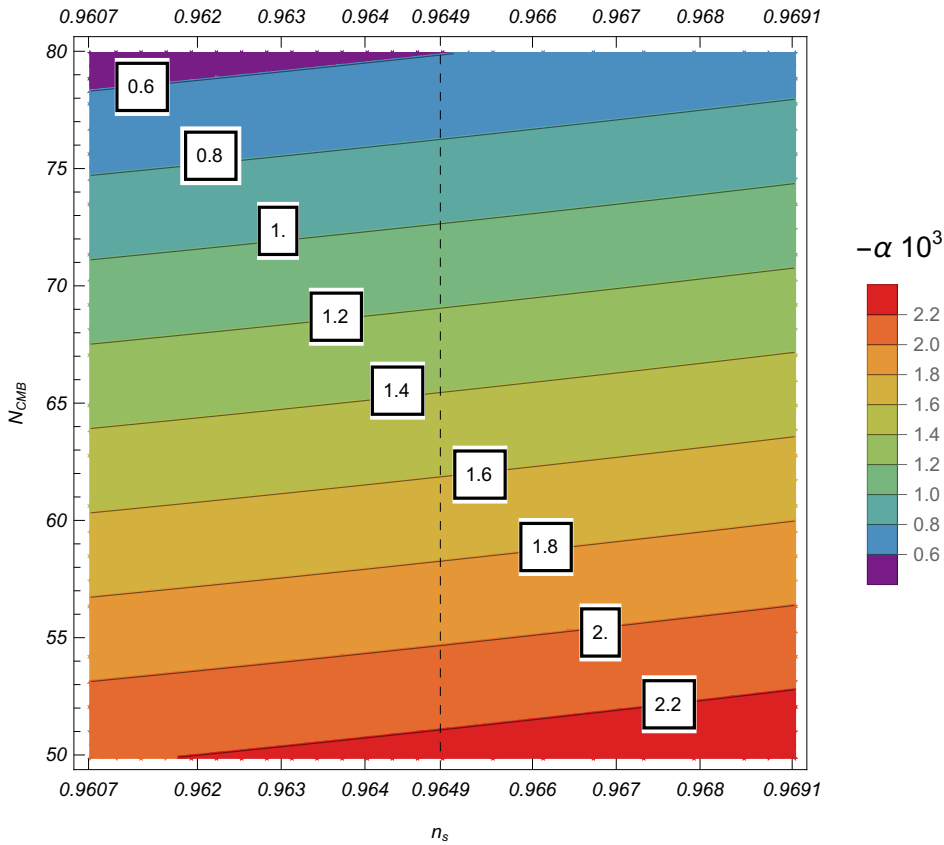
Figure 3.3: Prediction for the running of the spectral index $-\alpha/10^{-3}$ as functions of n_s and N_{CMB}. Our model predicts $\alpha \sim -10^{-3}$ when n_s lies in the vicinity of its current central value (vertical black dashed line) and $50 < N_{\text{CMB}} < 80$, which might be testable in future.

We would like to end this section with a few remarks on our model. It requires a very small but positive value of β, see Eq. (3.19). Eq. (3.26) shows that β varies approximately linearly when n_s and/or N_{CMB} are varied over their allowed ranges. In that sense β, while undoubtedly very small, is not very finely tuned. On the other hand, setting $\beta = 0$ does not enhance the symmetry of the potential. This means that radiative corrections to β – or, more accurately, to the first and second derivative of the potential at $\phi = \phi_0$ – need not be proportional to β. In order to compute these corrections, we first have to expand the scope of our model to include reheating. After inflation the inflaton field has to

decay away to produce relativistic Standard Model particles, i.e. radiation; otherwise no hot Big Bang will result. This requires some coupling(s) of the inflaton to lighter particles. These couplings will contribute to the radiative corrections to the inflaton potential. Before computing these corrections, we therefore need to discuss reheating. This leads to a discussion in Chapter 4, where the radiative stability of our model will also be investigated.

3.3 Summary and Conclusions

Simple monomial inflaton models have already been ruled out by latest experiments [22]. In this Chapter, we revisited a (next) simple renormalizable small field polynomial inflation model. This model reproduces cosmological data only if the potential possesses an "almost" inflection point ϕ_0, such that $\phi \simeq \phi_0$ during inflation. Expanding in $\phi_0 - \phi$ allowed us to derive accurate analytical expressions for all relevant quantities. This includes the number of $e-$folds of inflation after the pivot scale crossed out of the horizon, N_{CMB}, given in Eq. (3.11), as well as the power spectrum, spectral index, its running, and the tensor–to–scalar ratio r, as shown in Eqs. (3.12)-(3.16).

As usual for small–field models of inflation, r is too small to be detectable by currently conceivable experiments. This also means that a convincing detection of gravitational waves of inflationary origin would exclude our model. A second prediction is a negative running of the spectral index, given by $\alpha = -1.43 \times 10^{-3} + 5.56 \times 10^{-5} \left(N_{\mathrm{CMB}} - 65\right)$, which might be detectable in future [94]. Note that this is independent of ϕ_0, which is the only free parameter of our model once we have fixed the overall power of the density perturbations, their spectral index, and N_{CMB}.

The least attractive feature of this model is that one has to engineer ϕ_0 to "almost" be an inflection point; specifically, the parameter β, which controls the flatness of the potential around ϕ_0, has to be of order $10^{-6}\phi_0^4$, see Eq. (3.19). Actually, when written in the form of Eq. (3.5) the finetuning is not obvious; after all, β, while small, is not terribly finely tuned. On the other hand, the coefficient of the cubic term *is* tuned.

Note that the model we consider is renormalizable, and can thus serve as the inflationary sector of some well motivated extensions of the standard model of particle physics; examples are the νMSM [95, 96], or the new minimal standard model (NMSM) [97] which can explain cosmological dark matter, neutrino masses and the baryon asymmetry of the Universe. This offers clear avenues for future research. In Chapter 5, we will investigate dark matter production after polynomial inflation and in Chapter 6 leptogenesis will be investigated.

Note that the model parameters, as shown in Eqs. (3.18)-(3.20), and the inflationary predictions are controlled by the location of ϕ_0. Thereafter working out the parameter space of allowed ϕ_0 is necessary, which brings us to the discussions in the next Chapter.

Heating the Universe

After inflation terminates, the inflaton field oscillates around the potential minimum and transfers energy to other degree of freedoms. Such a process is usually called reheating. In general it consists of a non–perturbative "preheating" epoch [98–101], which is followed by the perturbative decay of the remaining inflaton particles. Finally, the produced daughter particles have to thermalize, giving rise to a thermal Universe. In this Chapter we are devoted to investigating the reheating phenomenology after polynomial infaltion, in particular working out the allowed reheating temperature. In a simple perturbative scenario, the reheating temperature is determined by the coupling strength. Note that reheating temperature can not be arbitrarily large in order to guarantee the loop corrections not spoiling the inflationary prediction; it should also be not too small to allow successful Big Bang Nucleosynthesis (BBN), in which a radiation epoch is required. These two constraints on reheating temperature turn out to generate a lower bound on ϕ_0, as will be discussed in the following.

This Chapter is organized as follows. In Sec. 4.1 we calculate the reheating temperature and discuss the corresponding constraints from BBN; we will analyze two scenarios, where the inflaton dominantly decays into two fermions or two bosons, respectively. In Sec. 4.2, the radiative stability of the potential under one–loop correction is investigated and the resulting lower bound on ϕ_0 is derived. In Sec. 4.3, we investigate the inflationary scale and reheating temperature within the parameter space we have obtained. In Sec. 4.4, we briefly describe a possible "prehistory" of our model, starting from a phase of eternal inflation. Finally, in Sec. 4.5 we sum up our findings and end with some prospects to embed our inflation model into some well motivated BSM scenarios. This chapter is based on Ref. [2]

4.1 Reheating

In this section, we first focus on the simplest possibility, namely the perturbative decays of the inflaton through trilinear couplings of the inflaton to lighter particles. Such a coupling is always required, since otherwise at least some inflaton particles would remain at the end of the reheating period. Then at the end of this Section we will argue that the non–perturbative effects cannot significantly deplete the inflaton number in our model. In next Section we will argue in order to guarantee the loop corrections to do not jeopardize the inflationary predictions, all the inflaton couplings have to be so small. This leads to inflaton annihilation reactions are completely negligible.

By using instantaneous decay approximation, one can estimate the reheating temperature, denoted as T_{rh}. In particular we have set the inflaton energy density, $\rho_\phi = m_\phi n_\phi$, equal to the radiation density

$\rho_R = \pi^2 g_* T_{\rm rh}^4 / 30$ at time $t = 2/(3\mathcal{H}) = 1/\Gamma_\phi$, with $\mathcal{H}^2 = \rho/3$ as usual in FRLW cosmology, one finds (in Planckian units)

$$T_{\rm rh} \simeq 1.41 g_\star^{-1/4} \Gamma_\phi^{1/2} . \tag{4.1}$$

Here g_* denotes the number of light degrees of freedom in the thermal plasma, and Γ_ϕ is the perturbative inflaton decay rate. And for $T_{\rm rh} > 1$ GeV, g_* is of order 100.

We allow the inflaton to decay into a Dirac fermion χ and/or a scalar ϕ' for completeness. Since ϕ is a singlet under the SM gauge group, χ would have to be in a vector–like representation of that group, i.e. it cannot be an SM fermion. On the other hand, ϕ' might be the Higgs field of the SM. We will treat this as our standard case, i.e. we will assume that ϕ' contains four degrees of freedom, just like the Dirac fermion χ. The Lagrangian respecting renormalizability is given by

$$\mathcal{L} = i\bar{\chi}\gamma^\mu \partial_\mu \chi + (\partial_\mu \phi')^\dagger \partial^\mu \phi' - m_\chi \bar{\chi}\chi - y\phi\bar{\chi}\chi - m_{\phi'}^2 |\phi'|^2 - g\phi|\phi'|^2 - \lambda\phi^2|\phi'|^2 - \lambda_{\phi'}|\phi'|^4 . \tag{4.2}$$

The total decay width of the inflaton is then given by

$$\Gamma_\phi = \frac{y_\chi^2 m_\phi}{8\pi} \left(1 - \frac{4m_\chi^2}{m_\phi^2}\right)^{3/2} + \frac{g^2}{8\pi m_\phi} \sqrt{1 - \frac{4m_{\phi'}^2}{m_\phi^2}} \simeq \frac{y^2}{8\pi} m_\phi + \frac{g^2}{8\pi m_\phi} , \tag{4.3}$$

where the inflaton mass is

$$m_\phi^2 = \left.\frac{\partial^2 V}{\partial \phi^2}\right|_{\phi=0} \simeq \frac{9}{16} dA^2 = 4d\phi_0^2 . \tag{4.4}$$

Note that this is the inflaton mass after inflation, and therefore not directly related to the SR parameter η_V, which is also computed from the second derivative of the inflaton potential. In the following analysis we will assume that one of the two terms in Eq. (4.3) dominates; the other one may then even vanish. Moreover, we assume that the mass of χ or ϕ' is much smaller than m_ϕ, which minimizes the lower bound on the couplings y and g which we wish to derive.

When fermionic decays dominate, the reheating temperature is given by

$$T_{\rm rh}^\chi \simeq 1.41 g_\star^{-1/4} \left(2\phi_0 \frac{y^2}{8\pi} \sqrt{d}\right)^{1/2} , \tag{4.5}$$

while for the bosonic decay mode,

$$T_{\rm rh}^{\phi'} \simeq 1.41 g_\star^{-1/4} \left(\frac{g^2}{8\pi \, 2\phi_0 \sqrt{d}}\right)^{1/2} . \tag{4.6}$$

Successful BBN requires $T_{\rm rh} \geq 4$ MeV, i.e. $T_{\rm rh} \geq 1.67 \cdot 10^{-21}$ in Planckian units [86, 87]. Taking $g_\star = 10.75$, as appropriate for a temperature of 4 MeV, and $d = 6.61 \times 10^{-16} \phi_0^2$ from Eq. (3.20) in previous chapter, we finally obtain lower bounds on the inflaton couplings:

$$y\phi_0 \geq 4.7 \times 10^{-17} , \tag{4.7}$$

if fermionic decays dominate, and

$$\frac{g}{\phi_0} \geq 2.4 \times 10^{-24} \, , \tag{4.8}$$

for bosonic inflaton decays. The scaling with ϕ_0 can be understood from the observation that $m_\phi \propto \sqrt{d}\phi_0 \propto \phi_0^2$, from Eqs. (4.4) and (3.20). Eq. (4.1) shows that a constant reheat temperature corresponds to a constant decay width Γ_ϕ. From Eq. (4.3) this requires constant $y^2 m_\phi$, i.e. constant $y^2\phi_0^2$, if fermionic decays dominate, but constant g^2/m_ϕ, i.e. constant g^2/ϕ_0^2 for bosonic inflaton decays; note that g has dimension of mass in natural units, whereas y is dimensionless.

We now come back to the issue of non–perturbative inflaton depletion mechanisms. In principle the couplings in the Lagrangian (4.2) allow both fermionic and bosonic preheating. However, due to Pauli blocking, fermionic preheating is usually very inefficient [102, 103], i.e. it reduces the initial inflaton energy by less than 1%.

Let's first focus on bosonic inflaton decays; the trilinear $\phi|\phi'|^2$ coupling gives rise to a tachyonic instability if $|g\phi| > m_{\phi'}^2$, where the squared mass of the daughter particle is negative for part of each oscillation of the inflaton field. As shown in [104, 105] this can build up a sizable ϕ' number density after a very small number of ϕ oscillations. However, even with very small ϕ' self–interactions of $O(10^{-6})$ this only allows to transfer less than 10% of the initial inflaton energy [104]. In our default scenario, where ϕ' is the SM Higgs field, ϕ' does have a sizable self interaction of the form $\lambda_{\phi'}\phi'^4$ (with $\lambda_{\phi'} \sim O(0.1)$). This gives an extra positive effective squared mass $\sim \lambda_{\phi'}\langle\phi'^2\rangle$ (with $\langle\phi'^2\rangle$ denoting the variance) once the daughter ϕ' particles are copiously produced. This back–reaction counteracts the negative tachyonic mass and quickly terminates preheating, making it even less efficient [104]. With the help of a lattice simulation [106], we found that less than 1% of the initial inflaton energy is depleted through preheating. Results with typical couplings will be presented in the next section. Preheating can thus indeed be neglected in our model, and our simple perturbative analysis to estimate the reheating temperature shall work well.[1]

4.2 Radiative Corrections and Stability

Once the couplings of inflaton to the daughter particles are considered, we have to make sure the radiative corrections do not spoil the flatness of the inflaton potential. The lower bounds (4.7) and (4.8) on the inflaton couplings imply lower bounds on the radiative corrections to the inflaton potential caused by these couplings. The self–couplings of the inflaton, described by the potential (3.5), also contribute to the radiative corrections. In this Section we investigate the impact of these corrections in 1–loop order. This will lead to upper bounds on the couplings; together with the lower bounds derived in the previous Section this will finally yield a lower bound on the remaining free parameter ϕ_0.

Our starting point of this analysis is the expression for the 1–loop effective potential, in the formalism

---

[1] We note that in the literature on preheating some scenarios have been suggested which could deplete inflaton energy more efficiently, see e.g. instant preheating [107] or combined reheating [108–110]. Here one introduces additional perturbative decay channels for the produced daughter particles in order to get rid of the back reaction problem. However, the decay width of the SM Higgs, our default bosonic decay product, is just 4 MeV, which is 5 orders of magnitude smaller than the minimal allowed value of m_ϕ in our model (see below). The preheating time scale, which is $O(1/m_\phi)$, is thus very much shorter than the ϕ' lifetime, in which case ϕ' decays cannot affect the preheating dynamics.

of Coleman and Weinberg (CW) [111]:

$$\Delta V(\phi) = \frac{1}{64\pi^2} \sum_\psi (-1)^{2s_\psi} g_\psi \widetilde{m}_\psi(\phi)^4 \left(\ln\left(\frac{\widetilde{m}_\psi(\phi)^2}{Q_0^2} \right) - \frac{3}{2} \right). \tag{4.9}$$

The sum runs over all fields ψ that couple to the inflaton field ϕ. s_ψ is the spin of ψ; the factor $(-1)^{2s_\psi}$ therefore implies that bosons (fermions) contribute with positive (negative) sign to ΔV. g_ψ is the number of degrees of freedom of the field ψ; it includes a spin multiplicity factor $2s_\psi + 1$. Finally, $\widetilde{m}_\psi(\phi)$ is the ϕ−dependent mass of ψ (not to be confused with the physical mass), and Q_0 is a renormalization scale.

In our case, up to three fields couple to the inflaton: the inflaton itself, as well as the fermionic and bosonic decay products χ and ϕ' introduced in the previous Section. Their field–dependent masses are given by:

$$\widetilde{m}_\phi^2(\phi) = 12d\phi^2 + 6dA(1 - \beta)\phi + \frac{9}{16}dA^2\,;$$
$$\widetilde{m}_\chi^2(\phi) = \left(m_\chi + y\phi \right)^2\,; \tag{4.10}$$
$$\widetilde{m}_{\phi'}^2(\phi) = m_{\phi'}^2 + g\phi\,.$$

In order to make sure that the predictions derived in Chapter 3 are stable under radiative corrections, we need to investigate the potential around the point ϕ_0, where inflation happens. In fact, the tree–level potential V_0 itself is not particularly suppressed at $\phi = \phi_0$: $V_0(\phi_0) \to d\phi_0^4/3$ as $\beta \to 0$. On the other hand, it is essential that the first and second derivatives of the potential *are* suppressed at ϕ_0; this is why ϕ_0 is a near inflection point. Recall also that V_0' and V_0'' directly determine N_{CMB} and n_s, respectively. From Eq. (3.5) with $A = -8\phi_0/3$ we have

$$V_0'(\phi_0) = 8d\beta\phi_0^3\,;$$
$$V_0''(\phi_0) = 16d\beta\phi_0^2\,. \tag{4.11}$$

On the other hand, from Eq. (4.9) the derivatives of the CW correction to the potential can be written as

$$\Delta V' = \frac{1}{32\pi^2} \sum_\psi (-1)^{2s_\psi} g_\psi \widetilde{m}_\psi^2 \widetilde{m}_\psi^{2\prime} \left(\ln\left(\frac{\widetilde{m}_\psi^2}{Q_0^2} \right) - 1 \right)\,;$$
$$\Delta V'' = \frac{1}{32\pi^2} \sum_\psi (-1)^{2s_\psi} g_\psi \left\{ \left[\left(\widetilde{m}_\psi^{2\prime} \right)^2 + \widetilde{m}_\psi^2 \widetilde{m}_\psi^{2\prime\prime} \right] \ln\left(\frac{\widetilde{m}_\psi^2}{Q_0^2} \right) - \widetilde{m}_\psi^2 \widetilde{m}_\psi^{2\prime\prime} \right\}\,. \tag{4.12}$$

Here $\widetilde{m}_\psi^{2\prime}$ and $\widetilde{m}_\psi^{2\prime\prime}$ are the first and second derivatives of $\widetilde{m}_\psi^2$ with respect to ϕ.

The loop corrections are minimized if the bare masses m_χ and $m_{\phi'}$ vanish. Recall also that these masses must be below half the physical inflaton mass; using Eqs. (4.4) and (3.20) this implies m_χ, $m_{\phi'} < \sqrt{d}\phi_0 = 2.6 \cdot 10^{-8}\phi_0^2$, which is already quite small. In the subsequent analysis we will therefore assume $m_\chi \ll y\phi_0$ and $m_{\phi'}^2 \ll g\phi_0$, so that the bare mass terms can be neglected. Moreover, we set $Q_0 = \phi_0$, since this is the field value we are interested in; this means that the Lagrangian

parameters y and g should be interpreted as running couplings, taken at scale Q_0. The derivatives of the correction to the potential at $\phi = \phi_0$ are then given by:

$$\Delta V'(\phi_0) = \frac{\phi_0^3}{4\pi^2}\left[y^4 - 16d^2\beta - y^4\ln(y^2) + 16d^2\beta\ln(16d\beta)\right] + \frac{g^2\phi_0}{8\pi^2}\left[\ln\left(\frac{g}{\phi_0}\right) - 1\right];$$

$$\Delta V''(\phi_0) = \frac{\phi_0^2}{4\pi^2}\left[y^4 - 3y^4\ln(y^2) + 8d^2\ln(16d\beta)\right] + \frac{g^2}{8\pi^2}\ln\left(\frac{g}{\phi_0}\right).$$

(4.13)

In the first Eq. (4.13) we have ignored terms of order $d^2\beta^2$. We see that all corrections from the inflaton self–coupling d are proportional to β, which means that these terms are automatically smaller than the tree–level result given in the first Eq. (4.11). In the second Eq. (4.13) we neglected also terms linear in β. We see that nevertheless a finite one–loop correction $\propto d^2$ remains.

In order to ensure stability of our inflationary model against radiative corrections, we will require that the terms $\propto d^2$, $\propto y^4$ and $\propto g^2$ are separately smaller than the tree–level results of Eqs. (4.11). We just saw that in case of d^2 only the correction to the second derivative of the potential can be dangerous. Demanding that it is smaller in magnitude than the tree–level result leads to the constraint

$$\left|\frac{d^2\ln(16d\beta)}{\pi^2}\right| < 8d\beta.$$

(4.14)

Using the numerical values from Eqs. (3.19) and (3.20) this implies

$$|\ln(10^{-20}\phi_0^6)| < 1.16 \cdot 10^{11}\phi_0^2,$$

which in turn implies

$$\phi_0 > 3 \cdot 10^{-5}.$$

(4.15)

The strongest upper bound on the Yukawa coupling also comes from the second derivative of the potential:

$$\left|\frac{y^4 - 3y^4\ln(y^2)}{4\pi^2}\right| < 16d\beta.$$

(4.16)

In order to turn this into a lower bound on ϕ_0, we again use Eqs. (3.19) and (3.20) for the right–hand side, and insert the lower limit (4.7) from reheating for y; this gives

$$\phi_0 > 3.4 \cdot 10^{-5},$$

(4.17)

which is slightly stronger than the bound (4.15).

On the other hand, the strongest bound on the coupling g originates from the first derivative of the potential; it reads

$$\frac{g^2}{8\pi^2}\left|\ln\left(\frac{g}{\phi_0}\right) - 1\right| < 8d\beta\phi_0^2.$$

(4.18)

Replacing g by its lower bound (4.8) then implies

$$\phi_0 > 3.1 \cdot 10^{-5},$$

(4.19)

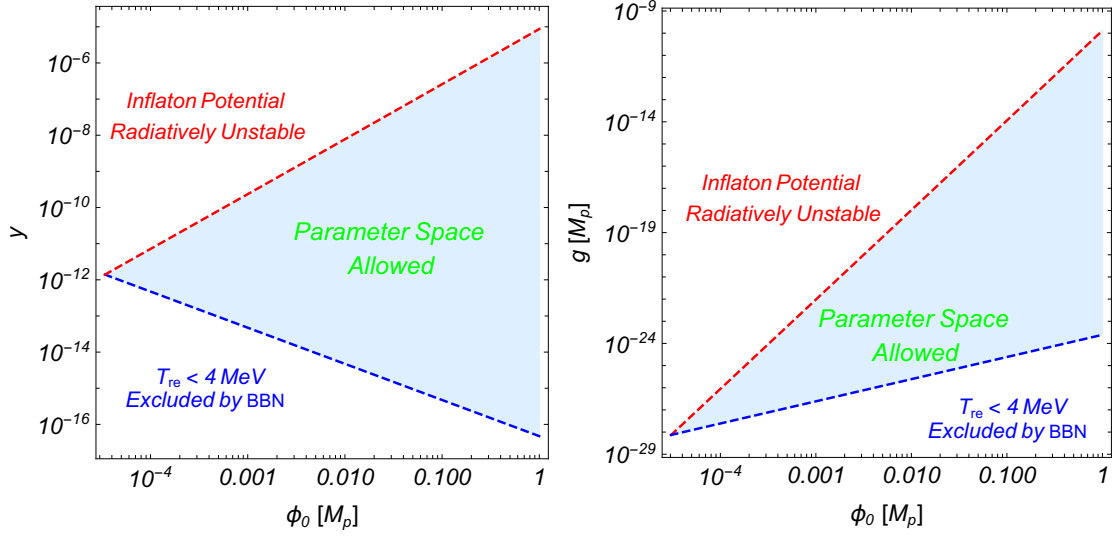very close to the bound (4.15) which is independent of reheating.

Figure 4.1: The light blue region is the allowed parameter space, yielding reheating temperature $T_{\text{re}} \equiv T_{\text{rh}} \geq 4$ MeV while keeping the inflaton potential stable against radiative corrections. The left (right) frame is for fermionic (bosonic) inflaton decays.

The constraints on the parameter space spanned by ϕ_0 and the coupling that is responsible for reheating are shown in Fig. 4.1; the left and right frames correspond to fermionic and bosonic inflaton decays, respectively. The allowed parameter space, shown in blue, ends at the values of ϕ_0 given by the bounds (4.17) and (4.19). Evidently the allowed range of couplings opens up when ϕ_0 increases; for the maximal value we consider, $\phi_0 = 1$, it ranges over 11 orders of magnitude for y, and 13 orders of magnitude for g. Nevertheless, even for $\phi_0 = 1$ the maximal allowed value of the Yukawa coupling is about 10^{-5}, which is only slightly larger than the Yukawa coupling of the electron in the SM.

Recall that we assumed that four (bosonic or fermionic) degrees of freedom couple to the inflaton, i.e. $g_{\phi'} = g_\chi = 4$. In case of bosonic decays, both the lower bound on g^2 from reheating and the upper bound from radiative stability scale like $1/g_{\phi'}$, i.e. the resulting lower bound (4.19) does not depend on $g_{\phi'}$. On the other hand, for fermionic decays the lower bound on y^2 scales like $1/g_\chi$ while the upper bound scales like $1/\sqrt{g_\chi}$; the bound (4.17) therefore roughly scales like $g_\chi^{-1/10}$. However, it is in any case already quite close to the bound (4.15) which is independent of reheating.

In our discussion on (p)reheating we have ignored a possible quartic coupling $\lambda \phi^2 |\phi'|^2$. Such a coupling would also contribute to the CW corrections to the potential. Demanding that this contribution to the first derivative of the inflaton potential at ϕ_0 does not exceed the tree–level value gives the quite stringent upper bound $\lambda \sqrt{|\ln(\lambda)|} < 4.5 \cdot 10^{-10} \phi_0^3$. The largest quartic coupling λ allowed by this bound is of $\mathcal{O}(10^{-10})$ even for $\phi_0 = 1$. Preheating with such small coupling is not efficient [98], i.e. reheating has to proceed via perturbative inflaton decay as we analyzed in Sec. 4.1.

We finally note that the upper bounds on the inflaton couplings we derived in this Section imply that the rate for inflaton annihilation reactions, $\phi\phi \rightarrow \chi\bar{\chi}$ or $\phi\phi \rightarrow \phi'\bar{\phi}'$, is always much smaller than the Hubble rate $\mathcal{H}$. The annihilation rate is given by $\langle \sigma v \rangle n_\phi$, where σ is the relevant annihilation cross section, $\langle \ldots \rangle$ denotes averaging over the ensemble of inflaton particles, and n_ϕ is the inflaton density. Right after inflation one can estimate $n_\phi \sim V_{\text{inf}}/m_\phi$ and $\mathcal{H} \sim \mathcal{H}_{\text{inf}} \sim \sqrt{V_{\text{inf}}}$, but even at this high

inflaton density the annihilation rate is many orders of magnitude smaller than the Hubble rate. The ratio becomes even smaller at later times, since $\mathcal{H} \propto 1/t$ while $n_\phi \propto 1/t^2$ during matter domination. Therefore inflaton annihilation plays no role in the dynamics of reheating.

4.3 The Scales of Inflation

In previous section, we have derived a lower bound on ϕ_0, with which we can discuss the range of energy scales during and just after inflation that can be realized in our model. Here we mean both the vacuum energy during inflation (or, equivalently, the Hubble parameter), and the range of reheating temperatures after inflation.

Note that ϕ_{CMB} is very close to ϕ_0, the inflationary scale $\mathcal{H}_{\mathrm{inf}}$ is thus essentially equal to that at the inflection-point ϕ_0. From eqs. (3.5) and (3.20) we have

$$V(\phi_0) = \frac{1}{3} d\phi_0^4 \simeq 2.2 \cdot 10^{-16} \phi_0^6 , \qquad (4.20)$$

where we have neglected β and used $A = -8\phi_0/3$. This corresponds to a Hubble parameter

$$\mathcal{H}_{\mathrm{inf}} = \sqrt{\frac{V(\phi_0)}{3}} \simeq 8.6 \cdot 10^{-9} \phi_0^3 . \qquad (4.21)$$

In the previous section we saw that $\phi_0 \gtrsim 3 \cdot 10^{-5}$; the lower bound on the bound on the Hubble parameter during inflation is thus

$$\mathcal{H}_{\mathrm{inf}} \gtrsim 2.3 \times 10^{-22} \simeq 0.6\,\mathrm{MeV} . \qquad (4.22)$$

With such a low scale inflationary scenario, the cosmological moduli problem can be relaxed [90]. Besides the isocurvature bound of QCD axion can be easily satisfied, making our model a good candidate to embed QCD axion as dark matter, which can even allow a wider cosmological window with larger decay constant f_a [88, 89]. On the other hand, for $\phi_0 \simeq 1$, $\mathcal{H}_{\mathrm{inf}} \sim 10^{10}$ GeV is possible, which allows for the non–thermal production of various particles, and hence non–standard post–inflationary cosmologies.

It is instructive to compare the inflationary Hubble parameter (4.21) with the change of the inflaton field during one Hubble time due to the slow–roll of the field. The latter is given by

$$\Delta\phi = \frac{|\dot{\phi}|}{\mathcal{H}} = \frac{|V'|}{3\mathcal{H}^2} = \frac{|V'|}{V} = \frac{24\beta}{\phi_0} = 2.3 \cdot 10^{-5} \phi_0^3 , \qquad (4.23)$$

which is much larger than $\mathcal{H}_{\mathrm{inf}}/(2\pi)$. This means that even near the inflection point the dynamics of the inflaton field is entirely dominated by the classical (SR) equation of motion.

Another energy scale of interest in inflationary model building is the reheating temperature. As long as we don't fix the relevant coupling y or g, we cannot make a firm prediction; however, the upper bounds on these couplings that we derived in the previous Section allow to derive an upper bound on T_{rh} for given ϕ_0. This is shown in Fig. 4.2, where we have again used the instantaneous reheating approximation. We see that for fermionic (bosonic) inflaton decay, the reheating temperatures as high as $4 \cdot 10^8$ GeV (10^{11} GeV) are possible. This allows for standard thermal leptogenesis [91]. Of course,
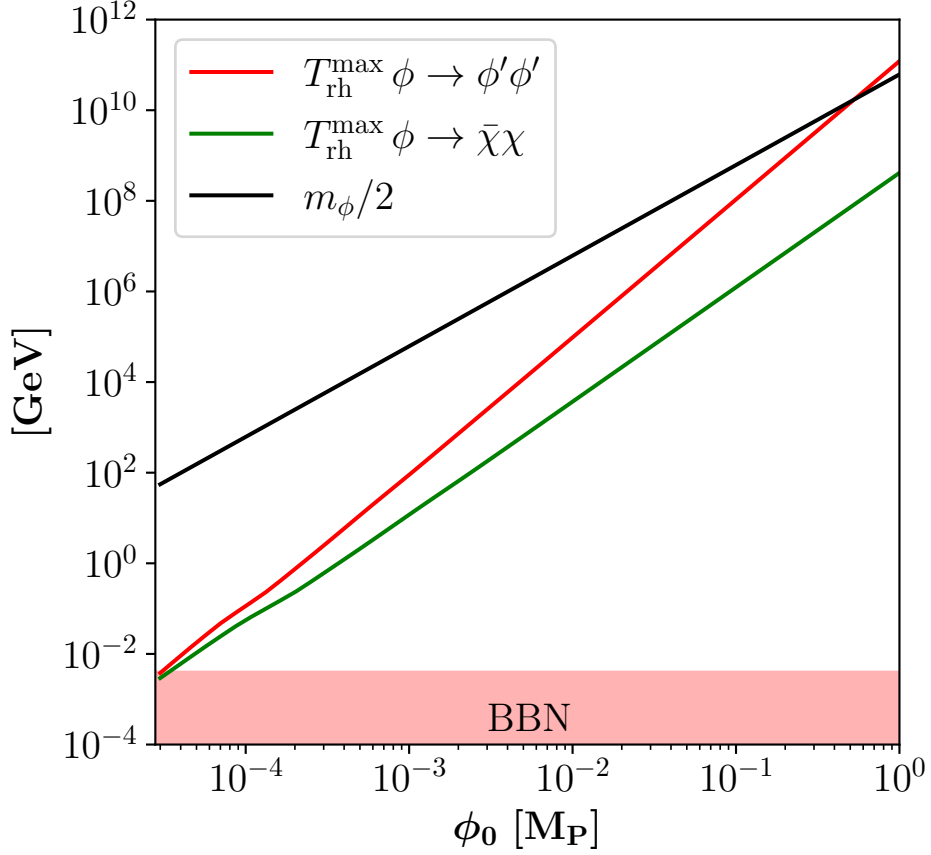
Figure 4.2: Allowed range of the post–inflationary reheat temperature as a function of ϕ_0 (in the range $[3 \cdot 10^{-5}, 1]$), for bosonic (red) and fermionic (green) inflaton decays. The blue line shows the lower bound of 4 MeV from BBN considerations, and the purple line denotes half of inflaton mass within the parameter space.

the fermionic decay product χ might itself be right–handed neutrinos (which contribute $g_\chi = 2$ for each generation), allowing for non–thermal leptogenesis if the coupling y is (well) below its upper bound. We will investigate leptogenesis in detail in Chapter 6.

The slopes of the curves depicted in Fig. 4.2 can be understood as follows. For fermionic decays, $\Gamma_\phi \propto y^2 m_\phi$, with $m_\phi \propto \phi_0^2$ from Eqs. (4.4) and (3.20) while $y_{\text{max}}^2 \propto \phi_0^3$ (up to logarithmic corrections) from the constraint (4.16), hence $T_{\text{rh,max}} \propto \Gamma_{\phi,\text{max}}^{1/2} \propto \phi_0^{5/2}$. For bosonic decays, $\Gamma_\phi \propto g^2/m_\phi$ and $g_{\text{max}}^2 \propto \phi_0^8$ (again up to logarithmic corrections) from (4.18), hence $T_{\text{rh,max}} \propto \phi_0^3$. In these simple estimates we have ignored the dependence of g_* on T_{rh}, which has been included in Fig. 4.2. When the temperature is around 0.1 GeV, the QCD deconfinement transition happens, leading to a rapid change of $g_\star$ [112]; this is the reason for the features in the red and green curves at $T_{\text{rh,max}} \sim 0.1$ GeV.

Recall from Eq. (4.4) that $m_\phi/2 = \sqrt{d}\phi_0 = 6.2 \cdot 10^{10}$ GeV $\times (\phi_0/M_P)^2$, which is somewhat above the maximal reheat temperature for fermionic inflaton decays as shown in Fig. 4.2. For fermionic decays a scenario with $T_{\text{rh}} > m_\phi/2$ is difficult to realize; instead, Pauli blocking would delay inflaton decays such that $T_{\text{rh}} \lesssim m_\phi/2$. For bosonic decays $T_{\text{rh}} > m_\phi/2$ is possible, since several relative soft bosons can combine into a smaller number of more energetic bosons.

Before ending this section, we would like to remind the reader that the highest temperature of the thermal background can be considerably higher than T_{rh} [113]; parametrically, in Planckian units $T_{\text{max}} \sim \sqrt{T_{\text{rh}}} \mathcal{H}_{\text{inf}}^{1/4} \sim \phi_0^{3/4} \sqrt{T_{\text{rh}}}$. In our case this is indeed always several orders of magnitude above T_{rh}, with $T_{\text{max}}/T_{\text{rh,max}}$ scaling like $\phi_0^{-1/2}$ ($\phi_0^{-3/4}$) for fermionic (bosonic) inflaton decays. However, for fermionic inflaton decays one also has to require $T_{\text{max}} \leq m_\phi/2$, as we argued above.

4.4 Prehistory

Our analysis so for has only been concerned with field values $\phi \lesssim \phi_0$, which we limited to be not larger than 1 (in Planckian units). In that sense our model is a "small field" model of inflation.

In this Section we nevertheless wish to briefly describe the dynamics at much larger field values. After all, except for possible quantum gravity effects our model can be UV complete, i.e. it might describe the dynamics also at much larger field values.

For field values $\phi \gg \phi_0$ the potential (3.5) is dominated by the quartic term $d\phi^4$. The dynamics in this range is therefore that of quartic chaotic inflation [114]. In particular, the deterministic change of ϕ during one Hubble time, $|\dot\phi|/\mathcal{H}$, will be smaller than the random variation $\mathcal{H}/(2\pi)$ if

$$\phi > \phi_{\text{ch, min}} = 1.2 \cdot 10^3 \phi_0^{-1/3} \, , \tag{4.24}$$

where we have again used Eq. (3.20) for the strength of the quartic coupling. If ϕ ever satisfied this bound, a period of "eternal" inflation started; in fact, in this case it should continue even now in "most" of space. This epoch of eternal inflation might allow to sample a "landscape" of minima of the (total) effective potential, which seems to be a feature of superstring theory [83].

Of course, in our patch of the universe eternal inflation must have ended at some point. It would have been followed by a long period of deterministic inflation, since for $\phi \lesssim \phi_{\text{ch, min}}$ the SR parameters are still very small. This first phase of deterministic SR inflation ended at

$$\phi = \phi_{\text{e,1}} \simeq \sqrt{12} + \frac{2}{3}\phi_0 \, , \tag{4.25}$$

where we have neglected terms of order ϕ_0^2. This first phase of deterministic inflation, where $\phi_{\text{ch, min}} > \phi > \phi_{\text{e,1}}$, lasted for

$$N_{\text{det, 1}} \simeq 1.8 \cdot 10^5 \phi_0^{-2/3} \tag{4.26}$$

e−folds. It should be noted that any initial field value $\phi_i > \phi_{\text{e,1}}$ would lead to large−field SR inflation; large field inflation is much less sensitive to initial conditions than small−field inflation [115]. Of course, if our universe indeed underwent a period of eternal inflation, the question of initial conditions might be moot [59].

For $\phi < \phi_{\text{e,1}}$ the field underwent fast roll (or overshooting), until it reached the vicinity of the near−inflection point ϕ_0 [1]. Here we can use an expansion as in Eq. (3.8) again, but now δ is negative, at least initially. SR inflation then starts again once $|\eta_V| < 1$, which is true for

$$\phi < \phi_{\text{b}} \simeq \phi_0 \left(1 + \frac{\phi_0^2}{24} - \frac{\phi_0^4}{384} + O(\phi_0^6)\right) \, . \tag{4.27}$$

Here we have neglected terms of order β. Eventually ϕ reached the value $\phi_{\text{CMB}} = \phi_0(1 - \delta_{\text{CMB}})$, with δ_{CMB} given by Eq. (3.18). SR inflation with $\phi_{\text{b}} > \phi > \phi_{\text{CMB}}$ gave rise to another

$$N_{\text{pre-CMB}} \simeq 120 \tag{4.28}$$

$e-$folds of inflation, with Hubble parameter given by Eq. (4.21).

This second deterministic stage of SR inflation would have been sufficient to completely dilute any relics from possible earlier large–field inflationary phases, even before density perturbations on CMB scales were generated. Therefore the "pre–history" sketched in this Section most likely does not have any direct observational consequences.

4.5 Summary and Conclusions

A complete inflation scenario has to provide for a mechanism to reheat the universe after inflation terminates.

In this chapter, we have considered scenarios where inflaton decays into either fermions or bosons via trilinear interactions. For given ϕ_0 the corresponding coupling strengths are bounded from below by demanding that the reheating temperature is sufficiently high for a successful BBN. On the other hand, we showed that the radiative stability of the inflaton potential near the inflection point leads to upper bounds on these couplings, which again depend on ϕ_0. These constraints on the parameter space are summarized in Fig. 4.1. In particular, radiative stability requires $\phi_0 > 3 \cdot 10^{-5}$ in Planckian units. Within the allowed parameter space the Hubble parameter during inflation ($\mathcal{H}_{\text{inf}}$) can be as low as ~ 1 MeV, which makes our model a good candidate to embed QCD axion as dark matter allowing wider cosmological window [88, 89]. On the other hand, $\mathcal{H}_{\text{inf}}$ can also be as high as 10^{10} GeV if $\phi_0 \simeq 1$. In this case the reheat temperature can be as high as $4 \cdot 10^8$ (10^{11}) GeV for fermionic (bosonic) inflaton decays as shown in Fig. 4.2.

Having worked out the full model parameter space and range for reheating temperature, in next chapters we will then proceed to investigate DM production and leptogenesis where reheating temperature plays a key role.

Generating Dark Matter

This chapter is aimed to show that Dark Matter (DM) with correct relic density can be sourced after inflation within the polynomial inflationary framework. The discussions are based on Ref. [3]

5.1 The Model Setup

Here we assume a singlet Dirac fermion χ as DM candidate with a Lagrangian $\mathcal{L}_\chi$:

$$\mathcal{L}_\chi = i\,\bar{\chi}\,\gamma^\mu\,\partial_\mu\chi - m_\chi\,\bar{\chi}\,\chi - y_\chi\,\phi\bar{\chi}\,\chi\,, \tag{5.1}$$

where m_χ denotes DM mass, and y_χ corresponds to the Yukawa coupling between inflaton and DM field. Note that the Universe after reheating has to be a radiation phase, which means that only a small fraction of inflaton energy goes to DM. The rest of the energy would be transferred to the degrees of freedom in the standard model (SM). To this end, we consider a coupling between inflaton and the SM Higgs field:

$$\mathcal{L}_{\phi H} = -\lambda_{12}\phi|H|^2 - \lambda_{22}\phi^2|H|^2\,, \tag{5.2}$$

which plays the roles of reheating as analyzed in Chapter 4.

5.2 Dark Matter Production and Relic Density

DM in our scenario can be produced via different processes, and the corresponding Feynman diagrams are collected in Fig. 5.1. The main contributions come from *i*) direct decay of inflatons, *ii*) 2-to-2 annihilations of inflatons during the reheating era (mediated by the *s*-channel exchange of inflatons or gravitons, and the *t*-channel exchange of DM), and *iii*) 2-to-2 annihilations of SM particles mediated by gravitons and inflatons. The evolution of the DM number density n is governed by the Boltzmann equation

$$\frac{dn}{dt} + 3\mathcal{H}\,n = \gamma\,, \tag{5.3}$$

where γ denotes the DM production rate density and $\mathcal{H}$ corresponds to the Hubble expansion rate given by $\mathcal{H}^2 = (\rho_R + \rho_\phi)/(3M_P^2)$. Evolution of the inflaton and SM radiation energy densities (ρ_ϕ
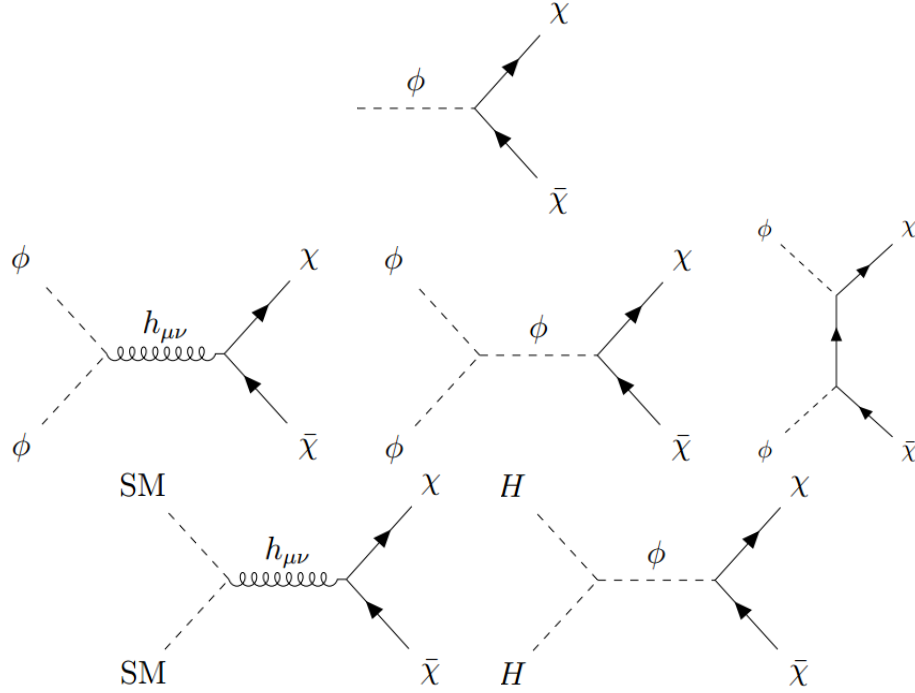
Figure 5.1: Feynman diagrams for the different DM productions channels described in the text. The three rows correspond to *i*) the decay of the inflaton, *ii*) inflaton scatterings, and *iii*) the scattering of SM particles.

and ρ_R, respectively) can be tracked via the coupled Boltzmann equations

$$\frac{d\rho_\phi}{dt} + 3\mathcal{H}\,\rho_\phi = -\Gamma\,\rho_\phi\,, \tag{5.4}$$

$$\frac{d\rho_R}{dt} + 4\mathcal{H}\,\rho_R = +\Gamma\,\rho_\phi\,(1 - \text{Br})\,, \tag{5.5}$$

where Br denotes the branching ratio for $\phi \to \bar{\chi}\chi$, and it is given by:

$$\text{Br} \equiv \frac{\Gamma_{\phi \to \bar{\chi}\chi}}{\Gamma_{\phi \to \bar{\chi}\chi} + \Gamma_{\phi \to H^\dagger H}} \simeq \frac{\Gamma_{\phi \to \bar{\chi}\chi}}{\Gamma_{\phi \to H^\dagger H}} \simeq 2.6 \times 10^{-15} \frac{\phi_0^4\,y_\chi^2}{M_P^2\,\lambda_{12}^2}\,. \tag{5.6}$$

Note that Br has to be very small so that the Universe ends with radiation epoch after reheating. The factor $(1 - \text{Br}) \simeq 1$ is the fraction of inflaton energy density that goes into SM radiation ρ_R, which first quickly maximizes at $T_{\max}$ and then decreases.

Here we mainly focus on DM generated during reheating, namely $T_{\text{rh}} \lesssim T \lesssim T_{\max}$, where the total energy density of the universe is still dominated by inflatons. Taking into account that $T \propto a^{-3/8}$ and that the inflaton energy density behaves as non relativistic matter, one then has

$$\rho_\phi(T) = \frac{\pi^2\,g_\star}{30}\,\frac{T^8}{T_{\text{rh}}^4}\,, \tag{5.7}$$

where $\rho_\phi(T_{\rm rh}) = \rho_R(T_{\rm rh})$ was assumed. Plugging Eq. (5.7) into the Friedmann equation, one can estimate the Hubble parameter:

$$\mathcal{H}(T) = \frac{\pi}{3}\sqrt{\frac{g_\star}{10}}\frac{T^4}{M_P T_{\rm rh}^2}\,. \tag{5.8}$$

Before moving on, we briefly revisit the estimation for $T_{\rm max}$, which plays an important role in this chapter. Considering the scaling of inflaton energy from the end of inflation, $\rho_\phi(a) = \rho_\phi(a_{\rm end})\left[\frac{a_{\rm end}}{a}\right]^3 = 3M_P^2\mathcal{H}_{\rm inf}^2\left[\frac{a_{\rm end}}{a}\right]^3$, one can solve Eq. (5.5) and obtain

$$\rho_R(a) = \frac{6}{5}M_P^2\,\Gamma\,\mathcal{H}_{\rm inf}\left(\frac{a_{\rm end}}{a}\right)^4\left[\left(\frac{a}{a_{\rm end}}\right)^{5/2} - 1\right], \tag{5.9}$$

which maximize at

$$a = a_{\rm max} \equiv (8/3)^{2/5} a_{\rm end}\,, \tag{5.10}$$

corresponding to

$$T_{\rm max}^4 = \frac{60}{\pi^2 g_\star}\left(\frac{3}{8}\right)^{8/5} M_P^2\,\Gamma\,\mathcal{H}_{\rm inf}\,. \tag{5.11}$$

Using Eq. (5.8) at $T = T_{\rm rh}$ and $H(T_{\rm rh}) = \frac{2}{3}\Gamma$, one has

$$T_{\rm rh} = \sqrt{\frac{2}{\pi}}\left(\frac{10}{g_\star}\right)^{1/4}\sqrt{M_P\Gamma}\,, \tag{5.12}$$

with which one can substitute Γ in Eq. (5.11) for $T_{\rm max}$ with respect to $T_{\rm rh}$. Finally one obtains

$$\frac{T_{\rm max}}{T_{\rm rh}} = \left(\frac{3}{8}\right)^{2/5}\left(\frac{\mathcal{H}_{\rm inf}}{\mathcal{H}\left(T_{\rm rh}\right)}\right)^{1/4} \simeq 4.8\times10^{-3}\left(\frac{\phi_0^3}{M_P T_{\rm rh}^2}\right)^{1/4}, \tag{5.13}$$

where we have used $\mathcal{H}_{\rm inf} \simeq \sqrt{\frac{V(\phi_0)}{3M_P^2}} \simeq 8.6\times10^{-9}\frac{\phi_0^3}{M_P^2}$ (cf. Eq. (4.21)).

Taking into account the fact that during the reheating the SM entropy density is not conserved due to the inflaton decay, it is usually convenient to rewrite Eq. (5.3) in terms of the comoving number density $N \equiv n\,a^3$ (rather than the usual yield $Y \equiv n/s$); this leads to:

$$\frac{dN}{dT} = -\frac{8}{\pi}\sqrt{\frac{10}{g_\star}}\frac{M_P\,T_{\rm rh}^{10}}{T^{13}}\,a^3(T_{\rm rh})\,\gamma\,. \tag{5.14}$$

After reheating ends, the universe enters a SM radiation dominated epoch with temperature $T < T_{\rm rh}$. In this regime, entropy is conserved, and Eq. (5.3) can be recast as a function of the DM yield $Y(T) \equiv n(T)/s(T)$, defined as a function of the SM entropy density $s(T) \equiv \frac{2\pi^2}{45}g_{\star s}T^3$, with $g_{\star s}(T)$ being the number of relativistic degrees of freedom contributing to the SM entropy. Therefore,

Eq. (5.3) becomes

$$\frac{dY}{dT} = -\frac{135}{2\pi^3 g_{\star s}}\sqrt{\frac{10}{g_\star}}\frac{M_P}{T^6}\,\gamma\,. \tag{5.15}$$

To match the observed DM energy density $\Omega_{\rm DM}h^2 \simeq 0.12$ [13], the DM yield has been fixed such that

$$m_\chi\, Y_0 = \Omega_\chi h^2\,\frac{1}{s_0}\,\frac{\rho_c}{h^2} \simeq 4.3 \times 10^{-10}\ {\rm GeV}\,, \tag{5.16}$$

with $\rho_c \simeq 1.05 \times 10^{-5}\,h^2$ GeV/cm^3 the critical energy density and $s_0 \simeq 2.9 \times 10^3$ cm^{-3} the present entropy density [45]. In the following we will investigate the aforementioned channels as shown in Fig. 5.1.

5.2.1 Inflaton Decay

Due to the presence of a trilinear coupling $y_\chi\,\phi\,\bar\chi\chi$, DM can be produced by direct decays of the inflaton [116]. In such case, corresponding to the first row of Fig. 5.1, the decay rate density is given by

$$\gamma = 2\,{\rm Br}\,\Gamma\,\frac{\rho_\phi}{m_\phi}\,, \tag{5.17}$$

where the factor 2 comes from the fact that each ϕ decays to a pair of DM particles. In the regime with $T_{\max} > T > T_{\rm rh}$, one can solve Eq. (5.14) analytically, and obtain

$$N \simeq \frac{2\pi\, g_\star}{15}\sqrt{\frac{10}{g_\star}}\frac{M_P\, T_{\rm rh}^2}{m_\phi}a^3(T_{\rm rh})\,{\rm Br}\,\Gamma\,. \tag{5.18}$$

We can further compute the DM yield:

$$Y_0 = \frac{N(T_{\rm rh})}{s(T_{\rm rh})\,a^3(T_{\rm rh})} \simeq \frac{3}{\pi}\frac{g_\star}{g_{\star s}}\sqrt{\frac{10}{g_\star}}\frac{M_P\,\Gamma}{m_\phi\,T_{\rm rh}}{\rm Br} \simeq \frac{3}{2}\frac{g_\star}{g_{\star s}}\frac{T_{\rm rh}}{m_\phi}{\rm Br}\,. \tag{5.19}$$

In order to produce the whole observed DM abundance, one needs:

$$y_\chi \simeq 1.2 \times 10^{-13}\sqrt{\frac{T_{\rm rh}}{m_\chi}}\,. \tag{5.20}$$

The Yukawa coupling y_χ required to reproduce the whole observed DM abundance via the direct decay of the inflaton is shown in Fig. 5.2. The colored bands correspond to different constraints BBN ($T_{\rm rh} \gtrsim 4$ MeV), radiative stability of inflaton potential (from inflaton and DM loops cf. Eq. (4.18) and Eq. (4.16)), Lyman-α (cf. Eq. (5.22)), and the kinematical threshold $m_\phi > 2\,m_\chi$. The white area corresponds to the allowed parameter space, with branching ratio $10^{-21} \lesssim {\rm Br} \lesssim 10^{-4}$; the upper bound on the branching fraction comes from the Lyman-α bound as shown in Eq. (5.23), while the lower bound corresponds to the case with $T_{\rm rh} \simeq 1.2 \times 10^{11}$ GeV and $m_\chi \simeq 6 \times 10^{10}$ GeV. The DM mass in the allowed parameter space can span from $O(10^{-5})$ GeV to $O(10^{11})$ GeV. Here we would like to stress that the allowed parameter space, namely the while region corresponds to the combinations of
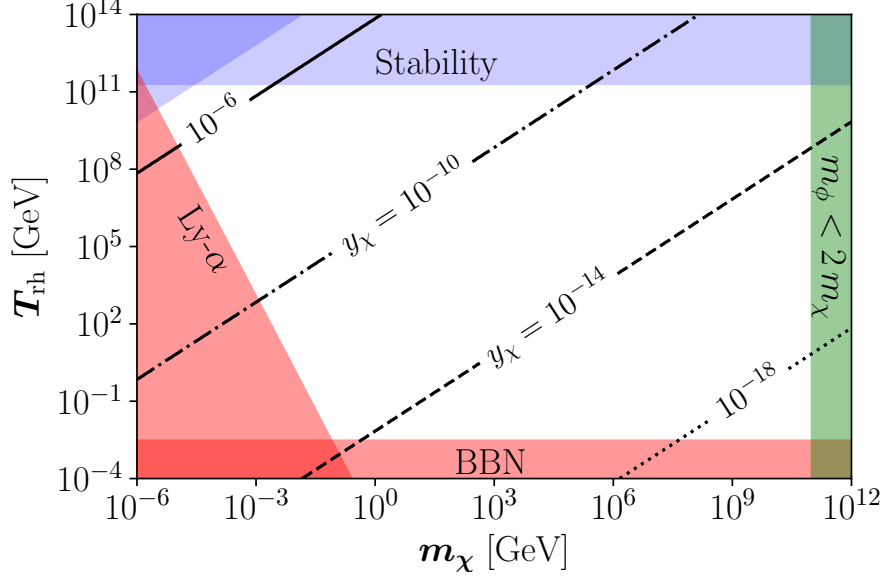
Figure 5.2: Reheating temperature $T_{\rm rh}$ as function of y_χ and DM mass m_χ in order to reproduce the whole observed DM abundance via the direct decay of the inflaton. The colored bands correspond to the different constraints as described in the text. The white region is the allowed parameter space with $10^{-21} \lesssim {\rm Br} \lesssim 10^{-4}$ and $O(10^{-5})\,{\rm GeV} \lesssim m_\chi \lesssim O(10^{11})\,{\rm GeV}$.

the bounds mentioned above with all possible ϕ_0 or equivalently m_ϕ.

Lyman-α Bound

Note that for those DM particles produced from inflaton decays, they were born to carry energy with half of the inflaton mass. And due to this large initial momentum of DM particles, they could have a rather large free-streaming length $\lambda_{\rm DM}$, leading to a smoothing of primordial inhomogeneities at scales smaller than $\lambda_{\rm DM}$ [117]. This typically causes a suppression on the structure formation at small scales. Note that the smaller DM mass is, the larger the suppression would be. By using the matter power spectrum inferred from small structure e.g. Lyman-α forest data, one is able to set lower bounds on DM mass [117, 118].

In our scenario here, DM has very suppressed interactions with the SM or with itself, so momentum of DM simply redshifts. And its present value p_0 is

$$p_0 = \frac{a_{\rm in}}{a_0} p_{\rm in} = \frac{a_{\rm in}}{a_{\rm eq}} \frac{\Omega_R}{\Omega_m} p_{\rm in} = \left[\frac{g_{\star s}(T_{\rm eq})}{g_{\star s}(T_{\rm rh})} \right]^{1/3} \frac{T_{\rm eq}}{T_{\rm rh}} \frac{\Omega_R}{\Omega_m} \frac{m_\phi}{2} \simeq 10^{-14} \frac{m_\phi}{T_{\rm rh}}\,{\rm GeV}\,, \qquad (5.21)$$

where $p_{\rm in} = m_\phi/2$ is the mean initial momentum at production (i.e., at $T = T_{\rm rh}$), $T_{\rm eq}$ and $a_{\rm eq}$ correspond to the temperature and the scale factor at the matter-radiation equality, respectively. Additionally, we have used $T_{\rm eq} \simeq 0.8$ eV, $\Omega_R \simeq 5.4 \times 10^{-5}$ and $\Omega_m \simeq 0.315$ [13, 45]. A lower bound on the DM mass can be used to obtain an upper bound on a typical velocity of warm dark matter (WDM) at present. Considering $m_{\rm WDM} \gtrsim 3.5$ KeV [119], one has the bounds on WDM velocity $v_{\rm WDM} \lesssim 10^{-8}$ by assuming that they are relativistic at decoupling [120]. Note that we have to require $v_{\chi,0} \lesssim v_{\rm WDM}$

if assuming χ particles accounting for the whole DM relic density, from which one finally obtains

$$\frac{m_\chi}{\text{KeV}} \gtrsim \frac{m_\phi}{T_{\text{rh}}} \, . \tag{5.22}$$

By using Eq. (5.19), we further obtain an upper bound on the branching ratio:

$$\text{Br} \lesssim 10^{-4}. \tag{5.23}$$

Such a small branching ratio is as expected since most of the inflaton energy shall be transferred to radiation at the end of reheating.

5.2.2 Inflaton Scattering

Alternatively, DM can be generated during reheating via 2-to-2 scatterings of inflatons mediated by the s-channel exchange of gravitons or inflatons, and the t-channel exchange of a DM particle, as shown in the second row of Fig. 5.1. However the second and third processes are *a*lways sub-dominant compared to the direct decay due to a further coupling suppression. We will therefore focus on the gravitational channel, which might dominate in particular if the branching ratio Br is suppressed.

In the case where the graviton mediation dominates, the interaction rate density for DM production out of nonrelativistic inflatons reads [121–123]

$$\gamma = \frac{\pi^3 g_\star^2}{3686400} \frac{T^{16}}{M_P^4 T_{\text{rh}}^8} \frac{m_\chi^2}{m_\phi^2} \left(1 - \frac{m_\chi^2}{m_\phi^2} \right)^{3/2} . \tag{5.24}$$

We present the detailed computation in the appendix A. The DM yield at the end of reheating can be analytically computed with Eq. (5.15) as

$$Y_0 \simeq \frac{g_\star^2}{81920 g_{\star s}} \sqrt{\frac{10}{g_\star}} \left(\frac{T_{\text{rh}}}{M_P} \right)^3 \left[\left(\frac{T_{\text{max}}}{T_{\text{rh}}} \right)^4 - 1 \right] \frac{m_\chi^2}{m_\phi^2} \left(1 - \frac{m_\chi^2}{m_\phi^2} \right)^{3/2}$$

$$\simeq 1.8 \times 10^{-2} \frac{T_{\text{rh}} m_\chi^2}{M_P^{5/2} m_\phi^{1/2}} \left(1 - \frac{m_\chi^2}{m_\phi^2} \right)^{3/2} , \tag{5.25}$$

where we have used Eq. (5.13) for T_{max}. However taking into account the stability constraint on the reheating temperature, i.e. $T_{\text{rh}} \lesssim 10^{11}$ GeV, it follows that DM production via inflaton scatterings can contribute at most to a few percent of the total DM abundance.

5.2.3 SM Particles Scattering

In our setup, DM could also be produced by the scattering of SM particles, as shown by the third row of Fig. 5.1. This channel, corresponding to the UV freeze-in, can be mediated by the s-channel exchange of gravitons or inflatons, and is presented in the following.

- Graviton Mediation.

Here we investigate production of DM via the scattering of SM particles with gravitons acting as the mediator. This gravitational production mechanism is unavoidable due to the universal couplings between the metric and the energy-momentum tensor $\sim g^{\mu\nu} h_{\mu\nu}$. The interaction rate density can be written as [124]

$$\gamma(T) = \alpha \, \frac{T^8}{M_P^4} \,, \tag{5.26}$$

where $\alpha \simeq 1.1 \times 10^{-3}$ for a fermonic DM. The DM abundance produced after reheating is given by integrating Eq. (5.15) with $m_\chi \lesssim T \lesssim T_{\rm rh}$, and therefore

$$Y_0 = \frac{45\alpha}{2\pi^3 g_{\star s}} \sqrt{\frac{10}{g_\star}} \left(\frac{T_{\rm rh}}{M_P}\right)^3 \,, \qquad \text{for } m_\chi \ll T_{\rm rh} \,. \tag{5.27}$$

In the case where DM is heavier than the reheating temperature (but still lighter than $T_{\rm max}$), one should compute the DM abundance during the reheating era. Equation (5.14) with $m_\chi \lesssim T \lesssim T_{\rm max}$ yields therefore

$$Y_0 = \frac{45\alpha}{2\pi^3 g_{\star s}} \sqrt{\frac{10}{g_\star}} \frac{T_{\rm rh}^7}{M_P^3 \, m_\chi^4} \,, \qquad \text{for } m_\chi \gg T_{\rm rh} \,. \tag{5.28}$$

However, in the present scenario this DM production mediated by the exchange of gravitons cannot generate enough DM relics as the reheating temperature of the universe is $T_{\rm rh} \lesssim 10^{11}$ GeV in order to not spoil the flatness of the inflaton potential by radiative corrections.

We now close this section with a few remarks regarding another purely gravitational production channel. Indeed any massive particle (which violates conformal invariance), and in particular the DM field, can be generated due to the effect of time variations of the background metric, in particular during inflaton oscillations [125–133]. Through this mechanism DM particles with mass $m_\chi \lesssim \mathcal{H}_{\rm inf}$ can be produced with typical number density $n_\chi \sim \mathcal{H}_{\rm inf}^3$ [128], and it is particularly relevant for $m_\chi \simeq \mathcal{H}_{\rm inf}$ [134, 135]. Via this mechanism, the DM relic density scales like $\Omega_\chi h^2 \sim \left(m_\chi/10^{11} \text{ GeV}\right)^2 (T_{\rm rh}/10^9 \text{ GeV})$ [128]. However, the upper bounds $\mathcal{H}_{\rm inf} \lesssim O(10^{10})$ GeV and $T_{\rm rh} \lesssim 10^{11}$ GeV imply that it is not very robust for the present scenario.

- Inflaton Mediation.

Alternatively, DM could also be produced by 2-to-2 scattering of SM particles, mediated by the s-channel exchange of inflatons, as shown by the last diagram in Fig. 5.1. In the regime with $T \ll m_\phi$, the corresponding interaction rate density is given by

$$\gamma(T) \simeq \frac{y_\chi^2 \lambda_{12}^2}{2\pi^5} \frac{T^6}{m_\phi^4} \,. \tag{5.29}$$

As in the present scenario, the reheating temperature is smaller than the inflaton mass, the DM abundance produced after reheating with $T < T_{\rm rh}$ can be then estimated with Eq. (5.15), and is

given by

$$Y_0 \simeq \frac{135 \, y_\chi^2 \, \lambda_{12}^2}{4\pi^8 \, g_{\star s}} \sqrt{\frac{10}{g_\star}} \, \frac{M_P \, T_{\rm rh}}{m_\phi^4} \, .$$

(5.30)

Note that this production channel mediated by the exchange of inflatons turns out to be subdominant with respect to the direct decay of the inflaton, smaller by a factor $\frac{T_{\rm rh}}{M_P} \left(\frac{T_{\rm rh}}{m_\phi}\right)^3 \ll 1$. This is kind of expected since the cross section for 2-to-2 scattering is suppressed by an extra coupling compared to the direct decays.

5.3 Summary and Conclusions

In this chapter, we have shown that after polynomial inflation, DM particles can be produced by a number of processes that counts the direct decay of the inflaton, the 2-to-2 scattering of standard model particles via the *s*-channel exchange of inflatons or gravitons, or purely gravitational interactions. However, due to the upper bounds on the reheating temperature (to guarantee the flatness of the inflaton potential), the pure gravitational channels are *not* robust to produce enough DM, and freeze-in is *always* subdominant compared to the direct decay. The viable parameter space to reproduce correct DM relics is shown in Fig. 5.2 by inflaton decay with branching ratio: $10^{-21} \lesssim \text{Br} \lesssim 10^{-4}$, where DM mass spans a large range, from the KeV scale up to $O(10^{11})$ GeV.

Producing Baryons

In this chapter we are devoted to showing that Baryogenesis can be easily realized within the polynomial inflationary setup. To that end, we will consider a simple Baryogenesis scenario via Leptogenesis, which could also account for the light neutrino masses simultaneously. It turns out that parameter space, consistent with inflationary predictions, neutrino oscillations data as well as baryon asymmetry of the Universe (BAU), exists as shown below. This chapter is based on Ref. [8]

This chapter is organised as follows. In Sec. 6.1 we give the model setup. And neutrino masses are revisited in Sec. 6.2. In Sec. 6.3 we investigate both the thermal and non-thermal channels for leptogenesis. Finally we sum up our findings in Sec. 6.4.

6.1 The Model Setup

We minimally extend the standard model (SM) of particle physics with a scalar inflaton field ϕ and three right-handed Majorana neutrinos (RHNs) denoted by N_I with $I = 1, 2, 3$. The Lagrangian for RHNs are given by:

$$\mathcal{L}_N = i\,\overline{N_I}\,\gamma^\mu\,\partial_\mu N_I - \left(\frac{1}{2}M_N\overline{N_I^c}N_I + h.c.\right) - \left(Y_{\alpha I}\,\bar{\ell}_\alpha\tilde{H}N_I + h.c.\right) - \left(y_I\,\phi\overline{N_I^c}N_I + h.c.\right) \quad (6.1)$$

where M_N denotes the Majorana mass, ℓ_α is lepton doublet, $\tilde{H} \equiv i\sigma_2 H^\star$, $Y_{\alpha I}$ and y_I are the Yukawa couplings. Note that the inflaton field ϕ admits the potential as shown in (3.1).

6.2 Neutrino Masses

In Eq. (6.1) using Euler-Lagrange equation for $\overline{N}_I$ field, namely $\partial_\mu \frac{\partial\mathcal{L}}{\partial(\partial_\mu\overline{N}_I)} - \frac{\partial\mathcal{L}}{\partial\overline{N}_I} = 0$, one can solve for N_I. By plugging N_I back to Eq. (6.1), one finds (after electroweak symmetry breaking) a Majorana mass term for the light active neutrino ν_α:

$$\mathcal{L} \supset \overline{\nu}_\alpha\left(-2\frac{v^2 Y_{\alpha I}Y_{\alpha I}^T}{M_N}\right)\nu_\alpha^c, \quad (6.2)$$

from which one has mass matrix:

$$\tilde{m}_\nu = -v^2 Y M_N^{-1} Y^T \,,$$ (6.3)

where $v = 174$ GeV denoting the vev of the Higgs field, and we have dropped the index for Yukawa couplings. In (6.3) $\tilde{m}_\nu$ can be diagonalized by using the Pontecorvo-Maki-Nakagawa-Sakata (PMNS) matrix such that $m_\nu = U^T \tilde{m}_\nu U$ with $m_\nu = \text{diag}(m_1, m_2, m_3)$. Here we assume a normal hierarchy with

$$m_1 = 0 \,, m_2 = \sqrt{\Delta m_\odot^2} = (8.6 \pm 0.1) \times 10^{-3} \,\text{eV} \,, m_3 = \sqrt{\Delta m_{\text{atm}}^2} = (5.02 \pm 0.03) \times 10^{-2} \,\text{eV} \,.$$ (6.4)

Using the Casas-Ibarra Parameterization [136], one can rewrite the Yukawa matrix Y with respect to the physical neutrino mass m_ν, PMNS matrix U and Majorana mass M:

$$Y = \frac{i}{v} U^\star \sqrt{m_\nu} R^T \sqrt{M} \,,$$ (6.5)

where R denotes some undetermined complex orthogonal matrix. With (6.5), one has

$$(R^T)_{ij} = -iv \frac{(U^T Y)_{ij}}{\sqrt{m_i}\sqrt{M_j}} \iff R_{ji} = -iv \frac{(U^T Y)_{ij}}{\sqrt{m_i}\sqrt{M_j}} \,.$$ (6.6)

In this work we will work with a mass hierarchy $M_3 \gg M_2 \gg M_1$, in particular we assume assumed $M_3 \to \infty$, so that the scenario corresponds to the minimal model with two RHNs [137]. Since $m_2 \neq 0$ and $m_3 \neq 0$, R_{32} and R_{33} have to vanish. On the other hand R_{31} might not be zero as we have also assumed that $m_1 \to 0$. Thereafter R takes the form

$$R = \begin{pmatrix} R_{11} & R_{12} & R_{13} \\ R_{21} & R_{22} & R_{23} \\ R_{31} & 0 & 0 \end{pmatrix} ; R^T = \begin{pmatrix} R_{11} & R_{21} & R_{31} \\ R_{12} & R_{22} & 0 \\ R_{13} & R_{23} & 0 \end{pmatrix} \,,$$ (6.7)

Since $RR^T = R^T R = \mathbb{1}$, one has

$$\mathbb{1} = \begin{pmatrix} R_{11}^2 + R_{12}^2 + R_{13}^2 & R_{11}R_{21} + R_{12}R_{22} + R_{13}R_{23} & R_{11}R_{31} \\ R_{11}R_{21} + R_{12}R_{22} + R_{13}R_{23} & R_{21}^2 + R_{22}^2 + R_{23}^2 & R_{21}R_{31} \\ R_{11}R_{31} & 0 & R_{31}^2 \end{pmatrix}$$

$$\mathbb{1} = \begin{pmatrix} R_{11}^2 + R_{21}^2 + R_{31}^2 & R_{11}R_{12} + R_{21}R_{22} & R_{11}R_{13} + R_{21}R_{23} \\ R_{11}R_{12} + R_{21}R_{22} & R_{12}^2 + R_{22}^2 & R_{12}R_{13} + R_{22}R_{23} \\ R_{11}R_{13} + R_{21}R_{23} & R_{12}R_{13} + R_{22}R_{23} & R_{13}^2 + R_{23}^2 \end{pmatrix}$$ (6.8)

which requires $R_{11} = R_{21} = 0$, $R_{31}^2 = 1$, $R_{12}^2 + R_{13}^2 = 1$, $R_{12}R_{22} + R_{13}R_{23} = 0$, $R_{22}^2 + R_{23}^2 = 1$, $R_{12}^2 + R_{22}^2 = 1$, $R_{12}R_{13} + R_{22}R_{23} = 0$, $R_{13}^2 + R_{23}^2 = 1$. Thereafter we can choose R matrix as [137]

$$R = \begin{pmatrix} 0 & \cos z & \sin z \\ 0 & -\sin z & \cos z \\ 1 & 0 & 0 \end{pmatrix} \,,$$ (6.9)

with z being a complex angle. Using Eq. (6.5) and Eq. (6.9), one has

$$(Y^\dagger Y)_{ij} = \frac{\sqrt{M_i M_j}}{v^2} \left(m_2 R_{i2}^\star R_{j2} + m_3 R_{i3}^\star R_{j3} \right) .$$ (6.10)

Here we present some useful quantities:

$$(Y^\dagger Y)_{11} = \frac{M_1}{v^2} \left(m_2 |\cos z|^2 + m_3 |\sin z|^2 \right) ;$$ (6.11)

$$(Y^\dagger Y)_{21} = \frac{\sqrt{M_1 M_2}}{v^2} \left[-m_2 (\sin z)^\star \cos z + m_3 \sin z (\cos z)^\star \right] ;$$ (6.12)

and

$$\begin{aligned}
\sum_\alpha \left(Y_{\alpha 1}^\star Y_{\alpha 1} \right) &= \sum_\alpha \frac{1}{v^2} \left(U_{\alpha i} \sqrt{m_i} R_{i1}^{T\star} \sqrt{M_1} \right) \left(U_{\alpha j}^\star \sqrt{m_j} R_{j1}^T \sqrt{M_1} \right) \\
&= \frac{M_1}{v^2} \sum_\alpha \left(U_{\alpha j}^\star U_{\alpha i} \sqrt{m_i} R_{1i}^\star \sqrt{m_j} R_{1j} \right) \\
&= \frac{M_1}{v^2} \sum_\alpha \left(U_{\alpha 2}^\star U_{\alpha 2} m_2 R_{12}^\star R_{12} + U_{\alpha 3}^\star U_{\alpha 3} m_3 R_{13}^\star R_{13} \right) \\
&= \frac{M_1}{v^2} \left(m_2 |\cos z|^2 + m_3 |\sin z|^2 \right) ,
\end{aligned}$$ (6.13)

where in the last step we have used the fact that $\sum_\alpha U_{\alpha i}^\star U_{\alpha i} = 1$, for $i = 1, 2, 3$. Note that $\sum_\alpha \left(Y_{\alpha 1}^\star Y_{\alpha 1} \right) \equiv (Y^\dagger Y)_{11}$. These expressions appear in the CP asymmetry parameter and matrix element for the three body decay of inflaton as presented in Appendix C.

6.3 Leptogenesis

Here we again focus on the minimal case with $I = 1, 2, 3$, with $M_3 \gg M_2 \gg M_1$, so only the lightest RHN, namely N_1 plays a role for leptogenesis. The interference of tree-level and one-loop correction for the decay of N_1 induce a CP asymmetry (due to the complex nature of Yukawa coupling), which turns out to be [54]

$$\epsilon_1 = \frac{1}{8\pi} \frac{1}{\left(Y^\dagger Y \right)_{11}} \text{Im} \left[\left(Y^\dagger Y \right)_{21}^2 \right] g \left(\frac{M_2^2}{M_1^2} \right) ,$$ (6.14)

with the Loop function given by

$$\begin{aligned}
g(z) &= \sqrt{z} \left[\frac{1}{1-z} + 1 - (1+z) \ln \left(\frac{1+z}{z} \right) \right] \\
&\simeq -\frac{3}{2} \left(\frac{1}{z} \right)^{1/2} - \frac{5}{6} \left(\frac{1}{z} \right)^{3/2} + O \left(\frac{1}{z} \right)^{5/2} \quad \text{for} \quad z \gg 1 .
\end{aligned}$$ (6.15)

Since

$$\left(Y^\dagger Y\right)^2_{21} = \frac{M_1 M_2}{v^4} \left[-m_2 (\sin z)^\star \cos z + m_3 \sin z (\cos z)^\star\right]^2$$
$$= \frac{M_1 M_2}{v^4} \left[m_2^2 (\sin z)^{\star 2} \cos z^2 + m_3^2 \sin z^2 (\cos z)^{\star 2} - 2m_2 m_3 |\sin z|^2 || \cos z|^2\right] , \quad (6.16)$$

one has

$$\mathrm{Im}\left[\left(Y^\dagger Y\right)^2_{21}\right] = \frac{M_1 M_2}{v^4} \mathrm{Im}\left[m_2^2 (\sin z)^{\star 2} \cos z^2 + m_3^2 \sin z^2 (\cos z)^{\star 2}\right]$$
$$= \frac{M_1 M_2}{v^4} (m_3^2 - m_2^2) \mathrm{Im}(\sin z)^2 \quad (6.17)$$

Now define $\cos^2 z = x + i\,y$, and $\sin^2 z = 1 - \cos^2 z = 1 - x - i\,y$ with $x, y \in \mathbb{R}$, so one has

$$\epsilon_1 = \frac{1}{8\pi} \frac{v^2}{M_1 \left(m_2 |\cos z|^2 + m_3 |\sin z|^2\right)} \mathrm{Im}\left[\left(Y^\dagger Y\right)^2_{21}\right] g\left(\frac{M_2^2}{M_1^2}\right)$$

$$= \frac{1}{8\pi} \frac{v^2}{M_1} \frac{M_1 M_2}{v^4} \frac{(m_3^2 - m_2^2) \mathrm{Im}\left(\sin^2 z\right)}{\left(m_2 |\cos z|^2 + m_3 |\sin z|^2\right)} \left(-\frac{3}{2} \frac{M_1}{M_2}\right) \left[1 + \frac{5M_1^2}{9M_2^2} + O\left(\frac{M_1^4}{M_2^4}\right)\right]$$

$$\simeq -\frac{3}{16\pi} \frac{M_1}{v^2} (m_3^2 - m_2^2) \frac{\mathrm{Im}\left(\sin^2 z\right)}{\left(m_2 |\cos z|^2 + m_3 |\sin z|^2\right)}$$

$$= -\frac{3}{16\pi} \frac{M_1}{v^2} (m_3^2 - m_2^2) \frac{-y}{\left(m_2 \sqrt{x^2 + y^2} + m_3 \sqrt{(1-x)^2 + y^2}\right)}$$

$$\lesssim \frac{3}{16\pi} \frac{M_1}{v^2} (m_3^2 - m_2^2) \frac{y}{\left(m_2 \sqrt{1 + y^2} + m_3 \sqrt{y^2}\right)}$$

$$\lesssim \frac{3}{16\pi} \frac{M_1}{v^2} (m_3 - m_2) \simeq 10^{-5} \left(\frac{M_1}{10^{11}\mathrm{GeV}}\right) . \quad (6.18)$$

The (BAU) today is given by

$$\eta_B = \frac{n_B}{n_\gamma} = \left(\frac{s}{n_\gamma}\right)_0 \left(\frac{n_B}{n_{B-L}}\right) \frac{n_{B-L}}{s}$$
$$\simeq 7 \times \frac{28}{79} Y_{B-L} , \quad (6.19)$$

where $n_\gamma = \frac{2\zeta(3)T_0^3}{\pi^2}$ and $s_0 = \frac{2\pi^2 g_{\star s} T_0^3}{45}$ denote present photon number and entropy densities respectively. At today $g_{\star s} = 2 + \frac{7}{8} 2 N_{\mathrm{eff}} \left(\frac{4}{11}\right) \simeq 3.9$ with a effective number of neutrino species N_{eff} close to three.

Note that if neutrino decouples instantaneously, one has $N_{\text{eff}} = 3$ and the factor $\frac{4}{11}$ orginates from the fact that $T_\nu = \left(\frac{4}{11}\right)^{1/3} T_\gamma$. And the 28/79 factor has already been discussed in Eq. (2.46). Using the BAU value reported by Planck 2018, namely Eq. (2.40) in Eq. (6.19), one has

$$\eta_B \sim 6 \times 10^{-10} \Rightarrow Y_{B-L} \sim 10^{-10}. \tag{6.20}$$

Thereafter to reproduce the measured BAU, one has to generate a $B - L$ yield around 10^{-10}. This brings to the discussions in the following sections.

6.3.1 Thermal Leptogenesis

First we assume that N_1 was merely generated by scattering of the thermal plasma after reheating. The B-L number yield, namely n_{B-L}/s is given by [54, 138]

$$Y_{B-L} = Y_{N_1}^{\text{eq}} \kappa_f \epsilon_1 = \frac{45}{\pi^4 g_{\star s}} \epsilon_1 \kappa_f. \tag{6.21}$$

As already mentioned earlier in Sec. 2.7.3, Y_{B-L} is mainly controlled the equilibrium N_1 yield, namely the numerical factor in Eq. (6.21), the CP asymmetry factor ϵ_1 and an efficiency factor (due to the washout effect from inverse decays). The efficiency factor in our setup can be written as [138]

$$\kappa_f \sim (2 \pm 1) \times 10^{-2} \left(\frac{0.01\text{eV}}{\tilde{m}_1}\right)^{1.1}, \tag{6.22}$$

where $\tilde{m}_1 = v^2 \left(Y^\dagger Y\right)_{11} / M_1 \geq m_2 \simeq 0.0086$ eV, so $\kappa_f \lesssim 10^{-2}$. More details are presented in Appendix B.

Using Eq. (6.21) with ϵ_1 given by (6.18) and the constraints on $\kappa_f \lesssim 10^{-2}$, we obtain a lower bound on M_1:

$$M_1 \gtrsim 10^{10} \text{ GeV}. \tag{6.23}$$

In order for the thermal leptogenesis to work, one has to require the reheating temperature $T_{\text{rh}} > M_1 \gtrsim 10^{10}$ GeV, as originally discussed in Ref. [91] by Davidson and Ibarra. In our model, the upper of reheating temperature can be as high as $T_{\text{rh}} \simeq 1.23 \times 10^{11}$ as depicted in Fig. 4.2, so the thermal channel is viable within our inflationary setup.

6.3.2 Non-thermal Leptogenesis

In this section we focus on the possibility that RHNs are produced non-thermally inflaton two body decays: $\phi \rightarrow N_1 N_1$ [139–144]. For lower reheating temperature with $T_{\text{rh}} < M_1$, thermal production of RHN is not viable, N_1 can nevertheless be generated via decay of inflaton $\phi \rightarrow N_1 N_1$ during reheating.[1]

---

[1] We noticed that there is a new and very interesting possibility to generate N_1 during reheating via inflaton three body decays: $\phi \rightarrow H\ell N_1$. However it turns out with this decay channel merely, *no* enough $B - L$ can be generated within the small field setup. See more details in Appendix C.

Within the regime where washout effect becomes Boltzmann suppressed by very low reheating temperature (i.e. $T_{\mathrm{rh}} < M_1$), the B-L number yield after reheating can be approximately as [141, 145]

$$Y_{B-L} = \frac{n_{B-L}}{s} = \left[\frac{3}{2} \frac{T_{\mathrm{rh}}}{m_\phi} \mathrm{BR}(\phi \to N_1 N_1) \right] \epsilon_1 , \tag{6.24}$$

where the formula within the bracket denotes the yield of N_1 from inflaton decay with BR being the corresponding branching ratio[2]. The larger BR is, the lower T_{rh} would be. In this section we will focus on the regime where inflaton dominantly decays to N_1 with BR $\simeq 1$.
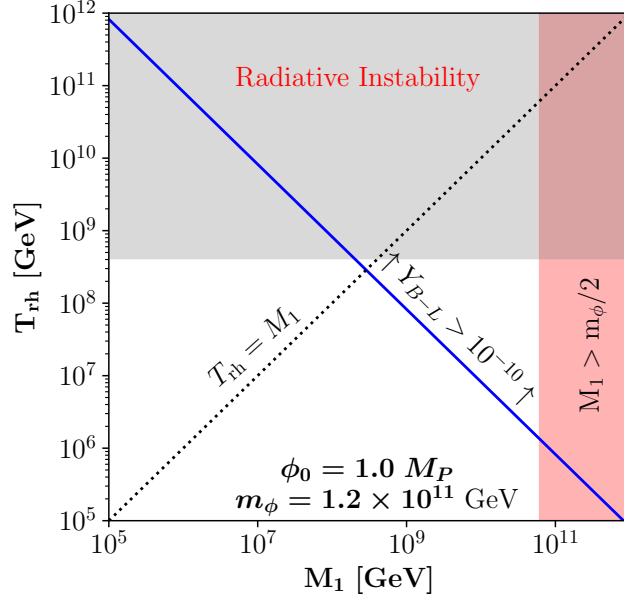

Figure 6.1: Reheating temperature T_{rh} as function of M_1 to yield the observed Baryon asymmetry via inflaton two body decays. Here we have take $\phi_0 = M_P$.

The allowed parameter space (T_{rh}, M_1) is shown in Fig. 6.1. The gray region with $T_{\mathrm{rh}} \gtrsim 4 \times 10^8$ GeV is not allowed since the radiative corrections from the N_1 loop would spoil the flatness of the inflaton potential at the near inflection point. The regime below the blue line corresponds to too small net lepton number. The red region is forbidden by the kinetic condition with $M_1 > m_\phi/2$. The black dotted line gives $T_{\mathrm{rh}} = M_1$, below which the effect of inverse decay is Boltzmann suppressed as we have assumed.

The allowed parameter space for successful leptogenesis while be consistent with both the inflationary observables and neutrino oscillation data is then

$$10^6 \text{ GeV} \lesssim T_{\mathrm{rh}} \lesssim 10^8 \text{ GeV} , \tag{6.25}$$

for reheating temperature, and the corresponding mass range for M_1 is

$$10^8 \text{ GeV} \lesssim M_1 \lesssim 10^{11} \text{ GeV} . \tag{6.26}$$

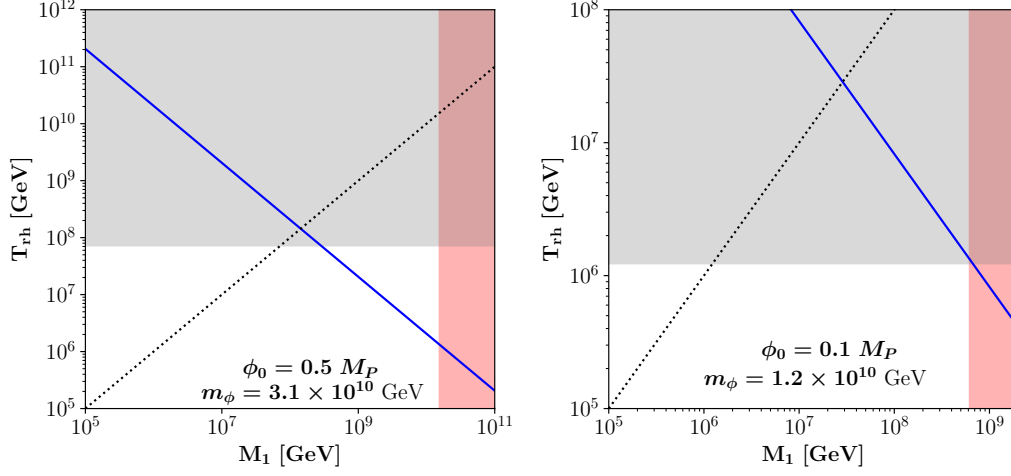[2] This is similar to Eq. (5.19) for the DM production from inflaton decay.

Figure 6.2: $T_{\rm rh}$ as function of M_1 to yield the observed Baryon asymmetry via inflaton two body decays. Here we have take $\phi_0 = 0.5\, M_P$ and $\phi_0 = 0.1\, M_P$.

Note that for different values of ϕ_0, the lowest reheating temperature constrained by Eq. (6.24) do not vary, which all correspond to the case when $M_1 \sim \frac{m_\phi}{2}$, implying $T_{\rm rh} \simeq 10^6$ GeV. Since the upper bound for reheating temperature, namely $T_{\rm rh}^{\rm max} \propto \phi_0^{5/2}$ and $m_\phi \propto \phi_0^2$, the smallest ϵ_1 (hence M_1) would corresponds to lager ϕ_0, thereafter the parameter space shown in Eqs. (6.25) and (6.26) cover the whole allowed M_1 and $T_{\rm rh}$ for all ϕ_0 ($\lesssim M_P$). For completeness, in Fig. 6.2 we show other two examples with $\phi_0 = 0.5\, M_P$ (left) and $\phi_0 = 0.1\, M_P$ (right). It turns out that for $\phi_0 \lesssim 0.1\, M_P$, no parameter space is allowed for non-thermal leptogenesis due to the radiative stability as well as kinematic threshold conditions.

6.4 Summary and Conclusions

In this chapter, we have shown that by extending the polynomial inflation model with three right handed neutrinos (RHNs), one can resolve the light neutrino masses as well Baryogenesis (via Leptogenesis) simultaneously.

Depending on the mass of the lightest RHN, one can have either thermal channel if 10^{10} GeV $\lesssim M_1 \lesssim 10^{11}$ GeV or non-thermal if 10^8 GeV $\lesssim M_1 \lesssim 10^{10}$ GeV, while being consist with neutrino oscillation data and inflationary predictions. For non-thermal leptogenesis, we found that the required reheating temperature can be as low as $T_{\rm rh} \sim O(10^6)$ GeV, which could potentially help to relax moduli problem.

We also noticed an interesting and unexplored possibility to generate N_1 during reheating via inflaton three body decays: $\phi \to H \ell N_1$. Note that once a bosonic reheating scenario is assumed, such a channel cannot be forbidden. We estimated B-L yield (shown in (C.11)) and found that with this three-body decay channel merely, *no* enough $B - L$ can be generated within the small field setup. However once the constraints on reheating temperature as well as inflaton masses are relaxed (e.g. in a large field framework), such a three-body decay channel could source the required B-L yield.

Large Field

In this chapter, we generalize the model to a large field regime. In particular we would like to explore the phenomenology of polynomial inflation with $\phi_0 \geq 1 \, M_P$. This chapter is based on Ref. [9]

This chapter is organized as follows. In Sec. 7.1, we give the general setup with emphasises on reparametrization the inflaton potential. In Sec. 7.2, methods to search for model parameters are shown; parameter space and predictions are also given. Radiative stability is analyzed in Sec. 7.3. And in sec. 7.4, we investigate eternal inflation with focus on the calculation of the scale for inflation to be eternal in the polynomial scenario. Finally, Sec. 7.5 summarizes this work. As a reminder we have set the reduced Planck mass $M_P = \sqrt{\frac{1}{8\pi G}} \simeq 2.4 \times 10^{18}$ GeV to be unity.

7.1 The Setup

In this section we first give the most general setup and inflationary analysis, and then we present the analytical results in some limits.

7.1.1 General Analysis

Action for the inflaton field in the Einstein frame is given by:

$$S = \int d^4x \sqrt{-g} \left[\frac{1}{2} g_{\mu\nu} \partial^\mu \phi \partial^\nu \phi - V(\phi) \right] , \tag{7.1}$$

where g is the determinant of the Friedmann-Robertson-Walker (FRW) metric which is defined as $g_{\mu\nu} = \text{diag}(+1, -a^2, -a^2, -a^2)$ with a denoting the scale factor. Using the Euler-Lagrange equation, one obtains the equation of motion for the classical background field:

$$\ddot{\phi} + 3\mathcal{H}\dot{\phi} - \frac{1}{a^2}\nabla^2\phi + V'(\phi) = 0 , \tag{7.2}$$

The Hubble parameter is defined by $H \equiv \frac{\dot{a}}{a}$ and determined by the Friedmann equation:

$$\mathcal{H}^2 = \frac{1}{3}\rho(\phi) = \frac{1}{3}\left[\frac{1}{2}(\dot{\phi})^2 + V(\phi) + \frac{1}{2a^2}(\nabla\phi)^2 \right] . \tag{7.3}$$

In this work we will assume the classical background ϕ is homogeneous, i.e. $\phi \equiv \phi(t)$ so that all gradient terms for the background field vanish. The potential we are considering is the general renormalizable one[1]:

$$V(\phi) = b\,\phi^2 + c\,\phi^3 + d\,\phi^4 \,. \tag{7.4}$$

To ensure the potential to be bound from below, we will consider $b > 0$, $d > 0$. Since the potential is symmetric under the transformation: $c \to -c$, $\phi \to -\phi$, in this work we will consider $c \leq 0$ without loss of generality [2]. Derivatives of the potential are given by:

$$V'(\phi) = 2b\,\phi + 3c\,\phi^2 + 4d\,\phi^3 \,; V''(\phi) = 2b + 6c\,\phi + 12d\,\phi^2 \,. \tag{7.5}$$

Suppose the potential features a saddle point at ϕ_0, and by using $V'(\phi_0) = V''(\phi_0) = 0$, one finds

$$\phi_0 = -\frac{3c}{8d} \,; b = \frac{9c^2}{32d} \,, \tag{7.6}$$

from which we learn that the ratio c/d determines the position of the saddle point. Since a potential with an exact saddle potential would be rather too flat, one can reparametrize the potential as

$$\begin{aligned} V(\phi) &= d\left[\phi^4 + \frac{c}{d}\,(1-\beta)\,\phi^3 + \frac{9}{32}\left(\frac{c}{d}\right)^2 \phi^2\right] \\ &= d\left[\phi^4 + A\,(1-\beta)\,\phi^3 + \frac{9}{32}A^2\phi^2\right] \,, \end{aligned} \tag{7.7}$$

where $A \equiv \frac{c}{d} \equiv -\frac{8}{3}\phi_0$, which roughly determines where the flat regions are. In this work, we mainly focus on the large field inflation scenario with $\phi_0 \geq 1$ and the detailed analysis for small field cases is shown in Chapter 3. The free parameter β ($0 < \beta \ll 1$) is utilized to control flatness configuration of potential in the vicinity of the plateau. If $\beta < 0$, a second minimum would exist where inflaton may get stuck so that inflation never ends thus no hot Big Bang. We do not consider the case with negative β in this work. If $\beta = 0$, one would have an exact saddle point at ϕ_0. And the larger β is, the more the potential deviates from a flat plateau ($\sim V(\phi_0)$). The parameter d determines the amplitude of the potential, which can be constrained by the power spectrum of primordial fluctuation near the plateau.

---

[1] The linear term can be shifted away. In this work, we also neglect the tiny cosmological constant term, which is sub-dominant during inflation.

[2] The two-term simper case with $c = 0$ has been investigated in Ref. [146]. In Ref. [147], the two-term scenario with radiative corrections are investigated.

To analyze inflationary predictions, the potential SR parameters shall be introduced:

$$\epsilon_{\rm v} = \frac{1}{2}\left(\frac{V'}{V}\right)^2 = \frac{2}{\phi^2}\left[\frac{9A^2 - 48A\,(\beta - 1)\,\phi + 64\phi^2}{9A^2 - 32A\,(\beta - 1)\,\phi + 32\phi^2}\right]^2 ;$$

$$\eta_{\rm v} = \frac{V''}{V} = \frac{6}{\phi^2}\left[\frac{3A^2 - 32A\,(\beta - 1)\,\phi + 64\phi^2}{9A^2 - 32A\,(\beta - 1)\,\phi + 32\phi^2}\right] ; \tag{7.8}$$

$$\xi_{\rm v}^2 = \frac{V'V'''}{V^2} = -\frac{384\,[A(\beta - 1) - 4\phi]}{\phi^3}\frac{\left(9A^2 - 48A\,(\beta - 1)\,\phi + 64\phi^2\right)}{\left(9A^2 - 32A\,(\beta - 1)\,\phi + 32\phi^2\right)^2} ,$$

which is merely function of β and A (or equivalently location of the plateau, i.e. ϕ_0). During SR inflation, all the parameters $\epsilon_{\rm v}$, $|\eta_{\rm v}|$ and $|\xi_{\rm v}^2| \ll 1$. End of inflation is defined by $\epsilon_{\rm v}(\phi_{\rm end}) = 1$. Since for larger ϕ_0 the term $9A^2 = 64\phi_0^2$ dominates over other terms in eq. (7.8) at smaller field regime, $\epsilon_{\rm v} \approx 2/\phi^2$ and $\eta_{\rm v} \approx 2/\phi^2$, hence one can approximately obtain $\phi_{\rm end} \approx 1.41$. Number of efolds for the scale $k_\star = 0.05{\rm Mpc}^{-1}$ crosses out the horizon till the end of inflation is given by[3]

$$N_{\rm CMB} = \int_{\phi_{\rm end}}^{\phi_{\rm CMB}} \frac{1}{\sqrt{2\epsilon_{\rm v}}} d\phi$$

$$\simeq \frac{1}{24}\left\{3\phi^2 - 4\phi\phi_0 + 15\phi_0^2 - \phi_0^2\sqrt{\frac{2}{\beta}}{\rm ArcTan}\left(\frac{\phi_0 - \phi}{\sqrt{2\beta}\phi_0}\right) - \phi_0^2\ln\left[(\phi_0 - \phi)^2\right]\right\}\Bigg|_{\phi_{\rm end}}^{\phi_{\rm CMB}} \tag{7.9}$$

where $\phi_{\rm CMB}$ denotes the value of the field when the scale with $k_\star = 0.05{\rm Mpc}^{-1}$ crosses out the horizon. To resolve the flatness problem, at least 50 efolds are needed. During SR inflation with a quai de Sitter spacetime, power spectrum of curvature perturbation can be approximated by

$$\mathcal{P}_\zeta = \frac{V}{24\pi^2\epsilon_{\rm v}} . \tag{7.10}$$

The spectral index and its running can be approximated as

$$n_{\rm s} = 1 - 6\epsilon_{\rm v} + 2\eta_{\rm v} \,; \alpha = 16\epsilon_{\rm v}\eta_{\rm v} - 24\epsilon_{\rm v}^2 - 2\xi_{\rm v}^2 , \tag{7.11}$$

which can be used to constrain the model parameters β and A. Tensor-to-scalar ratio r is given by

$$r = 16\epsilon_{\rm v} = \frac{32}{\phi^2}\left[\frac{9A^2 - 48A\,(\beta - 1)\,\phi + 64\phi^2}{9A^2 - 32A\,(\beta - 1)\,\phi + 32\phi^2}\right]^2 . \tag{7.12}$$

Planck 2018 measurements at the pivot scale $k_\star = 0.05{\rm Mpc}^{-1}$ with TT, TE, EE + lowE + lensing + BAO give [13]:

$$\mathcal{P}_\zeta = (2.1 \pm 0.1) \times 10^{-9} \,; n_s = 0.9659 \pm 0.0040 \,; \alpha = -0.0041 \pm 0.0067 . \tag{7.13}$$

---

[3] See Appendix E for more details.

For tensor-to-scalar ratio r, the recent BICEP/Keck 2018 results [22] offer a strong constraint on r (95% C.L.) up to date:

$$r < 0.035 \,. \tag{7.14}$$

The constraints on r^4 and n_s (adapted from Ref. [22]) are further shown in Fig. 7.1, where we also depict three parameter sets of (7.7) predicting $O(10^{-3}) \lesssim r \lesssim O(10^{-2})$, which is testable in the near future [148–151].
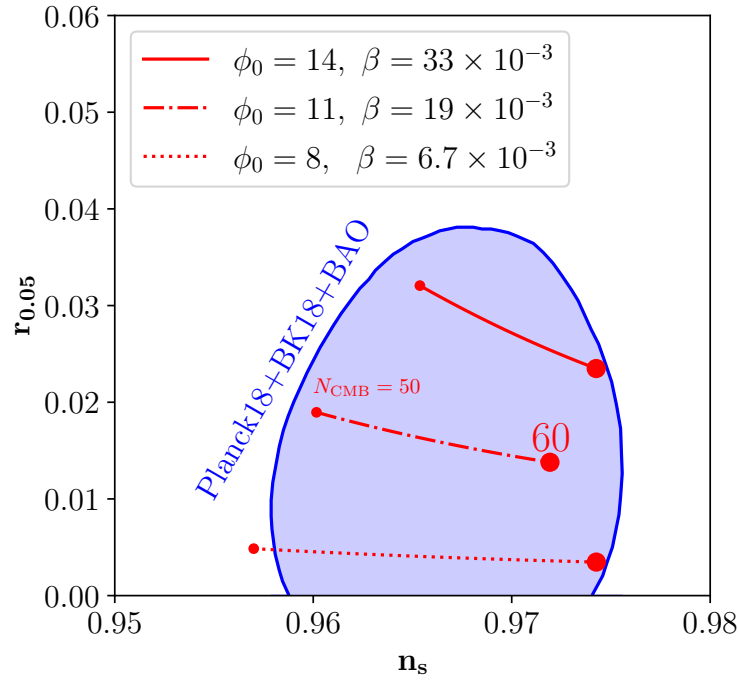

Figure 7.1: Blue curves are the current constraints for $r-n_s$ adapted from the recent BICEP/Keck 2018 results [22]. The red lines correspond to polynomial scenario (7.7) with three scenarios predicting $O(10^{-3}) \lesssim r \lesssim O(10^{-2})$ testable in the next generation CMB experiments. The small and big red dots denote $N_{\mathrm{CMB}} = 50$ and 60 respectively as usually depicted in Planck paper.

7.1.2 Analytical Approximation

In this section, we present the analytical approximation in some limit regimes.

1. $\phi \approx \phi_0$. In this regime, one could obtain analytical results for the inflationary predictions by rewriting the field as [2]:

$$\phi = \phi_0(1 - \delta) \,. \tag{7.15}$$

---

[4] Note that in the experimental literature (e.g. $r - n_s$ plot of Planck or BICEP/Keck) the bound for r is usually taken at scale with $k = 0.002 \mathrm{Mpc}^{-1}$, namely $r_{0.002}$. For pivot scale $k_\star = 0.05 \mathrm{Mpc}^{-1}$ as we are considering in this work, one has $r_{0.05} \equiv r_{0.002} \left(\frac{0.05}{0.002} \right)^{n_T} \simeq r_{0.002} \left(\frac{0.05}{0.002} \right)^{-r_{0.002}/8}$ with negligible running of tensor spectral index n_T.

Decreasing ϕ corresponds to increasing δ [5]. Since both δ and β are rather small (in practice $\beta \ll \delta \ll 1$), it will be sufficient to keep only linear term for β and up to quadratic term for δ in the analysis [6].

The SR parameters defined in (7.8) can be further approximated as [2]:

$$\epsilon_{\mathrm{v}} \simeq \frac{72\left(2\beta + \delta^2\right)^2}{\phi_0^2} ;\ \eta_{\mathrm{v}} \simeq \frac{24\left(2\beta - \delta\right)}{\phi_0^2} ;\ \xi_{\mathrm{v}}^2 \simeq \frac{288(2\beta + \delta^2)}{\phi_0^4} . \tag{7.16}$$

Number of efolds (7.9) in such case is shown to be [2]

$$
\begin{aligned}
N_{\mathrm{CMB}} &= \int_{\phi_{\mathrm{end}}}^{\phi_{\mathrm{CMB}}} \frac{1}{\sqrt{2\epsilon_{\mathrm{v}}}} d\phi \\
&= -\frac{\phi_0^2}{12} \int_{\delta_{\mathrm{end}}}^{\delta_{\mathrm{CMB}}} \frac{d\delta}{\left(2\beta + \delta^2\right)} \\
&\simeq \frac{\phi_0^2}{12\sqrt{2\beta}} \left[\frac{\pi}{2} - \mathrm{ArcTan}\left(\frac{\delta_{\mathrm{CMB}}}{\sqrt{2\beta}}\right) \right] .
\end{aligned}
\tag{7.17}
$$

Power spectrum, the spectral index and its running defined in (7.11) are approximated as [2]

$$\mathcal{P}_\zeta \simeq \frac{d\phi_0^6}{5184\pi^2(\delta^2 + 2\beta)^2} ; \tag{7.18}$$

$$n_s \simeq 1 - \frac{48\delta}{\phi_0^2} ; \tag{7.19}$$

$$\alpha \simeq -\frac{576(2\beta + \delta^2)}{\phi_0^4} . \tag{7.20}$$

And the tensor-to-scalar ratio r defined in (7.12) can be further expressed as [2]

$$r \simeq \frac{1152\left(2\beta + \delta^2\right)^2}{\phi_0^2} . \tag{7.21}$$

2. $\phi \gg \phi_0$. In this regime the quartic term dominates so that the potential becomes:

$$V \simeq d\phi^4 , \tag{7.22}$$

---

[5] We are mainly interested in the field dynamics on the left-side of ϕ_0, where the inflaton potential features concave shape so that $n_s < 1$ can be reproduced.

[6] In practice, δ^2 could be of the same magnitude of β, so one should in general keep it in the presence of linear term of β.

with which the SR parameters are shown to be

$$\epsilon_v = \frac{8 M_P^2}{\phi^2} \; ; \eta_v = \frac{12 M_P^2}{\phi^2} \, . \tag{7.23}$$

And spectral index is given by

$$n_s = 1 - 6\epsilon_v + 2\eta_v = 1 - \frac{24 M_P^2}{\phi^2} \, . \tag{7.24}$$

Considering the central value of Planck 2018 with $n_s = 0.9659$ (cf. Eq.(7.13)) , one has $\phi_{\text{CMB}} \simeq 27 M_P$, which implies $r = \frac{128 M_P^2}{\phi^2} \simeq 0.18$. The upper bound of r as shown in (7.13) rules out such a scenario.

3. $\phi > \phi_0$. In the regime with $\phi > \phi_0$ but neither $\phi \sim \phi_0$ nor $\phi \gg \phi_0$, the potential features a convex configuration, which is not favored by Planck data [93].

4. $\phi \ll \phi_0$. If $\phi \ll \phi_0$, the quadratic term in the potential cf. Eq. (7.7) dominates. In such case the model is similar as:

$$V(\phi) \simeq b \, \phi^2 \, , \tag{7.25}$$

with which the SR parameters are shown to be

$$\epsilon_v = \frac{2 M_P^2}{\phi^2} \; ; \eta_v = \frac{2 M_P^2}{\phi^2} \, . \tag{7.26}$$

And spectral index is given by

$$n_s = 1 - 6\epsilon_v + 2\eta_v = 1 - \frac{8 M_P^2}{\phi^2} \, . \tag{7.27}$$

Imposing central value of n_s measured by Planck 2018 (cf. eq.(7.13)), one has $\phi_{\text{CMB}} \simeq 15 M_P$. Prediction for tensor-to-scalar ratio is $r = \frac{32 M_P^2}{\phi^2} \simeq 0.14$, which was already disfavored.

5. $\phi < \phi_0$. In the regime with $\phi < \phi_0$ but neither with ϕ close to ϕ_0 nor $\phi \ll \phi_0$, it is possible for the potential to admit a concave shape due to the cubic term. With increase of ϕ_0, the potential is approaching to a quadratic one and correspondingly $\phi_{\text{CMB}} \to 15 M_P$. However the expansion based on $\phi - \phi_0$ (cf. Eq.(7.15)) fails and does not converge since in such cases ϕ_{CMB} is not close to ϕ_0 anymore. In this work we will investigate this regime in detail.

7.2 Model Parameters and Predictions

In this section, we first describe our methods to search for model parameters and then work out a full parameter space with predictions consistent the latest CMB experiments (7.13) and (7.14) at 2σ level.

ϕ_0	$d/10^{-14}$	$\beta/10^{-3}$	ϕ_{CMB}	n_s	$r/10^{-3}$	$\alpha/10^{-3}$	N_{CMB}
1	6.36×10^{-2}	0.0009	0.999203	0.9619	6.81×10^{-6}	−1.40	64.6
1	1.64×10^{-1}	0.0017	0.999285	0.9659	1.76×10^{-5}	−2.24	54.6
1	2.68×10^{-1}	0.0023	0.999368	0.9699	2.87×10^{-5}	−2.87	50.2
2	0.27	0.015	1.99356	0.9619	4.64×10^{-4}	−1.43	64.3
2	0.65	0.027	1.99418	0.9659	1.11×10^{-3}	−2.22	55.2
2	1.03	0.036	1.99482	0.9699	1.77×10^{-3}	−2.80	51.1
3	0.66	0.08	2.97783	0.9619	5.74×10^{-3}	−1.47	63.8
3	1.52	0.14	2.97976	0.9659	1.32×10^{-2}	−2.24	55.2
3	2.49	0.19	2.98175	0.9699	2.17×10^{-2}	−2.87	50.7
4	1.16	0.25	3.9461	0.9619	3.18×10^{-2}	−1.43	64.4
4	2.77	0.45	3.9499	0.9659	7.62×10^{-2}	−2.22	55.2
4	4.39	0.60	3.9542	0.9699	1.21×10^{-1}	−2.81	51.0
5	2.23	0.7	4.8899	0.9619	0.15	−1.55	61.9
5	4.29	1.1	4.8968	0.9659	0.29	−2.16	55.2
5	7.02	1.5	4.9037	0.9699	0.48	−2.77	50.6
8	4.54	4.0	7.4815	0.9619	2.04	−1.23	62.3
8	8.76	6.7	7.4879	0.9659	4.01	−1.72	55.0
8	13.05	9.0	7.5048	0.9699	6.07	−2.12	51.2
11	5.19	10	9.4906	0.9619	8.5	−0.84	62.1
11	9.43	19	9.4772	0.9659	16.1	−1.18	54.7
11	11.99	25	9.5432	0.9699	21.1	−1.35	52.7
14	6.93	26	10.6090	0.9619	29.8	−0.82	53.7
14	7.05	33	10.8235	0.9659	31.5	−0.83	55.3
14	7.36	41	11.0439	0.9699	34.2	−0.86	56.6
17	3.28	8	11.6109	0.9619	27.1	−0.49	61.1
17	3.43	22	11.8913	0.9659	30.0	−0.51	62.6
17	3.73	39	12.1859	0.9699	34.9	−0.55	63.6
20	2.25	3	12.4500	0.9651	32.9	−0.42	64.3
20	2.28	8	12.5183	0.9659	33.9	−0.42	64.6
20	2.30	13	12.6000	0.9668	34.7	−0.43	65.0

Table 7.1: Examples of model parameters and corresponding predictions. We have focused on those parameters predicting the central value of power spectrum, i.e. $\mathcal{P}_\zeta \simeq 2.1 \times 10^{-9}$. The predictions for n_s and α are perfectly consistent with Planck 2018 results (7.13) at 1σ level; the central value of n_s can also be obtained. Predictions for tensor-to-scalar ratio r are lower than current bound $r < 0.035$ (from the recent BICEP/Keck 2018 [22]) and range from $\mathcal{O}(10^{-8})$ to $\mathcal{O}(10^{-2})$.

7.2.1 Method to Find Model Parameters and Examples

we have learned that location of the plateau, i.e. ϕ_0, is determined by parameter A, which is treated as a free parameter in our analysis. The flatness of the plateau is shaped by β and amplitude of the plateau is controlled by d. With this in mind, a fast and convenient method to search for model parameters

is firstly to fix a ϕ_0, then search for β such that n_s and α are consistent with (7.13) at 2σ level. Of course, one should also guarantee that r is lower than the current bound. This will give a range for the inflaton field ϕ, in which ϕ_{CMB} lies. Meanwhile one shall guarantee that at least 50 efolds should be reproduced. Finally, one can use some $\mathcal{P}_\zeta > 2.1 \times 10^{-9}$ at the plateau ϕ_0 to fix the parameter d such that $\mathcal{P}_\zeta(\phi_{\mathrm{CMB}}) = 2.1 \times 10^{-9}$ (central value cf. (7.13)).

To first have some impression of the model parameters and corresponding predictions, we show a large set of examples with n_s in the vicinity of the central value in Table 7.1. The predictions for running of spectral index α agrees with (7.13) perfectly; meanwhile r ranges from $O(10^{-8})$ to $O(10^{-2})$. Besides, enough eflods can be obtained.

Now let us intuitively elaborate the dependence of predictions on the model parameters as shown in Table 7.1 in general. If one fixes ϕ_0 (or equivalently A), r tends to increase with β. Intuitively a large β corresponds to a steeper potential, thereafter r tends to be larger as well. For the spectral index, n_s increases with ϕ_{CMB}; this is because the larger ϕ_{CMB} is (or in other words the closer ϕ_{CMB} to ϕ_0), the flatter the potential would be, and further a more scale invariant power spectrum, thereafter a larger n_s is yielded (i.e. n_s becomes closer to 1). And to ensure $\mathcal{P}_\zeta = 2.1 \times 10^{-9}$, one has to lift the potential via increasing the parameter d, which is as shown in Table 7.1. Besides, N_{CMB} decreases with the increase of β; this is because the flatter the potential is, the longer it takes for the inflaton to pass the flat regime. For this reason, no enough N_{CMB} will be obtained if too large β is utilized; and rather large N_{CMB} will be generated with a very small β. In this work, we have focused on the range with $50 \lesssim N_{\mathrm{CMB}} \lesssim 65.$ [7]

7.2.2 Parameter Space

To obtain the full parameter space, we scan the four dimensional parameter $(\phi_0, \phi_{\mathrm{CMB}}, \beta, d)$ with constraints as depicted in Fig. 7.1. We have focused on predictions with power spectrum around the central value, namely $\mathcal{P}_\zeta \simeq 2.1 \times 10^{-9}$ and $50 \lesssim N_{\mathrm{CMB}} \lesssim 65$. The results are depicted in Fig. 7.2, and detailed model parameters and predictions for r, n_s with a fixed ϕ_0 are further shown in Fig. 7.3.

Upper left panel of Fig. 7.3 shows ϕ_{CMB} as function of ϕ_0. At small ϕ_0 regimes, $\phi_{\mathrm{CMB}} \simeq \phi_0$ and can be analytically obtained by:

$$\phi_{\mathrm{CMB}} = \phi_0(1 - \delta_{\mathrm{CMB}}) \simeq \phi_0 \left(1 - 7.10 \times 10^{-4} \phi_0^2 \right), \tag{7.28}$$

where we have used $\delta_{\mathrm{CMB}} \simeq 1 - \frac{\phi_0^2}{48}(1 - n_s)$ (cf. Eq.(7.19)) with $n_s = 0.9659$. The analytical approximation is shown by the red line, fitting well for the numerical results at small ϕ_0 regimes. At large ϕ_0 regimes, ϕ_{CMB} cannot be close to ϕ_0 anymore and tends to approach 12 (mainly due to the bound of r). Middle left panel of Fig. 7.3 gives β as function of ϕ_0. At small ϕ_0 regimes, analytically one has

$$\beta \simeq 1.65 \times 10^{-6} \phi_0^4, \tag{7.29}$$

with $N_{\mathrm{CMB}} = 55$ and $n_s = 0.9659$, describing well the numerical results at small ϕ_0 regimes. At a larger ϕ_0 regime, rather wide β is allowed, indicating that the predictions are (almost) independent

---

[7] It is shown that generically $N_{\mathrm{CMB}} < 65$ unless there is an exotic reheating phase following the end of inflation [152, 153]. For our case, inflation ends with a usual quadratic potential, so a standard upper value of 65 has been considered here.
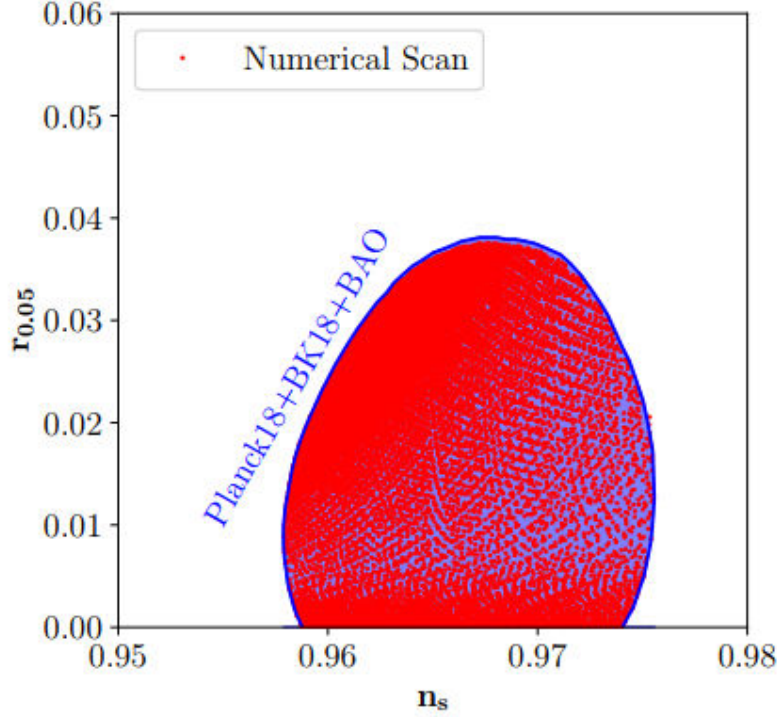
Figure 7.2: Scan of $r - n_s$.

from β once it is smaller than an upper bound. Lower left panel of Fig. 7.3 corresponds to d as function of ϕ_0. At small ϕ_0 regime, d can be analytically described as:

$$d \simeq 1.55 \times 10^{-15} \phi_0^2 \, , \tag{7.30}$$

with $\mathcal{P}_\zeta \simeq 2.1 \times 10^{-9}$, fitting well the numerical results at small ϕ_0 regimes. At the large ϕ_0 regime, smaller d is required in order to obtain the correct power spectrum. Upper right panel of Fig. 7.3 describes r as function of ϕ_0, and is given by

$$r \simeq 1.66 \times 10^{-8} \phi_0^6 \, , \tag{7.31}$$

at small ϕ_0 regimes. r increases with ϕ_0 and approaches to the current bound at large ϕ_0 regimes. Middle right panel of Fig. 7.3 is n_s as function of ϕ_0. With increase of ϕ_0, n_s tends to admit larger value in order to be consistent with the bound on r. When $\phi_0 \gtrsim 21.5$, *no* parameter space exist for $r - n_s$ being consistent with (7.13) at 2σ level. Lower right panel of Fig. 7.3 depicts N_{CMB} as function of ϕ_0. At large ϕ_0 regimes, N_{CMB} tends to be large since larger ϕ_{CMB} is required.

Let us end this section by summarizing the parameter space for the polynomial inflation model (7.7):

$$6 \times 10^{-16} \lesssim d \lesssim 2 \times 10^{-13} \, ; 0 < \beta \lesssim 4 \times 10^{-2} \, ; 1 \lesssim \phi_0 \lesssim 21.5 \, . \tag{7.32}$$
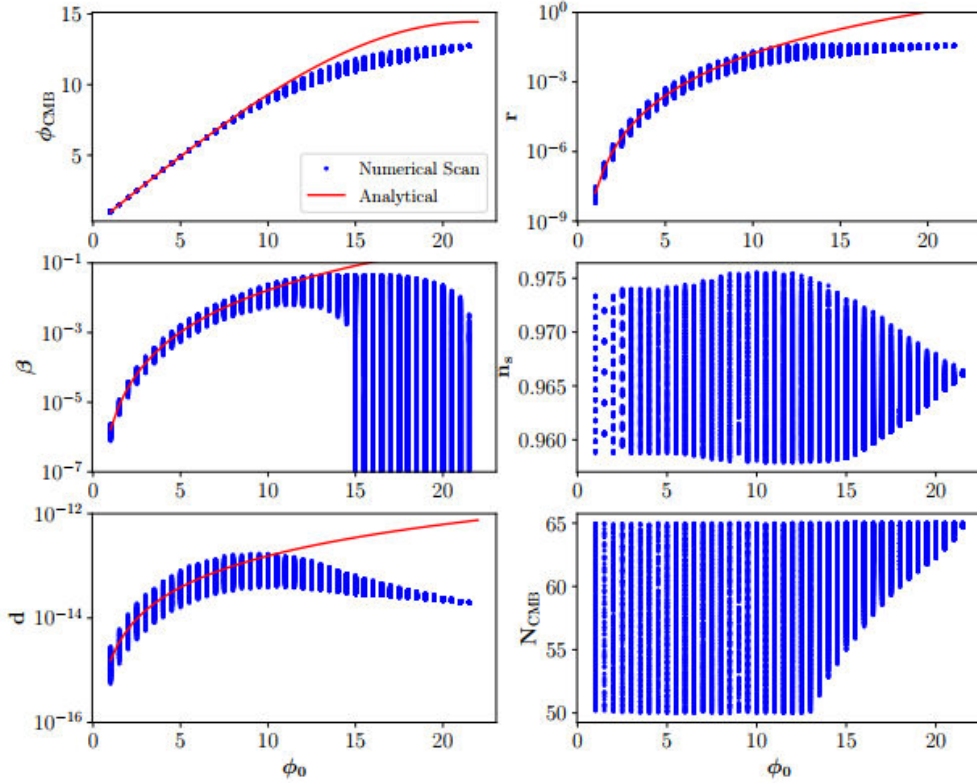
Figure 7.3: Blue dots represent scan of model parameters and predictions. Red line depicts an analytical approximation with a fixed n_s, $N_{\rm CMB}$ and $\mathcal{P}_\zeta$ as described in the text.

Since we have defined $A = -8\phi_0/3$, one also has a parameter space for A: $-57 \lesssim A \lesssim -3$. Predictions for n_s and α with parameters in (7.32) perfectly agree with Planck 2018 (7.13) at 2σ level; meanwhile the tensor-to-scalar ratio r ranges from $\mathcal{O}(10^{-8})$ to $\mathcal{O}(10^{-2})$. To our knowledge, this is the first time to work out such a comprehensive parameter space for polynomial inflation scenario [8]. Our results, in particular the upper bound of ϕ_0, can be further constrained once a more precise bound for r is obtained by next generation CMB experiments in the future.

7.3 Radiative Stability

In the last section we have found a rather full model parameter space. Now let us discuss the radiative stability of the polynomial inflation model with parameters in (7.32). One has to make sure that the loop corrections do not spoil the inflationary predictions. To this end one can first compute the leading order 1-loop Coleman-Weinberg (CW) potential(s) [111] and then require that they are subdominant compared to the tree-level potential, which guarantees the inflationary predictions. One can find

---

[8] This is the most complete parameter space for large field inflation scenario in polynomial model, and a detailed analysis for small field case is investigated in Chapter 3.

detailed procedures in Ref. [2]. First of all, for the inflaton self-couplings, it turns out that one requires

$$\left| \frac{d^2 \ln(16d\beta)}{\pi^2} \right| < 8d\beta \,, \tag{7.33}$$

which is always satisfied unless $\beta \ll d$. As depicted in Fig. 7.3, when $\phi_0 \gtrsim 14.5$, β can feature a small value. Note that there typically is $d \sim 10^{-14}$, implying that when $\beta \lesssim \mathcal{O}(10^{-14})$ the above inequality is saturated.

7.3.1 Reheating

On the other hand, the inflaton field has to couple to external particles for reheating. Here we assume ϕ couples to daughter particles with trilinear couplings in order to fully drain the inflaton energy so that a radiation dominated epoch is reproduced after reheating. For a scalar field ϕ', e.g. the standard model Higgs field, we introduce $\sim g\phi|\phi'|^2$ and for the Fermionic field χ, e.g. right-handed neutrino, we extend the model with a coupling $\sim y\phi\bar{\chi}\chi$. Applying the radiative stability conditions [2], one has:

$$\left| \frac{y^4 - 3y^4 \ln(y^2)}{4\pi^2} \right| < 16d\beta \,; \tag{7.34}$$

$$\frac{1}{8\pi^2} \left(\frac{g}{\phi_0} \right)^2 \left| \ln\left(\frac{g}{\phi_0} \right) - 1 \right| < 8d\beta \,. \tag{7.35}$$

For typical value of $d \sim 10^{-14}$ and $\beta \lesssim \beta^{\text{max}} \simeq 4 \times 10^{-2}$ (cf. Eq. (7.32)), one has

$$y \lesssim y^{\text{max}} \simeq 2.7 \times 10^{-4} \,; \tag{7.36}$$

$$\left(\frac{g}{\phi_0} \right) \lesssim \left(\frac{g}{\phi_0} \right)^{\text{max}} \simeq 1.2 \times 10^{-7} \,. \tag{7.37}$$

With the bounds on the couplings, one can further calculate the reheating temperature. Here we estimate the reheating temperature by utilizing the instantaneous decay approximation, with which one has [2]

$$T_{\text{rh}} \simeq 1.41 g_\star^{-1/4} \Gamma_\phi^{1/2} \,. \tag{7.38}$$

For the fermionic reheating channel, the reheating temperature is given by

$$T_{\text{rh}}^\chi \simeq 1.41 g_\star^{-1/4} \left(2\phi_0 \frac{y^2}{8\pi} \sqrt{d} \right)^{1/2} \lesssim 1.1 \times 10^{11} \text{ GeV} \,, \tag{7.39}$$

where we have considered $\phi_0 \simeq 20$, $g_\star = 106.75$ and Eq. (7.36) for upper bound on y. For the bosonic scenario,

$$T_{\text{rh}}^{\phi'} \simeq 1.41 g_\star^{-1/4} \left(\frac{g^2}{8\pi \, 2\phi_0 \sqrt{d}} \right)^{1/2} \lesssim 2.5 \times 10^{14} \text{ GeV} \,, \tag{7.40}$$

where the maximum value g^{max} reported in Eq. (7.37) has been utilized.

7.4 Eternal Polynomial Inflation

In previous sections, we have worked out the parameter space consistent with Planck 2018 (7.13) and BICEP/Keck 2018 (7.14) and and investigated the radiative stability for the polynomial inflation model. In this section we are devoted to investigating eternal inflation with a particular focus on the scale for inflation to be eternal using the parameter space we have found.

7.4.1 Eternal Phase I

During the SR phase, one can neglect the acceleration term in eq. (7.2), so that inflaton field evolves as

$$\dot{\phi} \approx -\frac{V'(\phi)}{3\mathcal{H}}\,, \tag{7.41}$$

leading to the classical field excursion during per Hubble time given by

$$\Delta\phi_{\text{cla}} = \frac{|\dot{\phi}|}{\mathcal{H}} \approx \frac{|V'(\phi)|}{3\mathcal{H}^2} \approx \frac{|V'(\phi)|}{V} = \sqrt{2\epsilon_{\text{v}}}\,. \tag{7.42}$$

Quantum fluctuation is assumed to follow a Gaussian probability distribution. In the quasi de Sitter background during SR inflation, typical size for quantum fluctuation over one Hubble time is given by $\delta\phi_{\text{qu}} = \frac{\mathcal{H}}{2\pi}$ [154, 155]. Eternal inflation can occur once the quantum fluctuation dominates over the classical field excursion, i.e. $\delta\phi_{\text{qu}} > \Delta\phi_{\text{cal}}$. In this case, it is possible that the quantum fluctuation driving the inflaton field to move uphill relative to the classical trajectory, leading to inflation may not end. By using (7.42) and $\delta\phi_{\text{qu}} = \frac{\mathcal{H}}{2\pi}$, one finds condition for eternal inflation is

$$\frac{\mathcal{H}}{2\pi} > \sqrt{2\epsilon_{\text{v}}} \Leftrightarrow \frac{\mathcal{H}^2}{8\pi^2\epsilon_{\text{v}}} > 1\,, \tag{7.43}$$

from which one sees that the condition for eternal inflation is identical to the case where the amplitude of curvature perturbation $\mathcal{P}_\zeta$ exceeds unity [156].

At large field regimes, effectively the polynomial inflation scenario behaves like quartic inflation similar as monomial $\lambda\phi^4$ inflation, as one can neglect the sub-dominated terms: $\sim A^2\phi^2$ and $\sim A\phi^3$ in (7.7). In this case, our model is simplified to be $V = d\,\phi^4$, and it is easy to show that:

$$\mathcal{H} = \sqrt{\frac{d}{3}}\phi^2\,, \tag{7.44}$$

and

$$\frac{\mathcal{H}^2}{8\pi^2\epsilon_{\text{v}}} = \frac{d\phi^6}{192\pi^2}\,. \tag{7.45}$$

Using the eternal conditions cf. Eq. (7.43), one finds the inflaton field should satisfy

$$\phi^2 > \left(\frac{192\pi^2}{d}\right)^{1/3} , \qquad (7.46)$$

corresponding to a threshold for Hubble parameter

$$\mathcal{H}^{\text{c}}_{\text{EI}} = 4\pi^{2/3} \left(\frac{d}{3}\right)^{1/6} , \qquad (7.47)$$

which depends merely on d. Once $\mathcal{H} > \mathcal{H}^{\text{c}}_{\text{EI}}$, an eternal inflationary phase can occur.

For the usual monomial chaotic $\lambda\phi^4$ inflation model with $\lambda \sim 10^{-12}$ [84] (to match the power spectrum), one can work out the threshold $\mathcal{H}^{\text{c}\prime}_{\text{EI}} \approx 0.07$ using the eq. (7.47). For the polynomial scenario, as we have shown in last section, the allowed range for d is: $6 \times 10^{-16} \lesssim d \lesssim 2 \times 10^{-13}$ in order to be consistent with Planck 2018 (7.13). Thereafter we find for the polynomial inflation model, the threshold for value of inflaton field is (in Planckian unit):

$$460 \lesssim \phi_{\text{c}} \lesssim 1211 , \qquad (7.48)$$

which justifies our previous approximation by neglecting $\sim A^2\phi^2$ and $\sim A\phi^3$ terms with $-57 \lesssim A \lesssim -3$. One can further work out the threshold of the corresponding inflationary scale (again in Planckian unit) :

$$0.02 \lesssim \mathcal{H}^{\text{c}}_{\text{EI}} \lesssim 0.05 , \qquad (7.49)$$

corresponding to an energy scale well below that in the Planckian, hence validating our above semi-classical estimation for the eternal scale without worrying about the quantum gravity effect.

We now end this section with a conclusion that eternal inflation can appear for the polynomial inflation models with predictions consistent with Planck 2018 (7.13). Besides, we find that even though the polynomial scenario behaves similar as the usual monomial $\lambda\phi^4$ model in large field regimes, the scale for inflation to be eternal in polynomial model is (slightly) lower than that in monomial $\lambda\phi^4$ model.

7.4.2 Eternal Phase II

The discussion in the previous section is one possibility for inflation to be eternal in the polynomial scenario. Now let us investigate another possibility. We have shown in Fig. 7.3 that the allowed parameter β can be as small as closing to zero in large ϕ_0 regimes. In the case where the potential features a very flat configuration near ϕ_0 with $\beta \to 0$, it is possible that the inflaton field may stay at ϕ_0 forever. Thereafter it is expected that a (second) eternal phase can also occur.

Since this eternal phase appears when the inflaton is in vicinity of saddle point ϕ_0, which is much smaller than those ϕ_{c} analyzed above, one can expect that the corresponding scale should be much lower than $\mathcal{H}^{\text{c}}_{\text{EI}}$ analyzed above.[9]

---

[9] This is similar as the eternal hilltop inflation as investigated in [156]. In our case, the inflaton first rolls down to a plateau around the saddle point similar as a very flat local hilltop, around which eternal inflation may occur.

To work out scale near the saddle point ϕ_0 where inflation is expected to be eternal, one can first compute $V(\phi_0)$ via eq. (7.7):

$$V(\phi_0) = d\left(\phi_0^4 + A\phi_0^3 + \frac{9}{32}A^2\phi_0^2\right) = \frac{1}{3}d\phi_0^4,\tag{7.50}$$

where we have neglected β and utilized $A = -8\phi_0/3$. With this we obtain

$$\mathcal{H}_{\text{EI}} = \sqrt{\frac{V(\phi_0)}{3}} = \frac{\sqrt{d}}{3}\phi_0^2,\tag{7.51}$$

which depends on both the parameter d and location of the saddle point ϕ_0. To obtain the rough magnitude of $\mathcal{H}_{\text{EI}}$, let us take $\phi_0 \sim 20$ with typical value of parameter $d \sim O(10^{-14})$ (cf Fig. 7.3), one then obtains:

$$\mathcal{H}_{\text{EI}} \sim 2 \times 10^{-5},\tag{7.52}$$

which is at least *three* magnitude smaller than the one given in (7.49). To obtain the magnitude of β needed in order to have the second eternal phase, we again use the eternal condition Eq. (7.43), identical to the power spectrum being larger than unity as mentioned earlier. Using $\delta \sim 0$, $d \sim 10^{-14}$, $\phi_0 \sim 20$ in (7.18), one finds $\beta \lesssim O(10^{-6})$ is needed.
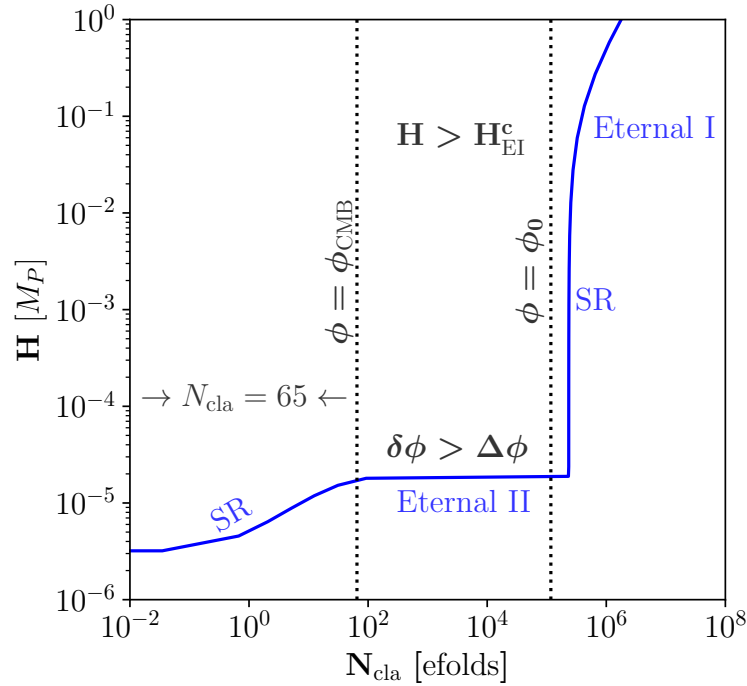
Figure 7.4: Evolution of Hubble parameter as functions of efolds N (depending on ϕ via Eq. (7.9)) with model parameter: $\phi_0 = 20$, $\beta = 10^{-7}$ and $d \simeq 2 \times 10^{-14}$. The gray region with $\mathcal{H} > \mathcal{H}_{\text{EI}}^c \simeq 0.04\, M_P$ denotes the corresponding scale where inflation can be eternal. Below that $\mathcal{H}_{\text{EI}}^c$, the usual SR inflation follows. Later ϕ rolls to the regime around ϕ_0, a second eternal phase may occur with a Hubble parameter as low as $\mathcal{H} \sim O(10^{-5})$.

Looking at Fig. 7.3 , one can conclude that model parameters (a subset of (7.32)) with:

$$15 \lesssim \phi_0 \lesssim 21.5 \, ; 0 < \beta \lesssim O(10^{-6}) \, ; 2 \times 10^{-14} \lesssim d \lesssim 6 \times 10^{-14} \, , \tag{7.53}$$

satisfying all constraints to have a second eternal inflationary phase. For model parameter in this subset, two stages of eternal inflation can appear; the first one can occur once the scale is above $\mathcal{H}_{\mathrm{EI}}^{\mathrm{c}} \sim O(10^{-2})$ while the second can appear near the saddle point with a rather low energy scale $\mathcal{H}_{\mathrm{EI}} \sim O(10^{-5})$. One example is shown in Fig. 7.4. To our knowledge, this is the first time to discover such phenomena in a specific inflation model, namely a model supporting *two distinct* eternal epochs.

Note that the second eternal phase can only appear at larger ϕ_0 regimes (cf. (7.53)), in which case the predictions for $r \sim O(10^{-2})$. This means that our finding regarding the (unusual) low scale second eternal phase can be tested by the next generation CMB experiments e.g. CORE [148], AliCPT [150], LiteBIRD [149] , CMB-S4 [151] which could reach $r \sim O(10^{-3})$.

7.5 Summary and Conclusions

In this chapter, we revisited the large field inflation with a polynomial of degree four with a near saddle point at ϕ_0, featuring a concave configuration, which is favoured by the Planck 2018 data.

In Sec. 7.1 we give the general setup for our analysis. We introduce three parameters: d, A and β to reparameterize the potential. Parameter d determines the overall amplitude of the potential, which is constrained by the power spectrum of curvature perturbation $\mathcal{P}_\zeta$. Parameter A gives location of (near) saddle point via $A = -\frac{8}{3}\phi_0$, and the parameter β shapes the flatness configuration of the potential in the vicinity of the saddle point. If $\beta = 0$, there is an exact saddle point at ϕ_0; the potential is less flat with larger β. In this work $0 < \beta \ll 1$ is considered. We also show that in the regime with $\phi \approx \phi_0$, one can derive analytical results for the inflationary predictions.

In Sec. 7.2 we are devoted to the search for a full parameter space consistent with most recent Planck and BICEP/Keck 2018 2σ level (cf. (7.13) and (7.14)), which is summarized in (7.32). The predictions for r range $O(10^{-8})$ to $O(10^{-2})$ and $\alpha \sim -O(10^{-3})$, which are testable in the near future. A very large set of examples are also given in Table 7.1. *To our knowledge, this is the first time to work out such a comprehensive parameter space by considering the most recent CMB data in polynomial scenario.* Our result (7.32), in particular the upper bound of ϕ_0, can be further constrained with more precise cosmic microwave background (CMB) experiments, such as CORE [148], AliCPT [150], LiteBIRD [149], CMB-S4 [151] which could reach $r \sim O(10^{-3})$.

In Sec. 7.3 we investigate radiative stability of the inflaton potential near the inflection-point ϕ_0. To that end, we write down the leading order 1-loop Coleman-Weinberg (CW) potential by considering a self-interacting real inflaon field. We find the tree-level potential is stable against loop correction for $d \ll \beta$, which is rather wide within the parameter space (7.32).

In Sec. 7.4, we study the scale of eternal inflation within the parameter space (7.32). Generally this can happen at a large scale. In a polynomial scenario, we find that eternal inflation can appear if the Hubble parameter is above a threshold $0.02 \lesssim \mathcal{H}_{\mathrm{EI}}^{\mathrm{c}} \lesssim 0.05$. We also show that even though the polynomial scenario behaves similar as the usual monomial $\lambda\phi^4$ model in large field regime, the threshold for inflation to be eternal in the polynomial scenario is lower in polynomial scenario than that in monomial $\lambda\phi^4$ (with $\mathcal{H}_{\mathrm{EI}}^{\mathrm{c}\prime} \approx 0.07$). More interestingly, we find there exists another possibility to realize eternal inflation in a polynomial scenario. This occurs when the potential admits a rather

flat configuration ϕ_0, in which case the quantum fluctuations can dominate over the classical evolution. Since ϕ_0 is not at the large field regimes, the scale for eternal inflation can be rather low. We show that for the full parameter space (7.32), there exists a subset (7.53) allowing such a possibility. The scale for eternal inflation in this case can be as low as $\mathcal{H} \sim O(10^{-5})$, and is of the same magnitude as that when the scale with $k_\star = 0.05\mathrm{Mpc}^{-1}$ crosses out the horizon. Note that in this subset there is another eternal scale with $\mathcal{H} \gtrsim O(10^{-2})$. In other words, there can be two phases of eternal inflation with scales at least three magnitudes differences. In this picture, eternal inflation appears at a very high scale, which is then followed by the usual non-eternal SR inflation. After that, eternal inflation can appear again when inflaton enters the rather flat part of the potential with a very low scale as shown in Fig. 7.4. *To the best of our knowledge, this is the first time to discover this kind of phenomenon in a concrete inflation model.* After showing inflation is also inevitable to be eternal for polynomial scenarios, we briefly discuss its further implications on initial conditions.

In summary, we have presented a successful large field polynomial model; worked out a comprehensive parameter space (7.32) and offered the corresponding inflationary predictions, in particular the tensor-to-scalar ratio r. Our analysis here together with the small field model investigated in Chapter 3 offers the most complete analysis for the polynomial inflation model after Planck and BICEP/Keck 2018. In this work we pointed out for the first time that two eternal phases with rather large scale hierarchy can appear in the inflationary history of the early Universe for a specific model.

Conclusion and Outlook

8.1 Conclusions

Cosmic inflation neatly resolves problems in standard cosmology. The most simple inflationary theory invokes a monomial potential of a form $\sim \phi^p$ for a single scalar field. However, the latest cosmic microwave background (CMB) experiments have ruled out these monomial inflationary scenarios, as they predict too large tensor-to-scalar ratio [22]. The next simple model would be a polynomial potential. Indeed if one assumes the inflaton field to be a sector in some UV complete theory, then in general all renormalizable terms in the potential shall be considered rather than a single term merely.

In this thesis, we have revisited the polynomial scenario with a renormalizable potential featuring a near inflection-point at ϕ_0 by confronting it to the latest CMB experiments. At small field regime, it turns out one can derive analytical results for power spectrum $\mathcal{P}_\zeta$, spectral index n_s, the running α, as well as the tensor-to-scalar ratio r. By considering the constraints on reheating temperature and radiative stability condition on the inflaton potential (near ϕ_0), we were able to derive a lower bound on location of the near inflection-point: $\phi_0 \gtrsim 3 \times 10^{-5} \, M_P$. The prediction for the tensor-to-scalar ratio is very small and takes a form $r \simeq 7.09 \times 10^{-9} (\phi_0/M_P)^6$, in the same fate as other small field inflation models; however the prediction for the running is $\alpha \simeq -1.43 \times 10^{-3}$, which is independent from ϕ_0 and testable in the near future.

To argue that a thermal Universe with sufficiently high temperature can be reproduced after polynomial inflation, we then consider reheating from inflaton decays to either bosons or fermions. We find that reheating temperature can lie between its lower bound of ~ 4 MeV and about $4 \times 10^8 (10^{11})$ GeV for fermionic (bosonic) reheating scenarios.

To show that dark matter (DM) problems can be easily resolved in the framework of polynomial inflation, we extend the model with a singlet field, which can be generated from *i*) direct decay of inflatons, *ii*) 2-to-2 annihilations of inflatons during the reheating era (mediated by the *s*-channel exchange of inflatons or gravitons, and the *t*-channel exchange of DM), and *iii*) 2-to-2 annihilations of SM particles mediated by gravitons and inflatons as shown in Fig. 5.1. With gravitational channels only, we found that one could not source enough DM density to match the measured value due to the radiative bound on reheating temperature. For the non-gravitational processes, direct decay always dominates. We find that DM field with mass in the range: O (KeV) $\lesssim m_\chi \lesssim O(10^{11})$ GeV can account for the correct relic density while being consistent with inflationary predictions and constraints from Lyman$-\alpha$ and kinematic threshold.

To demonstrate the aftermath of polynomial inflation can also resolve Baryogenesis, we consider the most simple scenario via leptogenesis. To this end, we extend the model with three right-handed-neutrinos (RHNs). Depending on the mass of the lightest RHN M_1, one can have either thermal channel if 10^{10} GeV $\lesssim M_1 \lesssim 10^{11}$ GeV or non-thermal if 10^8 GeV $\lesssim M_1 \lesssim 10^{10}$ GeV, while being consist with neutrino oscillation data and inflationary predictions. For non-thermal leptogenesis, we found that the required reheating temperature can be as low as $T_{\rm rh} \sim O(10^6)$ GeV, which could potentially help to relax moduli problem.

Finally we argue that if a large field version, namely $\phi_0 \geq 1$ of this model is admissible, the prediction for the gravitational wave or tensor-to-scalar ratio is testable in the near future. We also worked out the parameter space for the large field model, and found that $\phi_0 \lesssim 21.5$ in the Planckian unit in order to satisfy the current CMB experiment bounds.

8.2 Outlook

Here we list several interesting directions deserving further detailed studies.

- Realize polynomial inflation in supersymmetry framework.

  In current work, we have limited to the non-supersymmetric case. It would be tempting to realize the polynomial inflation scenario in the well motivated supersymmetry framework, in particular supergravity. For inflation model based on supergravity, one potential problem to overcome is the so-called η problem associated the spontaneously breaking of supersymmetry due to the requirement that the inflaton potential has to be positive.[1]

- Analyze DM production and leptogenesis in a large field model.

  We have showed that in large field scenario, the corresponding inflationary tensor-to-scalar ratio r (which is a function of ϕ_0 hence inflaton mass) is testable; this brings an interesting idea that utilizing r to constrain DM and leptogenesis from inflaton decays. Besides, as estimated in Appendix C, in the large field scenario the inflaton three-body decay could give rise to new and interesting contributions to leptogenesis.

- Fit CMB anomalies at large scale with inflaton overshooting.

  The success of the polynomial model is based on the assumption of existence of a near inflection-point ϕ_0. And it is expected that there is an overshooting behavior when inflaton approaches ϕ_0 (from $\phi > \phi_0$). Such overshooting would lead to a failure of slow-roll and hence a (sizable) breaking down of scale invariance of power spectrum. This is expected to leave some imprints in the CMB power spectrum at large scale. Indeed there exists some localised features, see e.g. around $l \sim 22$ in Fig. 1.3. It is thereafter interesting to investigate whether the overshooting behavior in the polynomial infaltion could offer better fit to the temperature power spectrum at large scale[2].

---

[1] In Appendix F we revisit inflation in Supergravity.

[2] It have been shown that, the power spectrum can feature both a dip and bump with an overshooting phase [1].

8.3 Contributions to Literature

In summary, this thesis has offered, for the first time, the most complete analysis for polynomial inflation to date. Our scenario, as the next simple single-field inflation model, fits well with current CMB data and is testable in the near future. We also showed that polynomial inflation with simple extensions can easily *i*) reproduce a thermal Universe with high enough reheating temperature, *ii*) give rise to successful generation of DM as well as Baryogenesis (via Leptogenesis). With these arguments, we would like to end this work with a statement that *polynomial inflation is indeed an acceptable cosmological model!* The current work also brings some new and interesting directions deserving future detailed studies[3].

---

[3] Good science usually offers new avenues except resolving the existing problems.

Dark Matter Production from Gravitational Inflaton Annihilation

In this chapter, we present the calculation for gravitational dark matter production from annihilation of inflatons during reheating [121]. In particular we offer the detailed computations for the scattering rate of inflaton annihilation to a pair of fermionic DM particles as shown on Fig. A.1. We collect
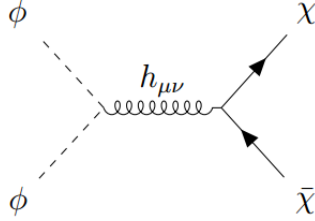
Figure A.1: Feynman diagrams for the DM production from gravitational annihilation of inflatons: $\phi(p_1)\,\phi(p_2) \to h_{\mu\nu}(q) \to \chi(p_3)\,\bar\chi(p_4)$.

relevant vertices from Refs. [123, 157], and they are given by:

$$-\frac{i}{2M_P}\left[p_{1\mu}p_{2\nu} + p_{1\nu}p_{2\mu} - \eta_{\mu\nu}\left(p_1 \cdot p_2 + m_\phi^2\right)\right] \tag{A.1}$$

for $\phi\phi h_{\mu\nu}$ and

$$-\frac{i}{4M_P}\left[\left(p_3 - p_4\right)_\mu \gamma_\nu + \left(p_3 - p_4\right)_\nu \gamma_\mu - 2\eta_{\mu\nu}\left(\slashed{p}_3 - \slashed{p}_4 - 2m_\chi\right)\right] \tag{A.2}$$

for $\bar\chi\chi h_{\mu\nu}$. The amplitude can be parametrized as:

$$\mathcal{M}^{\phi\chi} \propto \mathcal{M}_\phi^{\mu\nu}\Pi^{\mu\nu\rho\sigma}\mathcal{M}_{\rho\sigma}^\chi \,, \tag{A.3}$$

where the propagator is:

$$\Pi^{\mu\nu\rho\sigma} = \frac{1}{2q^2}\left(\eta^{\rho\nu}\eta^{\sigma\mu} + \eta^{\rho\mu}\eta^{\sigma\nu} - \eta^{\rho\sigma}\eta^{\mu\nu}\right) \,. \tag{A.4}$$

And relevant partial amplitudes are:

$$
\begin{aligned}
\mathcal{M}^{\mu\nu}_{\phi} &= \frac{1}{2}\left(p_{1\mu}p_{2\nu} + p_{1\nu}p_{2\mu} - \eta_{\mu\nu}p_1 \cdot p_2 - \eta_{\mu\nu}m_{\phi}^2 \right) ; \\
\mathcal{M}^{\chi}_{\rho\sigma} &= \frac{1}{4}\bar{v}\left(p_4 \right)\left[\gamma_\rho \left(p_3 - p_4 \right)_\sigma + \gamma_\sigma \left(p_3 - p_4 \right)_\rho \right] u\left(p_3 \right) .
\end{aligned}
$$
(A.5)

Thereafter the scattering amplitude in Eq. (A.3) is:

$$
\begin{aligned}
\mathcal{M}^{\phi\chi} \propto & \frac{1}{2}\left(p_{1\mu}p_{2\nu} + p_{1\nu}p_{2\mu} - \eta_{\mu\nu}p_1 \cdot p_2 - \eta_{\mu\nu}m_{\phi}^2 \right) \\
& \cdot \frac{1}{2q^2}\left(\eta^{\rho\nu}\eta^{\sigma\mu} + \eta^{\rho\mu}\eta^{\sigma\nu} - \eta^{\rho\sigma}\eta^{\mu\nu} \right) \cdot \frac{1}{4}\bar{v}\left(p_4 \right)\left[\gamma_\rho \left(p_3 - p_4 \right)_\sigma + \gamma_\sigma \left(p_3 - p_4 \right)_\rho \right] u\left(p_3 \right) \\
& = \frac{1}{16q^2}4 \cdot \bar{v}\left(p_4 \right)\left[\not{p}_2 p_1 \cdot \left(p_3 - p_4 \right) + \not{p}_1 p_2 \cdot \left(p_3 - p_4 \right) + m_{\phi}^2\left(\not{p}_3 - \not{p}_4 \right) \right] u\left(p_3 \right) .
\end{aligned}
$$
(A.6)

Since $p_1, p_2 = (m_\phi, 0)$, $p_3 = (m_\phi, \vec{p})$ and $p_4 = (m_\phi, -\vec{p})$, one has $p_1 \cdot (p_3 - p_4) = 0$, $p_2 \cdot (p_3 - p_4) = 0$ and $q^2 = (p_1 + p_2)^2 = 4m_\phi^2$. Thereafter the squared amplitude (after including the $1/M_P$ factor in each vertex):

$$
\begin{aligned}
\sum_{s_3, s_4} |\mathcal{M}|^2 &= \frac{1}{256\, M_P^4\, m_\phi^4} \cdot \mathrm{Tr}\left[m_\phi^2(\not{p}_3 - \not{p}_4)\,(\not{p}_3 + m_\chi)\, m_\phi^2(\not{p}_3 - \not{p}_4)\,(\not{p}_4 - m_\chi) \right] \\
&= \frac{1}{256\, M_P^4}\mathrm{Tr}\left[(\not{p}_3 - \not{p}_4)\not{p}_3(\not{p}_3 - \not{p}_4)\not{p}_4 - m_\chi^2(\not{p}_3 - \not{p}_4)^2 \right] \\
&= \frac{1}{256\, M_P^4}\mathrm{Tr}\left[4\left(2m_\chi^2(p_3 \cdot p_4) - 2m_\chi^4 \right) - m_\chi^2\left(8m_\chi^2 - 8(p_3 \cdot p_4) \right) \right] \\
&= \frac{1}{256\, M_P^4}\left[4\left(4m_\chi^2 m_\phi^2 - 4m_\chi^4 \right) - m_\chi^2(8m_\chi^2 - 8(2m_\phi^2 - m_\chi^2)) \right] \\
&= \frac{1}{128\, M_P^4}m_\chi^2(m_\phi^2 - m_\chi^2) ,
\end{aligned}
$$
(A.7)

where s_3, s_4 denotes the spins for the final states; $p_3 \cdot p_4 = 2m_\phi^2 - m_\chi^2$ has been used in the last second step. The $2 - 2$ cross section in the center of mass frame is

$$
(\sigma v) = \frac{1}{64\pi^2 m_\phi^2}\frac{|\vec{p}_f|}{\sqrt{s}}\int |\mathcal{M}|^2 d\Omega ,
$$
(A.8)

where the amplitude of the momentum for the final state is

$$
|\vec{p}_f| = \frac{\sqrt{s}}{2}\sqrt{1 - \frac{4m_\chi^2}{s}} .
$$
(A.9)

Plugging Eq. (A.7) into Eq. (A.8), one has

$$(\sigma v) = \frac{|\mathcal{M}|^2}{32\pi\, m_\phi^2} \sqrt{1 - \frac{m_\chi^2}{m_\phi^2}} \, , \tag{A.10}$$

with which one can further compute the interaction rate density $\gamma = (\sigma v) n_\phi^2$ as reported in Eq. (5.24).

Thermal Leptogenesis and Boltzmann Equations

In this chapter we revisit the Boltzmann equations for thermal leptogenesis and estimation for the $B - L$ yield in strong washout regime, which is favored by current neutrino oscillation data.

Evolution of RHN number density n_{N_1} is governed by the Boltzmann equation:

$$\frac{dn_{N_1}}{dt} + 3Hn_{N_1} = -\Gamma \left(n_{N_1} - n_{N_1}^{\text{eq}} \right) , \tag{B.1}$$

where Γ denotes the thermal averaged decay rate

$$\Gamma = \frac{K_1(M_1/T)}{K_2(M_1/T)} \frac{\left(Y^\dagger Y \right)_{11}}{8\pi} M_1 , \tag{B.2}$$

with K_1, K_2 denoting the modified Bessel function of the second kind. For convenience, we define $z \equiv M_1/T$. The equilibrium N_1 number density is given by [113]

$$n_{N_1}^{eq} = \frac{g\,T^3}{2\pi^2} z^2 K_2(z) \simeq \begin{cases} \frac{g\,T^3}{\pi^2} & \text{for } T \gg M_1 \, ; \\ g\left(\frac{M_1 T}{2\pi} \right)^{3/2} \exp\left(-\frac{M_1}{T} \right) & \text{for } T \ll M_1 \, . \end{cases} \tag{B.3}$$

To scale out the expansion, we define a comoving number density $N_{N_1} \equiv n_{N_1} a^3$, with which one cam rewrite Eq. (B.1) as

$$\frac{dN_{N_1}}{dt} = a^3 \left(\frac{dn_{N_1}}{dt} + 3HN_{N_1} \right) = -\Gamma \left(N_1 - N_{N_1}^{\text{eq}} \right) , \tag{B.4}$$

Now we try to write $\frac{dN_{N_1}}{dt}$ with respect to $\frac{dN_{N_1}}{dz}$. Using the definition $z = M/T$, one has

$$\frac{dz}{dt} = -z/T \frac{dT}{dt} . \tag{B.5}$$

And in radiation phase, the entropy is conserved, one has $d(s\,a^3)/dt = 0$, implying

$$
0 = \frac{2\pi^2\,g_{\star s}}{45}\left(3T^2a^3\dot{T} + 3T^3a^2\dot{a}\right) = \frac{2\pi^2\,g_{\star s}}{15}a^3T^3\left(\dot{T}/T + H\right)
$$
$$
\implies \dot{T}/T = -H\,.
\tag{B.6}
$$

Thereafter one has $\dot{z} = Hz$, so we can rewrite Eq. (B.4) as

$$
\frac{dN_1}{dz} = \frac{dN_1}{dt}\frac{dt}{dz} = -\frac{\Gamma}{H\,z}\left(N_1 - N_1^{\mathrm{eq}}\right)\,.
\tag{B.7}
$$

The Hubble parameter in a radiation phase is $H = \frac{\pi}{3}\sqrt{\frac{g_\star}{10}}\frac{T^2}{M_P}$, so

$$
\frac{\Gamma}{H\,z} = \frac{K_1(M_1/T)}{K_2(M_1/T)}\frac{\left(Y^\dagger Y\right)_{11}}{8\pi}M_1\left(\frac{3}{\pi}\frac{M_P}{T^2}\sqrt{\frac{10}{g_\star}}\right)\frac{T}{M_1}
$$
$$
= \frac{K_1(M_1/T)}{K_2(M_1/T)}K\,z\,,
\tag{B.8}
$$

where we have defined

$$
K \equiv \frac{\tilde{m}_1}{m_\star}\,,
\tag{B.9}
$$

and an effective mass neutrino mass as

$$
\tilde{m}_1 \equiv \frac{\left(Y^\dagger Y\right)_{11}v^2}{M_1}\,,
\tag{B.10}
$$

and a equilibrium neutrino mass, given by

$$
m_\star \equiv \frac{8\pi^2 v^2}{3M_P}\sqrt{\frac{g_\star}{10}} \simeq 10^{-3}\,\mathrm{eV}\,.
\tag{B.11}
$$

Thereafter the Boltzmann equation Eq. (B.7) becomes

$$
\frac{dN_{N_1}}{dz} = -\frac{K_1(M_1/T)}{K_2(M_1/T)}K\,z\left(N_{N_1} - N_{N_1}^{\mathrm{eq}}\right) = -D(z)\left(N_{N_1} - N_{N_1}^{\mathrm{eq}}\right)\,,
\tag{B.12}
$$

where we have defined:

$$
D(z) = \frac{K_1(M_1/T)}{K_2(M_1/T)}K\,z\,.
\tag{B.13}
$$

Similarly the Boltzmann equation for the co-moving B-L number density $N_{B-L} \equiv a^3 n_{B-L}$ can be

written as:

$$\frac{dN_{B-L}}{dz} = \epsilon_1 D(z) \left(N_{N_1} - N_{N_1}^{\text{eq}} \right) - W_{ID} N_{B-L} \,, \tag{B.14}$$

with

$$W_{ID}(z) = \frac{1}{2} D(z) \frac{N_{N_1}^{\text{eq}}(z)}{N_l^{eq}} \,, \tag{B.15}$$

accounting for washout effect coming from the inverse decays.

By solving Eq. (B.14) together with Eq. (B.12), one can the estimate N_{B-L}, with which the B-L yield, namely n_{B-L}/s can be further computed. A key parameter in the estimation is the parameter K, defined in Eq. (B.9). Using Eq. (6.11), one has

$$K = \frac{\left(m_2 |\cos z|^2 + m_3 |\sin z|^2 \right)}{m_\star} \geq \frac{m_2}{m_\star} > 1 \,, \tag{B.16}$$

where we have considered the present evidence for neutrino masses as presented in Eq. (6.4). In strong washout regime with $K > 1$, one has [54, 138]

$$Y_{B-L} = \frac{45}{\pi^4 g_{\star s}} \epsilon_1 \kappa_f \,, \tag{B.17}$$

where the factor $\frac{45}{\pi^4 g_{\star s}}$ comes from $Y_{N_1}^{\text{eq}} = n_{N_1}^{\text{eq}}/s$ and the efficiency factor given by [138]

$$\kappa_f \sim (2 \pm 1) \times 10^{-2} \left(\frac{0.01\text{eV}}{\tilde{m}_1} \right)^{1.1} \,. \tag{B.18}$$

Inflaton Three-Body Decay and Leptogenesis

In this chapter, we first calculate the rate of generating the lightest right-handed neutrino (RHN) via inflaton three-body decays during reheating: $\phi \to H \ell N_1$. Then we estimate the $B - L$ yield generated from further decay of N_1. Indeed once a bosoinc reheating scenario $\phi H^\dagger H$ is considered,
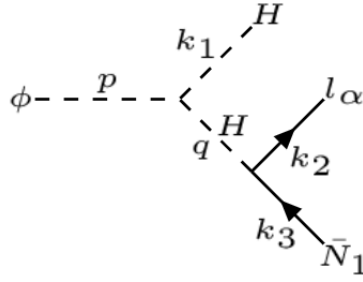
Figure C.1: Inflaton three-body decay for N_1 generation.

the three-body decay for N_1 production cannot be forbidden. In Sec. 6.3.2, we have focused on reheating via a fermionic channel and discussed the production of N_1 by introducing a lepton number violation operator $\sim \phi \bar{N}_1 N_1$. The scenario presented in this chapter is an alternative to that.

We label the momenta for particles involved as follows:

$$\phi(p) \to H(k_1)\,H(q) \to H(k_1)\,\ell(k_2)N_1(k_3)\,,$$

which is further depicted in Fig. C.1. Note that here we are focusing on inflaton couples the standard model (SM) Higgs via a trilinear coupling $\lambda_{12}\phi H^\dagger H$, which plays the role of reheating. The RHN N_1 couples to the SM Higgs and lepton through Yukawa coupling: $Y_{\alpha 1}\,\bar{\ell}_\alpha \tilde{H} N_1$, which is introduced in order to resolve the light neutrino masses as discussed in Sec. 6.2. The matrix element for a fixed lepton flavor α is given by

$$iM_\alpha = 2i\,\lambda_{12}\,\frac{i}{q^2 - m_H^2}\,Y_{\alpha 1}\bar{u}(k_2)\mathrm{v}(k_3)\,, \tag{C.1}$$

with which one can further compute squared matrix element with contributions from all lepton flavors:

$$|M|^2 = \sum_\alpha 4\,\lambda_{12}^2\,(Y_{\alpha 1}^\star Y_{\alpha 1})\left(4k_2 \cdot k_3 - 4M_1 m_{\ell_\alpha}\right)\frac{1}{q^4}$$

$$= 16\,\lambda_{12}^2 k_2 \cdot k_3 \frac{1}{q^4} \sum_\alpha (Y_{\alpha 1}^\star Y_{\alpha 1})\,, \qquad\qquad (C.2)$$

where we have neglected m_H and m_{ℓ_α}. The three-body phase space integral is given by:

$$\int d\Pi_3 = \int \int \int \frac{d^3\vec{k}_1}{(2\pi)^3\,2E_1}\frac{d^3\vec{k}_2}{(2\pi)^3\,2E_2}\frac{d^3\vec{k}_3}{(2\pi)^3\,2E_3}(2\pi)^4\delta^4\left[p - (k_1 + k_2 + k_3)\right]$$

$$= \int \int \frac{d^3\vec{k}_1}{(2\pi)^3\,2E_1}\frac{d^3\vec{k}_2}{(2\pi)^3\,2E_2}\left[\int \frac{d^4 k_3}{(2\pi)^3}\delta(E_3^2 - \vec{k}_3^2 - M_1^2)\theta(k_3^0)\right](2\pi)^4\delta^4\left[p - (k_1 + k_2 + k_3)\right]$$

$$= \int \int \frac{d^3\vec{k}_1}{(2\pi)^3\,2E_1}\frac{d^3\vec{k}_2}{(2\pi)^3\,2E_2}\delta(E_3^2 - \vec{k}_3^2 - M_1^2)(2\pi)\left(\int d^4 k_3\,\delta^4\left[p - (k_1 + k_2 + k_3)\right]\right)$$

$$= \int \int \frac{d^3\vec{k}_1}{(2\pi)^3\,2E_1}\frac{d^3\vec{k}_2}{(2\pi)^3\,2E_2}\delta(E_3^2 - \vec{k}_3^2 - M_1^2)(2\pi) \quad \text{with}\, p = (k_1 + k_2 + k_3)$$

$$= \frac{1}{(2\pi)^5}\int \int d^3\vec{k}_1 d^3\vec{k}_2 \frac{\delta\left[(m_\phi - E_1 - E_2)^2 - (\vec{k}_1 + \vec{k}_2)^2 - M_1^2\right]}{2E_1\,2E_2}$$

$$= \frac{1}{(2\pi)^5}\int \int \int 4\pi E_1^2 dE_2\,2\pi E_2^2 dE_2\,d\cos\theta\,\frac{\delta\left[m_\phi^2 - 2m_\phi(E_1 + E_2) + 2E_1 E_2(1 - \cos\theta) - M_1^2\right]}{2E_1\,2E_2}$$

$$= \frac{1}{32\pi^3}\int \int \int 2dE_1 dE_2\,d\cos\theta\,E_1 E_2\,\delta\left[m_\phi^2 - 2m_\phi(E_1 + E_2) + 2E_1 E_2(1 - \cos\theta) - M_1^2\right]$$

$$= \frac{1}{32\pi^3}\int \int 2dE_1 dE_2\,E_1 E_2 \frac{1}{2E_1 E_2} \quad \text{with}\,\left[m_\phi^2 - 2m_\phi(E_1 + E_2) + 2E_1 E_2(1 - \cos\theta) - M_1^2\right] = 0$$

$$= \frac{1}{32\pi^3}\int \int dx_1 dx_2 \frac{m_\phi}{2}\frac{m_\phi}{2}$$

$$= \frac{Q^2}{128\pi^3}\int \int dx_1 dx_2\,. $$

$$(C.3)$$

In the second step the Heaviside function $\theta(k_3^0)$ is utilized to change the three dimensional integral to four dimensional as well as to guarantee $k_3^0 \equiv E_3$ picking the positive value, namely $E_3 = \sqrt{\vec{k}_3^2 + M_1^2}$:

$$\int \frac{d^4 k_3}{(2\pi)^3}\delta(E_3^2 - \vec{k}_3^2 - M_1^2)\theta(k_3^0) = \int \frac{d^4 k_3}{(2\pi)^3}\delta\left[(E_3 + \sqrt{\vec{k}_3^2 + M_1^2})(E_3 - \sqrt{\vec{k}_3^2 + M_1^2})\right]\theta(k_3^0)$$

$$= \int \frac{d^4 k_3}{(2\pi)^3\,2E_3}\delta\left[(E_3 - \sqrt{\vec{k}_3^2 + M_1^2})\right] = \int \frac{d^3 k_3}{(2\pi)^3\,2E_3}\,. \quad (C.4)$$

We have defined $x_1 = 2E_1/m_\phi$, $x_2 = 2E_2/m_\phi$ and $x_3 = 2E_3/m_\phi - \gamma$ with $\gamma \equiv M_1^2/m_\phi^2$ and neglected

both lepton and Higgs masses. The integration boundaries can be fixed by using the condition:
$m_\phi^2 - 2m_\phi(E_1 + E_2) + 2E_1E_2(1 - \cos\theta) - M_1^2 = 0$ (arising from the integral of δ function in the last fourth step of Eq. (C.3)), from which one has

$$m_\phi^2 - 2m_\phi\left(\frac{m_\phi x_1}{2} + \frac{m_\phi x_2}{2}\right) + 2\frac{m_\phi x_1}{2}\frac{m_\phi x_2}{2}(1 - \cos\theta) - M_1^2 = 0$$

$$\implies m_\phi^2\left[1 - x_1 - x_2 + \frac{x_1 x_2}{2}(1 - \cos\theta) - \gamma\right] = 0$$

$$\implies x_1 + x_2 - 1 + \gamma = \frac{x_1 x_2}{2}(1 - \cos\theta)$$

$$\implies (1 - \cos\theta) = \frac{2(x_1 + x_2 - 1 + \gamma)}{x_1 x_2}$$

$$\implies 0 \le \frac{2(x_1 + x_2 - 1 + \gamma)}{x_1 x_2} \le 2$$

$$\implies x_1 + x_2 \ge 1 - \gamma \text{ and } (x_1 + x_2 - 1 + \gamma) \le x_1 x_2$$

$$\implies x_1 + x_2 \ge 1 - \gamma \text{ and } (x_2 - 1)(1 - x_1) + \gamma \le 0$$

$$\implies x_1 + x_2 \ge 1 - \gamma \text{ and } 1 - x_1 - \gamma \le x_2 \le 1 - \frac{\gamma}{1 - x_1}, \tag{C.5}$$

leading to phase space integral given by

$$\int d\Pi_3 = \frac{m_\phi^2}{128\pi^3} \int_0^{1-\gamma} dx_1 \int_{1-x_1-\gamma}^{1-\frac{\gamma}{1-x_1}} dx_2. \tag{C.6}$$

Using the following conditions,

$$(k_1 + k_2)^2 \equiv m_\phi^2(1 - x_3); (k_2 + k_3)^2 \equiv m_\phi^2(1 - x_1); (k_1 + k_3)^2 \equiv m_\phi^2(1 - x_2), \tag{C.7}$$

one then has $2k_2 \cdot k_3 = m_\phi^2(1 - x_1) - M_1^2 - m_{\ell_\alpha}^2 \simeq m_\phi^2(1 - x_1) - M_1^2$.

With Eq. (C.6) and Eq. (C.2), one can finally compute the three-body decay rate:

$$\Gamma_{\text{3-body}} \equiv \Gamma_{\phi \to \ell H N_1} = \frac{1}{2m_\phi} \int d\Pi_3 |M|^2$$

$$= \frac{1}{2m_\phi} \frac{m_\phi^2}{128\pi^3} \int_0^{1-\gamma} dx_1 \int_{1-x_1-\gamma}^{1-\frac{\gamma}{1-x_1}} dx_2 \left[8\lambda_{12}^2\left(m_\phi^2(1 - x_1) - M_1^2\right)\right] \frac{1}{m_\phi^4(1 - x_1)^2} \sum_\alpha (Y_{\alpha 1}^\star Y_{\alpha 1})$$

$$= \frac{\lambda_{12}^2}{32\pi^3 m_\phi} \int_0^{1-\gamma} dx_1 \int_{1-x_1-\gamma}^{1-\frac{\gamma}{1-x_1}} dx_2 \frac{(1 - x_1) - \gamma}{(1 - x_1)^2} \sum_\alpha (Y_{\alpha 1}^\star Y_{\alpha 1})$$

$$= \frac{\lambda_{12}^2}{32\pi^3 m_\phi} \sum_\alpha (Y_{\alpha 1}^\star Y_{\alpha 1}) \frac{1}{2}\left[\gamma^2 + 4\gamma - 5 - 2(1 + 2\gamma)\ln\gamma\right]. \tag{C.8}$$

Note that $0 < \gamma < 1$, and the dominated contribution comes from the term $-2\ln\gamma$ at small γ regime; when $\gamma \to 1$ or equivalently $M_1 \to m_\phi$, $\Gamma_{\text{3-body}} \to 0$, which is as expected since this process is kinematically blocked in such case.

The branching ratio for the channel $\phi \to \ell N_1 H$ is

$$\mathrm{BR}(\phi \to \ell N_1 H) = \frac{\Gamma_{3\text{-body}}}{\Gamma_{3\text{-body}} + \Gamma_{\phi \to H^\dagger H}} \simeq \frac{\Gamma_{3\text{-body}}}{\Gamma_{\phi \to H^\dagger H}}$$

$$= \frac{m_\phi}{8\pi^2 v^2}\left(m_2 |\cos z|^2 + m_3 |\sin z|^2\right) \cdot f(\gamma), \tag{C.9}$$

where $\Gamma_{\phi \to H^\dagger H} \simeq \frac{\lambda_{12}^2}{8\pi m_\phi}$ and Eq. (6.13) for $\sum_\alpha \left(Y_{\alpha 1}^\dagger Y_{\alpha 1}\right)$ have been applied. The function $f(\gamma)$ is defined as:

$$f(\gamma) = \sqrt{\gamma}\left[\gamma^2 + 4\gamma - 5 - 2(1 + 2\gamma)\ln \gamma\right], \tag{C.10}$$

which peaks at $\gamma \sim 0.0177$ with $f(\gamma)^{\max} \sim 0.456$.

If one neglects the washout effect, the generated $B - L$ yield would be similar to Eq. (6.24), and given by

$$Y_{B-L} = \left[\frac{3}{4}\frac{T_{\mathrm{rh}}}{m_\phi}\mathrm{BR}(\phi \to \ell N_1 H)\right]\epsilon_1$$

$$= \frac{3}{4}\frac{T_{\mathrm{rh}}}{m_\phi}\left[\frac{m_\phi}{8\pi^2 v^2}\left(m_2|\cos z|^2 + m_3|\sin z|^2\right)\cdot f(\gamma)\right]\left[-\frac{3}{16\pi}\frac{M_1}{v^2}(m_3^2 - m_2^2)\frac{\mathrm{Im}\left(\sin^2 z\right)}{\left(m_2|\cos z|^2 + m_3|\sin z|^2\right)}\right]$$

$$= -\frac{9}{512\pi^2}\frac{M_1 T_{\mathrm{rh}}}{v^4}(m_3^2 - m_2^2)\mathrm{Im}\left(\sin^2 z\right)\cdot f(\gamma)$$

$$\simeq 4.8 \times 10^{-11}\left(\frac{m_\phi}{10^{11}\mathrm{GeV}}\right)\left(\frac{T_{\mathrm{rh}}}{10^{11}\mathrm{GeV}}\right)\mathrm{Im}\left(\sin^2 z\right)\cdot \sqrt{\gamma}f(\gamma), \tag{C.11}$$

where in the first line the factor $3/2$ in Eq. (6.24) has been changed to be $3/4$ since only one N_1 is produced via the three-body decay, and in the third line we have utilized Eq. (6.18). Note that the function $\sqrt{\gamma}f(\gamma)$ peaks at $\gamma \simeq 0.08$ with maximum ~ 0.09. Within the small field polynomial inflationary setup $m_\phi \lesssim 10^{11}$ GeV, $T_{\mathrm{rh}} \lesssim 10^{11}$ GeV, thereafter with a typically value of $\mathrm{Im}\left(\sin^2 z\right) \sim O(1)$ the maximum value of the yield turns out to be $Y_{B-L}^{\max} \sim O\left(10^{-12}\right)$, which is too small compared to the required value as shown Eq. (6.20). Thereafter with such three-body decay alone, *no* enough B-L yield can be generated in the small field model.

Note that once the constraints on T_{rh} and m_ϕ are relaxed, such three-body decay could give rise to interesting contributions to the B-L yield. For example, in the large field scenario presented in Chapter 7, the inflaton mass $m_\phi \simeq \sqrt{2d}\phi_0$, can be as large as 10^{13} GeV by using Eq. (7.32), and the reheating temperature can be as high as $T_{\mathrm{rh}} \sim 10^{14}$ GeV (cf. Eq. 7.40). Also if one relaxes the radiative constraint on T_{rh} and treat it as a free parameter (might be possible in some other inflation model), T_{rh} can be as larger as $\sim 5.5 \times 10^{15}$ GeV (coming from CMB bound derived in Eq. (D.3)). Of course proper treatments on washout effect shall also be applied once N_1 mass is smaller than T_{rh}. We leave the detailed study regarding leptogenesis from inflaton three-body decay in the large field scenario for a future publication.

Upper Bounds on Inflationary Scale and Reheating Temperature from CMB

We start from the expression for the power spectrum:

$$\mathcal{P} = \frac{V}{24\pi^2 \epsilon M_P^4} \implies \epsilon_v = 6.0 \times 10^6 \left(\frac{2.1 \times 10^{-9}}{\mathcal{P}}\right) \left(\frac{\mathcal{H}_{\text{inf}}}{M_P}\right)^2$$

$$\implies \left(\frac{\mathcal{H}_{\text{inf}}}{M_P}\right)^2 = 1.0 \times 10^{-10} \left(\frac{\mathcal{P}}{2.1 \times 10^{-9}}\right) \left(\frac{r}{0.01}\right)$$

$$\implies \frac{\mathcal{H}_{\text{inf}}}{M_P} = 1.0 \times 10^{-5} \left(\frac{\mathcal{P}}{2.1 \times 10^{-9}}\right)^{1/2} \left(\frac{r}{0.01}\right)^{1/2}, \tag{D.1}$$

where the Friedmann equation $H^2 = V/(3\,M_P^2)$ and the relation $r = 16\epsilon_v$ have been applied in the first and second step, respectively. Applying the recent bound on $r < 0.035$ from CMB experiment [22] into Eq. (D.1), we obtain an upper bound on inflationary scale:

$$\mathcal{H}_{\text{inf}} < 2 \times 10^{-5} M_P. \tag{D.2}$$

Considering $\mathcal{H}(T_{\text{rh}})^2 = \frac{\pi^2 g_\star T_{\text{rh}}^4}{90 M_P^2}$ with $g_\star = 106.75$ being the degrees of freedoms in the standard model of particle physics contributing to energy density, and the fact that $\mathcal{H}(T_{\text{rh}}) < \mathcal{H}_{\text{inf}}$ one has

$$\left(\frac{T_{\text{rh}}}{M_P}\right)^4 = 8.5 \times 10^{-2} \left(\frac{\mathcal{H}(T_{\text{rh}})}{M_P}\right)^2 < 8.5 \times 10^{-12} \left(\frac{\mathcal{P}}{2.1 \times 10^{-9}}\right) \left(\frac{r}{0.01}\right)$$

leading to

$$T_{\text{rh}} < 2.3 \times 10^{-3} M_P \simeq 5.5 \times 10^{15} \text{ GeV}. \tag{D.3}$$

General Expression for e-folds

Here we present the general analytical expression for the number of e-folds for polynomial inflation. (See Eq. (7.9) for definition.) It is given by the the following integrals:

$$
\begin{aligned}
N_{\text{CMB}} &= \int_{\phi_{\text{end}}}^{\phi_{\text{CMB}}} \frac{1}{\sqrt{2\epsilon_{\text{v}}}} d\phi \\
&= \int_{\phi_{\text{end}}}^{\phi_{\text{CMB}}} \frac{\phi}{2} \left[\frac{32\phi^2 - 32A(\beta-1)\phi + 9A^2}{64\phi^2 - 48A(\beta-1)\phi + 9A^2} \right] d\phi \\
&= \int_{\phi_{\text{end}}}^{\phi_{\text{CMB}}} \frac{\phi}{2} \left[1 + \frac{-32\phi^2 + 16A(\beta-1)\phi}{64\phi^2 - 48A(\beta-1)\phi + 9A^2} \right] d\phi \\
&= \int_{\phi_{\text{end}}}^{\phi_{\text{CMB}}} \frac{\phi}{2} \left\{ 1 + \frac{-32\phi^2 + 16A(\beta-1)\phi}{[8\phi - 3A(\beta-1)]^2 - 9A^2(\beta^2 - 2\beta)} \right\} d\phi \\
&= \int_{\phi_{\text{end}}}^{\phi_{\text{CMB}}} \frac{\phi}{2} \left\{ 1 + \frac{-32\phi^2 + 16A(\beta-1)\phi}{64[\phi - 3/8A(\beta-1)]^2 - 9A^2(\beta^2 - 2\beta)} \right\} d\phi \\
&= \int_{\phi_{\text{end}}}^{\phi_{\text{CMB}}} \frac{\phi}{2} \left\{ 1 + \frac{-32\phi^2}{64\left[\phi - \frac{3}{8}A(\beta-1)\right]^2 - 9A^2(\beta^2 - 2\beta)} + \frac{+16A(\beta-1)\phi}{64\left[\phi - \frac{3}{8}A(\beta-1)\right]^2 - 9A^2(\beta^2 - 2\beta)} \right\} d\phi \\
&= \int_{\phi_{\text{end}}}^{\phi_{\text{CMB}}} \frac{\phi}{2} \left\{ 1 - \frac{1}{2} \frac{\phi^2}{\left[\phi + \phi_0(\beta-1)\right]^2 - \phi_0^2(\beta^2 - 2\beta)} - \frac{2}{3} \frac{\phi_0(\beta-1)\phi}{\left[\phi + \phi_0(\beta-1)\right]^2 - \phi_0^2(\beta^2 - 2\beta)} \right\} d\phi \, .
\end{aligned}
$$

$$\text{(E.1)}$$

The three integrals admit analytical expression as:

$$
\int d\phi \frac{\phi}{2} = \frac{\phi^2}{4} \, ; \tag{E.2}
$$

$$\int -\frac{1}{4} \frac{d\phi\,\phi^3}{[\phi - m]^2 + n^2}$$

$$= \frac{1}{8} \left\{ 5m^2 - 4m\,\phi - \phi^2 + \frac{2(m^3 - 3m\,n^2)}{n} \text{ArcTan}\left[\frac{m - \phi}{n}\right] - (3m^2 - n^2) \log\left[n^2 + (m - \phi)^2\right] \right\} \; ;$$

(E.3)

and

$$\int \frac{1}{3} \frac{d\phi\,m\,\phi^2}{[\phi - m]^2 + n^2}$$

$$= \frac{m}{3} \left\{ \phi - \frac{(m^2 - n^2)}{n} \text{ArcTan}\left[\frac{m - \phi}{n}\right] + m \log\left[n^2 + (m - \phi)^2\right] \right\} ,$$

(E.4)

with $m = \phi_0(1 - \beta)$, and $n^2 = \phi_0^2(2\beta - \beta^2)$. By combining them, we have

$$N_{\text{CMB}} = \frac{1}{24} \left\{ -2\frac{m^3 + 5mn^2}{n} \text{ArcTan}\left(\frac{m - \phi}{n}\right) + 15m^2 - 4m\phi + 3\phi^2 - (m^2 - 3n^2) \ln\left[n^2 + (m - \phi)^2\right] \right\} \Bigg|_{\phi_{\text{end}}}^{\phi_{\text{CMB}}}$$

$$\simeq \frac{1}{24} \left\{ 3\phi^2 - 4\phi\phi_0 + 15\phi_0^2 - \phi_0^2\sqrt{\frac{2}{\beta}} \text{ArcTan}\left(\frac{\phi_0 - \phi}{\sqrt{2\beta}\phi_0}\right) - \phi_0^2 \ln\left[(\phi_0 - \phi)^2\right] \right\} \Bigg|_{\phi_{\text{end}}}^{\phi_{\text{CMB}}} , \qquad \text{(E.5)}$$

corresponding to Eq. (7.9).

Inflation in Supergravity

In this chapter we briefly revisit the realization of inflation in the supergravity framework. We start from the F-term scalar potential, which is determined by superpotential W and Kähler potential K [158]:

$$V = e^K \left[(D_i W) K_{i\bar{j}}^{-1} (D_{\bar{j}} \bar{W}) - 3|W|^2 \right] , \tag{F.1}$$

where

$$D_i W = \frac{\partial W}{\partial \Phi_i} + \frac{\partial K}{\partial \Phi_i} W \, ; D_{\bar{j}} \bar{W} = \frac{\partial \bar{W}}{\partial \bar{\Phi}_j} + \frac{\partial K}{\partial \bar{\Phi}_j} \bar{W} , \tag{F.2}$$

and

$$K_{i\bar{j}} = \frac{\partial^2 K}{\partial \Phi_i \partial \bar{\Phi}_j} . \tag{F.3}$$

For successful inflation, the potential energy V has to be positive, thus breaking supersymmetry spontaneously and giving rise to an positive effective mass for any would-be inflaton field with the same magnitude as the Hubble parameter during inflation. This leads to the so-called η problem [158]. To see this point more clearly, let's consider a canonical Kähler potential $K = \sum_i |\Phi_i|^2$ and then expand the scalar potential in Eq. (F.1). This leads to

$$V \supset \left(1 + \sum_i \left| \Phi_i \right|^2 \right) \sum_i \left| \frac{\partial W}{\partial \Phi_i} \right|^2 = V^{\text{global}} + \sum_i \left| \Phi_i \right|^2 V^{\text{global}} \Rightarrow \eta = \frac{V''}{V} \sim 1 , \tag{F.4}$$

where $V^{\text{global}} = \sum_i |\frac{\partial W}{\partial \Phi_i}|^2$. Recall that slow-roll inflation requires $\eta \ll 1$; clearly Eq. (F.4) violates such conditions. This is the so-called η problem in supergravity inflation models [158].

A simple idea to resolve this problem is to construct Kähler potential with a shift symmetry [159]: $\Phi \to \Phi + iC$. This ensures that the imaginary part does not appear in the exponential of the scalar potential, thus allowing the imaginary component to be a viable inflaton candidate, free from the η problem [158].

Following the same spirit of Ref. [159], one can consider the following Kähler potential and superpotential [63, 160],

$$K = \frac{1}{2}(\Phi + \Phi^\dagger)^2 + |X|^2 \, ; \quad W = X(d_1 \Phi + d_2 \Phi^2) , \tag{F.5}$$

where Φ and X are two superfields and d_1, d_2 denote the couplings. Such construction has been considered to realize polynomial inflation scenarios. In particular a large field scenario was considered in Refs. [63, 160]. Here we briefly revisit the calculations and then derive the conditions for the Kähler potential and superpoetntial in Eq. (F.5) in order to arrive at our model namely Eq. (3.5). The introduction of superfield X is to make sure the scalar potential to be positive; during inflation X would quickly align itself to be the minimum such that the negative term $-3|W|^2$ does not contribute to the scalar potential. By expanding e^K up to $O(\Phi^2)$, and decomposing $\Phi \equiv \frac{1}{\sqrt{2}}(\chi + i\phi)$, one has the scalar potential:

$$
\begin{aligned}
V &\simeq \left[1 + \frac{1}{2}(\Phi^2 + \Phi^{\dagger 2} + 2\Phi\Phi^\dagger)\right]\left(d_1\Phi + d_2\Phi^2\right)\left(d_1^\star\Phi^\dagger + d_2^\star\Phi^{\dagger 2}\right) \\
&= \left(1 + \chi^2\right)\left[\frac{|d_1|^2}{2}(\chi^2 + \phi^2) + \frac{|d_2|^2}{4}(\chi^2 + \phi^2)^2 + \frac{d_1 d_2^\star}{2\sqrt{2}}(\chi^2 + \phi^2)(\chi - i\phi) + \frac{d_1^\star d_2}{2\sqrt{2}}(\chi^2 + \phi^2)(\chi + i\phi)\right] \\
&\supset \frac{|d_1|^2}{2}\phi^2 + \frac{|d_2|^2}{4}\phi^4 + \frac{(-id_1 d_2^\star + id_1^\star d_2)}{2\sqrt{2}}\phi^3 \\
&= \frac{m^2}{2}\phi^2 + \frac{\lambda^2}{4}\phi^4 - \frac{\sqrt{2}m\lambda\sin\theta}{2}\phi^3 ,
\end{aligned}
$$

(F.6)

where the angle θ denotes the relative phase for the two complex coupling parameters d_1 and d_2; we have also defined $|d_1| = m$ and $|d_2| = \lambda$.

Defining $b = \frac{m^2}{2}, c = -\frac{\sqrt{2}m\lambda\sin\theta}{2}$ and $d = \frac{\lambda^2}{4}$, one arrives at:

$$
V(\phi) = b\,\phi^2 + c\,\phi^3 + d\,\phi^4 ,
$$

(F.7)

as considered in Eq. (3.1). By applying the inflection-point conditions: $b = \frac{9c^2}{32d}$, $\phi_0 = -\frac{3c}{8d}$, (cf. from Eq. (3.3) and Eq. (3.4)) one has

$$
\frac{m^2}{2} = \frac{9m^2\lambda^2\sin^2\theta}{16\lambda^2} \Rightarrow \sin\theta = \frac{2\sqrt{2}}{3} ;
$$

(F.8)

and the location of the inflection-point is fixed by

$$
\phi_0 = \frac{3}{8}\frac{2\sqrt{2}m\sin\theta}{\lambda} = \frac{m}{\lambda} ,
$$

(F.9)

where only a positive solution of $\sin\theta$ has been considered since both m and λ are positive. So one sees that it could be possible to start from Kähler potential and superpoetntial constructed in (F.5), to realize the polynomial inflation scenario (3.5).

Bibliography

[1] M. Drees and Y. Xu,
Overshooting, Critical Higgs Inflation and Second Order Gravitational Wave Signatures,
Eur. Phys. J. C **81** (2021) 182, arXiv: `1905.13581` [`hep-ph`] (cit. on pp. vii, 39, 74).

[2] M. Drees and Y. Xu,
Small field polynomial inflation: reheating, radiative stability and lower bound,
JCAP **09** (2021) 012, arXiv: `2104.03977` [`hep-ph`] (cit. on pp. vii, 22, 31, 60, 61, 67).

[3] N. Bernal and Y. Xu, *Polynomial inflation and dark matter*, Eur. Phys. J. C **81** (2021) 877,
arXiv: `2106.03950` [`hep-ph`] (cit. on pp. vii, 41).

[4] N. Bernal, F. Hajkarim and Y. Xu, *Axion Dark Matter in the Time of Primordial Black Holes*,
Phys. Rev. D **104** (2021) 075007, arXiv: `2107.13575` [`hep-ph`] (cit. on p. vii).

[5] N. Bernal, Y. F. Perez-Gonzalez, Y. Xu and Ó. Zapata,
ALP dark matter in a primordial black hole dominated universe,
Phys. Rev. D **104** (2021) 123536, arXiv: `2110.04312` [`hep-ph`] (cit. on p. vii).

[6] B. Barman, N. Bernal, Y. Xu and Ó. Zapata,
Ultraviolet Freeze-in with a Time-dependent Inflaton Decay, (2022),
arXiv: `2202.12906` [`hep-ph`] (cit. on p. vii).

[7] N. Bernal, Y. F. Perez-Gonzalez and Y. Xu,
Superradiant Production of Heavy Dark Matter from Primordial Black Holes, (2022),
arXiv: `2205.11522` [`hep-ph`] (cit. on p. vii).

[8] M. Drees and Y. Xu, *A Minimal Model for Inflation, Neutrino Masses and Leptogenesis*,
(2022), arXiv: `22xx.xxxx` [`hep-ph`] (cit. on pp. vii, 49).

[9] M. Drees and Y. Xu,
"Large Field Polynomial Inflation: Parameter Space, Predictions and (Double) Eternal Nature",
2022, arXiv: `2209.07545` [`astro-ph.CO`] (cit. on pp. vii, 57).

[10] N. Bernal and Y. Xu, *WIMPs during Reheating*, (2022), arXiv: `2209.07546` [`hep-ph`]
(cit. on p. vii).

[11] `https://home.cern/news/series/lhc-physics-ten/recreating-big-bang-matter-earth` (cit. on p. 1).

[12] D. Wands, O. F. Piattella and L. Casarini,
Physics of the Cosmic Microwave Background Radiation, Astrophys. Space Sci. Proc. **45**
(2016) 3, ed. by J. C. Fabris, O. F. Piattella, D. C. Rodrigues, H. E. S. Velten and W. Zimdahl,
arXiv: `1504.06335` [`astro-ph.CO`] (cit. on p. 2).

[13] N. Aghanim et al., *Planck 2018 results. VI. Cosmological parameters*,
Astron. Astrophys. **641** (2020) A6, [Erratum: Astron.Astrophys. 652, C4 (2021)],
arXiv: `1807.06209` [`astro-ph.CO`] (cit. on pp. 2, 3, 5, 8, 17, 44, 45, 59).

[14] `https://www.esa.int/Science_Exploration/Space_Science/Planck/Planck_`
`and_the_cosmic_microwave_background` (cit. on p. 2).

[15] S. M. Carroll, *Spacetime and Geometry*, Cambridge University Press, 2019,
ISBN: 978-0-8053-8732-2, 978-1-108-48839-6, 978-1-108-77555-7 (cit. on p. 5).

[16] S. Weinberg, *The Cosmological Constant Problem*,
Rev. Mod. Phys. **61** (1989) 1, ed. by J.-P. Hsu and D. Fine (cit. on p. 6).

[17] `http://www.damtp.cam.ac.uk/user/tong/particle.html` (cit. on p. 6).

[18] D. Baumann, *Cosmology*, Cambridge University Press, 2022,
ISBN: 978-1-108-93709-2, 978-1-108-83807-8 (cit. on p. 6).

[19] J. Frieman, M. Turner and D. Huterer, *Dark Energy and the Accelerating Universe*,
Ann. Rev. Astron. Astrophys. **46** (2008) 385, arXiv: `0803.0982` [`astro-ph`] (cit. on p. 7).

[20] D. Baumann, "Inflation", *Theoretical Advanced Study Institute in Elementary Particle
Physics: Physics of the Large and the Small*, 2011 523, arXiv: `0907.5424` [`hep-th`]
(cit. on pp. 9, 11).

[21] A. D. Linde, *A New Inflationary Universe Scenario: A Possible Solution of the Horizon,
Flatness, Homogeneity, Isotropy and Primordial Monopole Problems*,
Phys. Lett. B **108** (1982) 389, ed. by L.-Z. Fang and R. Ruffini (cit. on pp. 10, 21).

[22] P. A. R. Ade et al., *Improved Constraints on Primordial Gravitational Waves using Planck,
WMAP, and BICEP/Keck Observations through the 2018 Observing Season*,
Phys. Rev. Lett. **127** (2021) 151301, arXiv: `2110.00483` [`astro-ph.CO`]
(cit. on pp. 11, 21, 26, 30, 60, 63, 73, 89).

[23] `https://en.wikipedia.org/wiki/Standard_Model` (cit. on p. 12).

[24] M. E. Peskin and D. V. Schroeder, *An Introduction to quantum field theory*,
Reading, USA: Addison-Wesley, 1995, ISBN: 978-0-201-50397-5 (cit. on p. 11).

[25] J. Rubio, *Higgs inflation*, Front. Astron. Space Sci. **5** (2019) 50,
arXiv: `1807.02376` [`hep-ph`] (cit. on p. 11).

[26] `https://en.wikipedia.org/wiki/Galaxy_rotation_curve` (cit. on p. 13).

[27] E. Corbelli and P. Salucci, *The Extended Rotation Curve and the Dark Matter Halo of M33*,
Mon. Not. Roy. Astron. Soc. **311** (2000) 441, arXiv: `astro-ph/9909252` (cit. on p. 13).

[28] `https://en.wikipedia.org/wiki/Galaxy_cluster` (cit. on p. 13).

[29] D. Clowe et al., *A direct empirical proof of the existence of dark matter*,
Astrophys. J. Lett. **648** (2006) L109, arXiv: `astro-ph/0608407` (cit. on p. 14).

[30] `https://camb.readthedocs.io/en/latest/` (cit. on p. 13).

[31] A. Lewis, A. Challinor and A. Lasenby,
Efficient computation of CMB anisotropies in closed FRW models,
Astrophys. J. **538** (2000) 473, arXiv: `astro-ph/9911177` (cit. on p. 13).

[32] M. Drees, *Dark Matter Theory*, PoS **ICHEP2018** (2019) 730,
arXiv: `1811.06406` `[hep-ph]` (cit. on p. 14).

[33] G. Arcadi et al., *The waning of the WIMP? A review of models, searches, and constraints*,
Eur. Phys. J. C **78** (2018) 203, arXiv: `1703.07364` `[hep-ph]` (cit. on p. 14).

[34] N. Bernal, M. Heikinheimo, T. Tenkanen, K. Tuominen and V. Vaskonen,
The Dawn of FIMP Dark Matter: A Review of Models and Constraints,
Int. J. Mod. Phys. A **32** (2017) 1730023, arXiv: `1706.07442` `[hep-ph]` (cit. on p. 14).

[35] D. J. E. Marsh, *Axion Cosmology*, Phys. Rept. **643** (2016) 1,
arXiv: `1510.07633` `[astro-ph.CO]` (cit. on p. 14).

[36] A. Boyarsky, M. Drewes, T. Lasserre, S. Mertens and O. Ruchayskiy,
Sterile neutrino Dark Matter, Prog. Part. Nucl. Phys. **104** (2019) 1,
arXiv: `1807.07938` `[hep-ph]` (cit. on p. 14).

[37] B. Carr and F. Kuhnel, *Primordial Black Holes as Dark Matter: Recent Developments*,
Ann. Rev. Nucl. Part. Sci. **70** (2020) 355, arXiv: `2006.02838` `[astro-ph.CO]`
(cit. on pp. 14, 27).

[38] G. Bertone and D. Hooper, *History of dark matter*, Rev. Mod. Phys. **90** (2018) 045002,
arXiv: `1605.04909` `[astro-ph.CO]` (cit. on p. 14).

[39] J. McDonald, *Gauge singlet scalars as cold dark matter*, Phys. Rev. D **50** (1994) 3637,
arXiv: `hep-ph/0702143` (cit. on p. 14).

[40] C. P. Burgess, M. Pospelov and T. ter Veldhuis,
The Minimal model of nonbaryonic dark matter: A Singlet scalar,
Nucl. Phys. B **619** (2001) 709, arXiv: `hep-ph/0011335` (cit. on p. 14).

[41] Y. G. Kim and K. Y. Lee, *The Minimal model of fermionic dark matter*,
Phys. Rev. D **75** (2007) 115012, arXiv: `hep-ph/0611069` (cit. on p. 14).

[42] Y. G. Kim, K. Y. Lee and S. Shin, *Singlet fermionic dark matter*, JHEP **05** (2008) 100,
arXiv: `0803.2932` `[hep-ph]` (cit. on p. 14).

[43] S. Baek, P. Ko and W.-I. Park,
Search for the Higgs portal to a singlet fermionic dark matter at the LHC,
JHEP **02** (2012) 047, arXiv: `1112.1847` `[hep-ph]` (cit. on p. 14).

[44] L. Lopez-Honorez, T. Schwetz and J. Zupan,
Higgs portal, fermionic dark matter, and a Standard Model like Higgs at 125 GeV,
Phys. Lett. B **716** (2012) 179, arXiv: `1203.2064` `[hep-ph]` (cit. on p. 14).

[45] P. A. Zyla et al., *Review of Particle Physics*, PTEP **2020** (2020) 083C01
(cit. on pp. 15, 17, 44, 45).

[46] M. D. Schwartz, *Quantum Field Theory and the Standard Model*,
Cambridge University Press, 2014, ISBN: 978-1-107-03473-0, 978-1-107-03473-0
(cit. on pp. 15, 18).

[47] I. Esteban, M. C. Gonzalez-Garcia, A. Hernandez-Cabezudo, M. Maltoni and T. Schwetz,
*Global analysis of three-flavour neutrino oscillations: synergies and tensions in the
determination of θ_{23}, δ_{CP}, and the mass ordering*, JHEP **01** (2019) 106,
arXiv: `1811.05487` `[hep-ph]` (cit. on p. 16).

[48] S. Weinberg, *Baryon and Lepton Nonconserving Processes*, Phys. Rev. Lett. **43** (1979) 1566 (cit. on p. 16).

[49] P. Minkowski, $\mu \to e\gamma$ *at a Rate of One Out of* 10^9 *Muon Decays?*, Phys. Lett. B **67** (1977) 421 (cit. on p. 17).

[50] S. Davidson, E. Nardi and Y. Nir, *Leptogenesis*, Phys. Rept. **466** (2008) 105, arXiv: `0802.2962` [`hep-ph`] (cit. on p. 17).

[51] A. Riotto, "Theories of baryogenesis", *ICTP Summer School in High-Energy Physics and Cosmology*, 1998 326, arXiv: `hep-ph/9807454` (cit. on p. 18).

[52] V. A. Rubakov and D. S. Gorbunov, *Introduction to the Theory of the Early Universe: Hot big bang theory*, Singapore: World Scientific, 2017, ISBN: 978-981-320-987-9, 978-981-320-988-6, 978-981-322-005-8 (cit. on p. 18).

[53] M. Fukugita and T. Yanagida, *Baryogenesis Without Grand Unification*, Phys. Lett. B **174** (1986) 45 (cit. on pp. 19, 22).

[54] C. S. Fong, E. Nardi and A. Riotto, *Leptogenesis in the Universe*, Adv. High Energy Phys. **2012** (2012) 158303, arXiv: `1301.3062` [`hep-ph`] (cit. on pp. 19, 51, 53, 83).

[55] A. A. Starobinsky, *A New Type of Isotropic Cosmological Models Without Singularity*, Phys. Lett. B **91** (1980) 99, ed. by I. M. Khalatnikov and V. P. Mineev (cit. on p. 21).

[56] A. H. Guth, *The Inflationary Universe: A Possible Solution to the Horizon and Flatness Problems*, Phys. Rev. D **23** (1981) 347, ed. by L.-Z. Fang and R. Ruffini (cit. on p. 21).

[57] A. Albrecht and P. J. Steinhardt, *Cosmology for Grand Unified Theories with Radiatively Induced Symmetry Breaking*, Phys. Rev. Lett. **48** (1982) 1220, ed. by L.-Z. Fang and R. Ruffini (cit. on p. 21).

[58] A. Vilenkin, *The Birth of Inflationary Universes*, Phys. Rev. D **27** (1983) 2848 (cit. on p. 21).

[59] A. D. Linde, *ETERNAL CHAOTIC INFLATION*, Mod. Phys. Lett. A **1** (1986) 81 (cit. on pp. 21, 39).

[60] J. Martin, C. Ringeval and V. Vennin, *Encyclopædia Inflationaris*, Phys. Dark Univ. **5-6** (2014) 75, arXiv: `1303.3787` [`astro-ph.CO`] (cit. on p. 21).

[61] H. M. Hodges, G. R. Blumenthal, L. A. Kofman and J. R. Primack, *Nonstandard Primordial Fluctuations From a Polynomial Inflaton Potential*, Nucl. Phys. B **335** (1990) 197 (cit. on p. 21).

[62] C. Destri, H. J. de Vega and N. G. Sanchez, *MCMC analysis of WMAP3 and SDSS data points to broken symmetry inflaton potentials and provides a lower bound on the tensor to scalar ratio*, Phys. Rev. D **77** (2008) 043509, arXiv: `astro-ph/0703417` (cit. on p. 21).

[63] K. Nakayama, F. Takahashi and T. T. Yanagida, *Polynomial Chaotic Inflation in the Planck Era*, Phys. Lett. B **725** (2013) 111, arXiv: `1303.7315` [`hep-ph`] (cit. on pp. 21, 93, 94).

[64] G. Aslanyan et al., *Ultracompact minihalos as probes of inflationary cosmology*, Phys. Rev. Lett. **117** (2016) 141102, arXiv: `1512.04597` [`astro-ph.CO`] (cit. on p. 21).

[65] N. Musoke and R. Easther, *Expectations for Inflationary Observables: Simple or Natural?*, JCAP **12** (2017) 032, arXiv: `1709.01192` [`astro-ph.CO`] (cit. on p. 21).

[66] E. D. Stewart, *Flattening the inflaton's potential with quantum corrections*, Phys. Lett. B **391** (1997) 34, arXiv: `hep-ph/9606241` (cit. on p. 21).

[67] E. D. Stewart, *Flattening the inflaton's potential with quantum corrections. 2.*, Phys. Rev. D **56** (1997) 2019, arXiv: `hep-ph/9703232` (cit. on p. 21).

[68] G. Ballesteros and C. Tamarit, *Radiative plateau inflation*, JHEP **02** (2016) 153, arXiv: `1510.05669` [`hep-ph`] (cit. on p. 21).

[69] K. Dimopoulos, C. Owen and A. Racioppi, *Loop inflection-point inflation*, Astropart. Phys. **103** (2018) 16, arXiv: `1706.09735` [`hep-ph`] (cit. on p. 21).

[70] N. Okada and D. Raut, *Inflection-point Higgs Inflation*, Phys. Rev. D **95** (2017) 035035, arXiv: `1610.09362` [`hep-ph`] (cit. on p. 21).

[71] N. Okada, S. Okada and D. Raut, *Inflection-point inflation in hyper-charge oriented $U(1)_X$ model*, Phys. Rev. D **95** (2017) 055030, arXiv: `1702.02938` [`hep-ph`] (cit. on p. 21).

[72] N. Okada, D. Raut and Q. Shafi, *Inflation, proton decay, and Higgs-portal dark matter in $SO(10) \times U(1)_\psi$*, Eur. Phys. J. C **79** (2019) 1036, arXiv: `1906.06869` [`hep-ph`] (cit. on p. 21).

[73] N. Okada, D. Raut and Q. Shafi, *Inflection-Point Inflation with Axion Dark Matter in light of Trans-Planckian Censorship Conjecture*, Phys. Lett. B **812** (2021) 136001, arXiv: `1910.14586` [`hep-ph`] (cit. on p. 21).

[74] N. Okada, D. Raut and Q. Shafi, *SMART $U(1)_X$ − standard model with axion, right handed neutrinos, two Higgs doublets and $U(1)_X$ gauge symmetry*, Eur. Phys. J. C **80** (2020) 1056, arXiv: `2002.07110` [`hep-ph`] (cit. on p. 21).

[75] N. Okada and D. Raut, *Running non-minimal inflation with stabilized inflaton potential*, Eur. Phys. J. C **77** (2017) 247, arXiv: `1509.04439` [`hep-ph`] (cit. on p. 21).

[76] R. Allahverdi, K. Enqvist, J. Garcia-Bellido and A. Mazumdar, *Gauge invariant MSSM inflaton*, Phys. Rev. Lett. **97** (2006) 191304, arXiv: `hep-ph/0605035` (cit. on p. 21).

[77] N. Itzhaki and E. D. Kovetz, *Inflection Point Inflation and Time Dependent Potentials in String Theory*, JHEP **10** (2007) 054, arXiv: `0708.2798` [`hep-th`] (cit. on p. 21).

[78] R. Allahverdi, B. Dutta and A. Mazumdar, *Unifying inflation and dark matter with neutrino masses*, Phys. Rev. Lett. **99** (2007) 261301, arXiv: `0708.3983` [`hep-ph`] (cit. on p. 21).

[79] M. Badziak and M. Olechowski, *Volume modulus inflection point inflation and the gravitino mass problem*, JCAP **02** (2009) 010, arXiv: `0810.4251` [`hep-th`] (cit. on p. 21).

[80] K. Enqvist, A. Mazumdar and P. Stephens, *Inflection point inflation within supersymmetry*, JCAP **06** (2010) 020, arXiv: `1004.3724` [`hep-ph`] (cit. on p. 21).

[81] S. Hotchkiss, A. Mazumdar and S. Nadathur, *Inflection point inflation: WMAP constraints and a solution to the fine-tuning problem*, JCAP **06** (2011) 002, arXiv: `1101.6046` [`astro-ph.CO`] (cit. on p. 21).

[82] T.-J. Gao and Z.-K. Guo, *Inflection point inflation and dark energy in supergravity*, Phys. Rev. D **91** (2015) 123502, arXiv: `1503.05643` [`hep-th`] (cit. on p. 21).

[83] L. Susskind, *The Anthropic landscape of string theory*, (2003), ed. by B. J. Carr, arXiv: `hep-th/0302219` (cit. on pp. 21, 39).

[84] A. H. Guth, *Eternal inflation and its implications*, J. Phys. A **40** (2007) 6811, ed. by J. Sola, arXiv: `hep-th/0702178` (cit. on pp. 21, 69).

[85] S. Winitzki, *Predictions in eternal inflation*, Lect. Notes Phys. **738** (2008) 157, arXiv: `gr-qc/0612164` (cit. on p. 21).

[86] M. Kawasaki, K. Kohri and N. Sugiyama, *MeV scale reheating temperature and thermalization of neutrino background*, Phys. Rev. D **62** (2000) 023506, arXiv: `astro-ph/0002127` (cit. on pp. 22, 32).

[87] S. Hannestad, *What is the lowest possible reheating temperature?*, Phys. Rev. D **70** (2004) 043506, arXiv: `astro-ph/0403291` (cit. on pp. 22, 32).

[88] F. Takahashi, W. Yin and A. H. Guth, *QCD axion window and low-scale inflation*, Phys. Rev. D **98** (2018) 015042, arXiv: `1805.08763` [`hep-ph`] (cit. on pp. 22, 37, 40).

[89] S.-Y. Ho, F. Takahashi and W. Yin, *Relaxing the Cosmological Moduli Problem by Low-scale Inflation*, JHEP **04** (2019) 149, arXiv: `1901.01240` [`hep-ph`] (cit. on pp. 22, 37, 40).

[90] G. D. Coughlan, W. Fischler, E. W. Kolb, S. Raby and G. G. Ross, *Cosmological Problems for the Polonyi Potential*, Phys. Lett. B **131** (1983) 59 (cit. on pp. 22, 37).

[91] S. Davidson and A. Ibarra, *A Lower bound on the right-handed neutrino mass from leptogenesis*, Phys. Lett. B **535** (2002) 25, arXiv: `hep-ph/0202239` (cit. on pp. 22, 37, 53).

[92] D. H. Lyth and A. R. Liddle, *The primordial density perturbation: Cosmology, inflation and the origin of structure*, 2009 (cit. on pp. 23, 25).

[93] Y. Akrami et al., *Planck 2018 results. X. Constraints on inflation*, Astron. Astrophys. **641** (2020) A10, arXiv: `1807.06211` [`astro-ph.CO`] (cit. on pp. 26, 62).

[94] J. B. Muñoz, E. D. Kovetz, A. Raccanelli, M. Kamionkowski and J. Silk, *Towards a measurement of the spectral runnings*, JCAP **05** (2017) 032, arXiv: `1611.05883` [`astro-ph.CO`] (cit. on pp. 27, 30).

[95] T. Asaka, S. Blanchet and M. Shaposhnikov, *The nuMSM, dark matter and neutrino masses*, Phys. Lett. B **631** (2005) 151, arXiv: `hep-ph/0503065` (cit. on p. 30).

[96] M. Shaposhnikov and I. Tkachev, *The nuMSM, inflation, and dark matter*,
Phys. Lett. B **639** (2006) 414, arXiv: `hep-ph/0604236` (cit. on p. 30).

[97] H. Davoudiasl, R. Kitano, T. Li and H. Murayama, *The New minimal standard model*,
Phys. Lett. B **609** (2005) 117, arXiv: `hep-ph/0405097` (cit. on p. 30).

[98] L. Kofman, A. D. Linde and A. A. Starobinsky,
Towards the theory of reheating after inflation, Phys. Rev. D **56** (1997) 3258,
arXiv: `hep-ph/9704452` (cit. on pp. 31, 36).

[99] R. Allahverdi, R. Brandenberger, F.-Y. Cyr-Racine and A. Mazumdar,
Reheating in Inflationary Cosmology: Theory and Applications,
Ann. Rev. Nucl. Part. Sci. **60** (2010) 27, arXiv: `1001.2600 [hep-th]` (cit. on p. 31).

[100] M. A. Amin, M. P. Hertzberg, D. I. Kaiser and J. Karouby,
Nonperturbative Dynamics Of Reheating After Inflation: A Review,
Int. J. Mod. Phys. D **24** (2014) 1530003, arXiv: `1410.3808 [hep-ph]` (cit. on p. 31).

[101] K. D. Lozanov, *Lectures on Reheating after Inflation*, (2019),
arXiv: `1907.04402 [astro-ph.CO]` (cit. on p. 31).

[102] P. B. Greene and L. Kofman, *Preheating of fermions*, Phys. Lett. B **448** (1999) 6,
arXiv: `hep-ph/9807339` (cit. on p. 33).

[103] P. B. Greene and L. Kofman, *On the theory of fermionic preheating*,
Phys. Rev. D **62** (2000) 123516, arXiv: `hep-ph/0003018` (cit. on p. 33).

[104] J. F. Dufaux, G. N. Felder, L. Kofman, M. Peloso and D. Podolsky,
Preheating with trilinear interactions: Tachyonic resonance, JCAP **07** (2006) 006,
arXiv: `hep-ph/0602144` (cit. on p. 33).

[105] A. A. Abolhasani, H. Firouzjahi and M. M. Sheikh-Jabbari,
Tachyonic Resonance Preheating in Expanding Universe, Phys. Rev. D **81** (2010) 043524,
arXiv: `0912.1021 [hep-th]` (cit. on p. 33).

[106] G. N. Felder and I. Tkachev,
LATTICEEASY: A Program for lattice simulations of scalar fields in an expanding universe,
Comput. Phys. Commun. **178** (2008) 929, arXiv: `hep-ph/0011159` (cit. on p. 33).

[107] G. N. Felder, L. Kofman and A. D. Linde, *Instant preheating*, Phys. Rev. D **59** (1999) 123523,
arXiv: `hep-ph/9812289` (cit. on p. 33).

[108] J. Garcia-Bellido, D. G. Figueroa and J. Rubio,
Preheating in the Standard Model with the Higgs-Inflaton coupled to gravity,
Phys. Rev. D **79** (2009) 063531, arXiv: `0812.4624 [hep-ph]` (cit. on p. 33).

[109] J. Repond and J. Rubio,
Combined Preheating on the lattice with applications to Higgs inflation, JCAP **07** (2016) 043,
arXiv: `1604.08238 [astro-ph.CO]` (cit. on p. 33).

[110] J. Fan, K. D. Lozanov and Q. Lu, *Spillway Preheating*, JHEP **05** (2021) 069,
arXiv: `2101.11008 [hep-ph]` (cit. on p. 33).

[111] S. R. Coleman and E. J. Weinberg,
Radiative Corrections as the Origin of Spontaneous Symmetry Breaking,
Phys. Rev. D **7** (1973) 1888 (cit. on pp. 34, 66).

[112] M. Drees, F. Hajkarim and E. R. Schmitz,
The Effects of QCD Equation of State on the Relic Density of WIMP Dark Matter,
JCAP **06** (2015) 025, arXiv: `1503.03513` [`hep-ph`] (cit. on p. 38).

[113] G. F. Giudice, E. W. Kolb and A. Riotto,
Largest temperature of the radiation era and its cosmological implications,
Phys. Rev. D **64** (2001) 023508, arXiv: `hep-ph/0005123` (cit. on pp. 39, 81).

[114] A. D. Linde, *Chaotic Inflation*, Phys. Lett. B **129** (1983) 177 (cit. on p. 39).

[115] K. Clough et al., *Robustness of Inflation to Inhomogeneous Initial Conditions*,
JCAP **09** (2017) 025, arXiv: `1608.04408` [`hep-th`] (cit. on p. 39).

[116] R. Allahverdi and M. Drees, *Production of massive stable particles in inflaton decay*,
Phys. Rev. Lett. **89** (2002) 091302, arXiv: `hep-ph/0203118` (cit. on p. 44).

[117] A. Garzilli, A. Magalich, O. Ruchayskiy and A. Boyarsky,
How to constrain warm dark matter with the Lyman-α forest,
Mon. Not. Roy. Astron. Soc. **502** (2021) 2356, arXiv: `1912.09397` [`astro-ph.CO`]
(cit. on p. 45).

[118] M. Viel, J. Lesgourgues, M. G. Haehnelt, S. Matarrese and A. Riotto,
*Constraining warm dark matter candidates including sterile neutrinos and light gravitinos
with WMAP and the Lyman-alpha forest*, Phys. Rev. D **71** (2005) 063534,
arXiv: `astro-ph/0501562` (cit. on p. 45).

[119] V. Iršič et al., *New Constraints on the free-streaming of warm dark matter from intermediate
and small scale Lyman-α forest data*, Phys. Rev. D **96** (2017) 023522,
arXiv: `1702.01764` [`astro-ph.CO`] (cit. on p. 45).

[120] I. Masina, *Dark matter and dark radiation from evaporating primordial black holes*,
Eur. Phys. J. Plus **135** (2020) 552, arXiv: `2004.04740` [`hep-ph`] (cit. on p. 45).

[121] Y. Mambrini and K. A. Olive, *Gravitational Production of Dark Matter during Reheating*,
Phys. Rev. D **103** (2021) 115009, arXiv: `2102.06214` [`hep-ph`] (cit. on pp. 46, 77).

[122] N. Bernal and C. S. Fong, *Dark matter and leptogenesis from gravitational production*,
JCAP **06** (2021) 028, arXiv: `2103.06896` [`hep-ph`] (cit. on p. 46).

[123] B. Barman and N. Bernal, *Gravitational SIMPs*, JCAP **06** (2021) 011,
arXiv: `2104.10699` [`hep-ph`] (cit. on pp. 46, 77).

[124] N. Bernal et al., *Spin-2 Portal Dark Matter*, Phys. Rev. D **97** (2018) 115020,
arXiv: `1803.01866` [`hep-ph`] (cit. on p. 47).

[125] L. H. Ford, *Gravitational Particle Creation and Inflation*, Phys. Rev. D **35** (1987) 2955
(cit. on p. 47).

[126] V. Kuzmin and I. Tkachev, *Matter creation via vacuum fluctuations in the early universe and
observed ultrahigh-energy cosmic ray events*, Phys. Rev. D **59** (1999) 123006,
arXiv: `hep-ph/9809547` (cit. on p. 47).

[127] D. J. H. Chung, E. W. Kolb and A. Riotto, *Superheavy dark matter*,
Phys. Rev. D **59** (1998) 023501, arXiv: `hep-ph/9802238` (cit. on p. 47).

[128] D. J. H. Chung, P. Crotty, E. W. Kolb and A. Riotto,
On the Gravitational Production of Superheavy Dark Matter, Phys. Rev. D **64** (2001) 043503,
arXiv: `hep-ph/0104100` (cit. on p. 47).

[129] D. J. H. Chung, E. W. Kolb, A. Riotto and L. Senatore,
Isocurvature constraints on gravitationally produced superheavy dark matter,
Phys. Rev. D **72** (2005) 023511, arXiv: `astro-ph/0411468` (cit. on p. 47).

[130] Y. Ema, R. Jinno, K. Mukaida and K. Nakayama, *Gravitational Effects on Inflaton Decay*,
JCAP **05** (2015) 038, arXiv: `1502.02475 [hep-ph]` (cit. on p. 47).

[131] Y. Ema, R. Jinno, K. Mukaida and K. Nakayama, *Gravitational particle production in
oscillating backgrounds and its cosmological implications*, Phys. Rev. D **94** (2016) 063517,
arXiv: `1604.08898 [hep-ph]` (cit. on p. 47).

[132] Y. Ema, K. Nakayama and Y. Tang, *Production of Purely Gravitational Dark Matter*,
JHEP **09** (2018) 135, arXiv: `1804.07471 [hep-ph]` (cit. on p. 47).

[133] Y. Ema, K. Nakayama and Y. Tang,
Production of purely gravitational dark matter: the case of fermion and vector boson,
JHEP **07** (2019) 060, arXiv: `1903.10973 [hep-ph]` (cit. on p. 47).

[134] M. Garny, M. Sandora and M. S. Sloth,
Planckian Interacting Massive Particles as Dark Matter, Phys. Rev. Lett. **116** (2016) 101302,
arXiv: `1511.03278 [hep-ph]` (cit. on p. 47).

[135] M. Garny, A. Palessandro, M. Sandora and M. S. Sloth,
Theory and Phenomenology of Planckian Interacting Massive Particles as Dark Matter,
JCAP **02** (2018) 027, arXiv: `1709.09688 [hep-ph]` (cit. on p. 47).

[136] J. A. Casas and A. Ibarra, *Oscillating neutrinos and $\mu \to e, \gamma$*, Nucl. Phys. B **618** (2001) 171,
arXiv: `hep-ph/0103065` (cit. on p. 50).

[137] A. Ibarra and G. G. Ross, *Neutrino phenomenology: The Case of two right-handed neutrinos*,
Phys. Lett. B **591** (2004) 285, arXiv: `hep-ph/0312138` (cit. on p. 50).

[138] W. Buchmuller, P. Di Bari and M. Plumacher, *Leptogenesis for pedestrians*,
Annals Phys. **315** (2005) 305, arXiv: `hep-ph/0401240` (cit. on pp. 53, 83).

[139] G. Lazarides and Q. Shafi, *Origin of matter in the inflationary cosmology*,
Phys. Lett. B **258** (1991) 305 (cit. on p. 53).

[140] G. F. Giudice, M. Peloso, A. Riotto and I. Tkachev,
Production of massive fermions at preheating and leptogenesis, JHEP **08** (1999) 014,
arXiv: `hep-ph/9905242` (cit. on p. 53).

[141] T. Asaka, K. Hamaguchi, M. Kawasaki and T. Yanagida, *Leptogenesis in inflationary universe*,
Phys. Rev. D **61** (2000) 083512, arXiv: `hep-ph/9907559` (cit. on pp. 53, 54).

[142] V. N. Senoguz and Q. Shafi,
GUT scale inflation, nonthermal leptogenesis, and atmospheric neutrino oscillations,
Phys. Lett. B **582** (2004) 6, arXiv: `hep-ph/0309134` (cit. on p. 53).

[143] F. Hahn-Woernle and M. Plumacher, *Effects of reheating on leptogenesis*,
Nucl. Phys. B **806** (2009) 68, arXiv: `0801.3972 [hep-ph]` (cit. on p. 53).

[144]   S. Antusch, J. P. Baumann, V. F. Domcke and P. M. Kostka,
        Sneutrino Hybrid Inflation and Nonthermal Leptogenesis, JCAP **10** (2010) 006,
        arXiv: `1007.0708` [`hep-ph`] (cit. on p. 53).

[145]   E. W. Kolb and M. S. Turner, *The Early Universe*, vol. 69, 1990, ISBN: 978-0-201-62674-2
        (cit. on p. 54).

[146]   T. Kobayashi and O. Seto, *Polynomial inflation models after BICEP2*,
        Phys. Rev. D **89** (2014) 103524, arXiv: `1403.5055` [`astro-ph.CO`] (cit. on p. 58).

[147]   V. N. Senoguz and Q. Shafi, *Chaotic inflation, radiative corrections and precision cosmology*,
        Phys. Lett. B **668** (2008) 6, arXiv: `0806.2798` [`hep-ph`] (cit. on p. 58).

[148]   F. R. Bouchet et al., *COrE (Cosmic Origins Explorer) A White Paper*, (2011),
        arXiv: `1102.2181` [`astro-ph.CO`] (cit. on pp. 60, 71).

[149]   T. Matsumura et al., *Mission design of LiteBIRD*, J. Low Temp. Phys. **176** (2014) 733,
        arXiv: `1311.2847` [`astro-ph.IM`] (cit. on pp. 60, 71).

[150]   H. Li et al., *Probing Primordial Gravitational Waves: Ali CMB Polarization Telescope*,
        Natl. Sci. Rev. **6** (2019) 145, arXiv: `1710.03047` [`astro-ph.CO`] (cit. on pp. 60, 71).

[151]   K. Abazajian et al., *CMB-S4 Science Case, Reference Design, and Project Plan*, (2019),
        arXiv: `1907.04473` [`astro-ph.IM`] (cit. on pp. 60, 71).

[152]   A. R. Liddle and S. M. Leach,
        How long before the end of inflation were observable perturbations produced?,
        Phys. Rev. D **68** (2003) 103503, arXiv: `astro-ph/0305263` (cit. on p. 64).

[153]   E. H. Tanin and T. Tenkanen, *Gravitational wave constraints on the observable inflation*,
        JCAP **01** (2021) 053, arXiv: `2004.10702` [`astro-ph.CO`] (cit. on p. 64).

[154]   A. A. Starobinsky, *Dynamics of Phase Transition in the New Inflationary Universe Scenario
        and Generation of Perturbations*, Phys. Lett. B **117** (1982) 175 (cit. on p. 68).

[155]   A. D. Linde,
        Scalar Field Fluctuations in Expanding Universe and the New Inflationary Universe Scenario,
        Phys. Lett. B **116** (1982) 335 (cit. on p. 68).

[156]   G. Barenboim, W.-I. Park and W. H. Kinney, *Eternal Hilltop Inflation*, JCAP **05** (2016) 030,
        arXiv: `1601.08140` [`astro-ph.CO`] (cit. on pp. 68, 69).

[157]   S. Y. Choi, J. S. Shim and H. S. Song, *Factorization and polarization in linearized gravity*,
        Phys. Rev. D **51** (1995) 2751, arXiv: `hep-th/9411092` (cit. on p. 77).

[158]   M. Yamaguchi, *Supergravity based inflation models: a review*,
        Class. Quant. Grav. **28** (2011) 103001, arXiv: `1101.2488` [`astro-ph.CO`] (cit. on p. 93).

[159]   M. Kawasaki, M. Yamaguchi and T. Yanagida, *Natural chaotic inflation in supergravity*,
        Phys. Rev. Lett. **85** (2000) 3572, arXiv: `hep-ph/0004243` (cit. on p. 93).

[160]   K. Harigaya, M. Ibe, M. Kawasaki and T. T. Yanagida,
        Revisiting the Minimal Chaotic Inflation Model, Phys. Lett. B **756** (2016) 113,
        arXiv: `1506.05250` [`hep-ph`] (cit. on pp. 93, 94).

List of Figures

106

List of Tables